Università degli Studi di Cagliari

DOTTORATO DI RICERCA

Scienze della Terra

Ciclo XXVII

Geochemical studies on antimony: antimony dispersion in water draining Su Suergiu mine area; removal of Sb(V) from aqueous solution by layered double hydroxides (LDH)

Settori scientifici disciplinari di afferenza

GEO/06 - GEO/08

Presentata da	Dott.ssa Elisabetta Dore
Coordinatore Dottorato	Prof. Marcello Franceschelli
Tutor	Prof.ssa Rosa Cidu
	Prof. Franco Frau

Esame finale anno accademico 2013 – 2014

Acknowledgment

It is a pleasure to thank those people who made this thesis possible.

First I would like to express my gratitude to my supervisors Prof.ssa Rosa Cidu and Prof. Franco Frau.

I wish to thank to Dr. Gregory Lefèvre (ENSCP/CNRS LECIME, Paris) and Dr. Athenais Davantès (Universty P.Curie UPMC-Paris 6) for hosting me in their laboratories, allowing me to collect new interesting data for implementing my work.

A special thank to Dr. Paola Meloni and Dr. Ombretta Cocco of "*Laboratorio per la Didattica e Ricerca per la Salvaguardia dei Beni Culturali "Colle di Bonaria""* for let me use their laboratory and for their kindness.

I would like to thanks Prof. Piero Lattanzi (coordinator of PRIN 2010-2011) and Prof. Marcello Franceschelli (coordinator of doctoral course).

Thanks to Dr. Giorgio Contis for the analyses by Ionic Chromatography and his kindness, and Dr. Francesca Podda for her technical support.

A special thank to Dr. D. Kirk Nordstrom for hosting me at U.S.Geological Survey in Boulder, Colorado, for his help and very useful suggestions in writing and for his careful review of this thesis.

In particular I would like to thanks Dott. Richard B. Wanty for his kindness and frienship when I was in Colorado.

Table of Contents

Abstract

Antimony (Sb) is considered a pollutant of priority interest, it is largely used in several industrial sectors (> 100,000 tons year worldwide) and is heavily mined worldwide (Leuz et al., 2006). In this work the hydrogeochemical behavior of Sb has been studied in water draining the abandoned antimony mine of Su Suergiu, SE Sardinia. Waters flowing at Su Suergiu show high Sb concentration and impact the main river of South Sardinia, the Flumendosa River that supplies water for agricultural and domestic uses. The main source of contamination at Su Suergiu is represented by the foundry slag heaps, in fact the slag drainages contain up to 30,000 μg L^{-1} Sb(tot) (median value 13,000 μg L^{-1} Sb(tot)). The determination of Sb specie in solution has been carried out through the analyses of both Sb(tot) (by ICP-MS and/or ICP-OES) and Sb(III) (by ASV). The Sb(III) concentration was determined on filtered (pore-size 0.45 μm) water samples stabilized with L(+) tartaric acid plus nitric acid, that, among several stabilizations of Sb(III) tested, has been evaluated as the most effective. Results obtained, showed that Sb(V) prevails in water sampled at Su Suergiu and surrounding area as $Sb(OH)_6^-$ species, in agreement with the circumneutral-slightly alkaline pH values and oxidizing condition (Sb(III) ≤6% of Sb(tot)). The Sb(V) is less toxic but more mobile than Sb(III); the Sb behavior in water analyzed seems to be conservative, and the most important natural attenuation process of Sb contamination appears to be dilution. First in the water of Riu Ciurixeda (whose catchment collect all mine drainage), and after in the Flumendosa River, the Sb concentration decreases significantly, from 10^4 to 10^1 μg L^{-1}, but in the Flumendosa River it still exceeded the limit recommended by both the World Health Organization (20 μg L^{-1}) and the European Union (5 μg L^{-1}), especially under extremely high flow conditions (Sb(tot) = 51 μg L^{-1}; median relative to all flow conditions Sb(tot) = 22 μg L^{-1}).

In view of these results Sb(V) removal from solution was tested using a synthetic mineral belonging to the class of layered double hydroxides, that has the advantage, with respect to the other sorbents (metal oxy-hydroxides, organic polymers, etc...), of being able to remove contaminants from solutions at circumneutral pH values often found in the environment. The LDH are characterized by a layered structure composed by brucite-like sheets ($[M^{2+}_{1-x}M^{3+}_x(OH)_2]^{x+}$), stacked along the *c* axis and positively charged, due to the partial substitution of bivalent cations (M^{2+} = Mg^{2+}, Zn^{2+}, Ca^{2+}) by trivalent cations (M^{3+} = Al^{3+}, Fe^{3+}). The positive charges are compensated by anions or anionic complexes (A^{n-} = Cl^-, NO_3^-, CO_3^{2-}) in the interlayer, where also structural water can occur. From an environmental point of view, LDH have anion exchange capacity, sorption capacity, high specific surface area and the "memory effect", which is the capacity of the calcined phases which have undergone structural collapse from the loss of interlayer water and anions, to recover its structure when immerged in aqueous solution. Calcined and nitrate LDH were tested; the calcined resulted are the most effective. Among them the Mg(AlFe)-c oxides, derived from the calcination of hydrotalcite-like compounds

{$Mg_6Al_2(OH)_{16}CO_3 \cdot 4H_2O$}, removed $Sb(OH)_6^-$ from solution through the rehydration and formation of a brandholzite-like compound {$Mg[Sb(OH)_6]_2 \cdot 6H_2O$}. The 2ZnAl-c oxides derived from the calcination of zaccagnaite-like compounds ($Zn_4Al_2(OH)_{12}CO_3 \cdot 3H_2O$) kept $Sb(OH)_6^-$ from solution by its intercalation in the interlayer during the reconstruction of zincalstibite-like LDH {$Zn_2Al(OH)_6[Sb(OH)_6]$}. The $Sb(OH)_6^-$ removal capacity of both sorbents is seriously affected by the presence of coexistent equal concentrations of As in solution, while the carbonate species and the SO_4^{2-} result lower competition with respect to $Sb(OH)_6^-$. Sorption tests with selected calcined LDH, Mg(AlFe)-c and 2ZnAl-c, were performed on water collected in the slag drainage of Su Suergiu, characterized by slightly alkaline pH and high concentration of SO_4^{2-} (1006 mg L^{-1}), HCO_3^- (485 mg L^{-1}), As (3386 µg L^{-1}) and Sb(tot) (9900 µg L^{-1}). Results show substantial capacity of Sb removal from solution, and also of As. Due to the relatively low concentration of Sb in Su Suergiu water with respect to the synthetic solution used in the sorption test, the main removal process of Sb resulted for both sorbents used in the intercalation in the interlayer during the reconstruction of carbonate(hydroxyl) LDH structure, also As seem to be removed through the same mechanism. In several experiments the dissolution of sorbents was observed, therefore it is necessary consider the impact from the dissolution of the metals composing them.

The solid/liquid ratio strongly influences the removal processes, therefore future studies should address this aspect to assess the potential use of LDH in Sb removal from solution at circumneutral pH usually found in the environment.

Preface

This PhD work has been developed in the frameworks of the projects PRIN 2009 "*study of geochemical behavior of antimony: speciation in the aqueous phase and dispersion in abandoned mining areas"* (coordinator Cidu R.) and PRIN 2012 "i*nteraction between biosphere and minerals: consequences for the environment and human health"* (coordinator Lattanzi P.) of the Research Unit of the Department of Chemical and Geological Science of University of Cagliari. The aims of these projects were to improve the knowledge of the geochemical behavior of antimony (PRIN 2009), and the development of remediation strategies for the decontamination of water polluted by heavy metals (PRIN 2012).

In these contexts, part of this work was dedicated to the study of the hydrogeochemistry of antimony, with particular regards to the determination of antimony species in solution through the study of antimony behavior in water draining an important mine area in the south east of Sardinia, the abandoned antimony mine of Su Suergiu, and the impact of these polluted waters on the Flumendosa River, the main river of the South Sardinia.

Another part of this study was dedicated to the experimentation of the antimony removal from solution by means of synthetic minerals. Taking into account that at the environmental conditions of surface water usually the Sb(V) prevail as anionic complex dissolved in solution, the synthetic minerals belonging to the class of layered double hydroxides were chosen because they are able to remove contaminants that are stable as anionic species in solution at circumneutral pH. Their removal capacity of antimony was tested both on synthetic solutions and on natural waters.

CHAPTER 1. Introduction

Antimony is heavily mined due to its usefulness in several industrial applications(> 100,000 tons year consumed worldwide) (Leuz et al., 2006; Mitsunobu et al., 2009); for instance, it is used as alloys in storage batteries and ammunition, as a pigment for paint or lacquers, in the smelting industry and in the textile industry (Krachler et al., 2001; Mitsunobu et al., 2009). Antimony is a non-essential element, ubiquitously distributed in the lithosphere and present in the aquatic environment as a result of natural processes such as weathering of Sb-bearing minerals and geothermal activity, and anthropogenic sources, like mining and industrial activities.

The World Health Organization (WHO, 2011) and the European Community (Directive 98/83/EC) have established a guideline value of 20 μg L^{-1} Sb and 5μg L^{-1} for drinking water, respectively; while the US Environmental Protection Agency set the limit of Sb in drinking water at 6 μg L^{-1} (USEPA, 1979). In unpolluted waters the antimony concentration is commonly below 1 μg L^{-1}, but close to mine areas or other anthropogenic sources it can reach up to 100 times natural levels. Particularly high concentrations of antimony have been detected in water draining abandoned mine and smelter sites (Cidu et al., 2008b; Filella et al., 2002a; Hiller et al., 2012).

In the last few decades, antimony's anthropogenic emissions have been significantly increasing, and being a pollutant element, with toxicity similar to arsenic, environmental effects linked to its extraction are arising great interest by several authors (Filella et al., 2002a;). Inorganic antimony compounds are considered more toxic than organic ones, and Sb(III) is considered more toxic than Sb(V) (Filella et al., 2002b; Gebel 1997). The mobility, bioavailability and toxicology of antimony depend on its chemical speciation. Total concentration is not sufficient to assess antimony environmental effects (Filella et al., 2002a, b). Even though several studies have been done, at present the geochemical behavior of antimony is not completely understood. Antimony can be present in natural waters as both dissolved Sb(III) and dissolved Sb(V); in the simple chemical system Sb-H-O under reducing conditions, aqueous antimony prevails as antimonous acid $Sb(OH)_3$ while under oxidizing conditions the $Sb(OH)_6^-$ specie is stable in a wide range of pH. Nevertheless Sb(III) has been also detected under oxidizing conditions, where it is thermodynamically unstable, as well as Sb(V) oxidized species has been reported in anoxic environments (Filella et al., 2002b and references therein). These observations suggest that the kinetics of redox reactions may play a significant role in defining the impact of Sb in the environment (Quentel et al., 2004).

This work focused on the study of the geochemical behavior of antimony in water draining the abandoned mining area of Su Suergiu (SE Sardinia) and the impact of this water on the main river of South Sardinia, the Flumendosa River. Previous studies showed that waters draining Su Suergiu mine area which contain high antimony concentrations (up to 10^3-10^4 μg L^{-1}) flowed untreated in the Flumendosa River, which supplies water for agricultural and domestic uses, and the antimony

contamination persists for several kilometer after its confluence (Cidu et al., 2008 a, b).

To achieve a better understanding of the processes that control antimony dispersion in the aqueous system of this area, both Sb(III) and total antimony in solution were determined. The determination of Sb(III) in oxygenated water is difficult because of its thermodynamic instability and considerable efforts were devoted to assess the most appropriate water sampling and stabilization conditions.

Several sorbents, like metal oxides and hydroxides, organic polymers, clay minerals, have higher removal capacity at low pH values than circumneutral or slightly alkaline conditions (Carriazo et al., 2007); previous studies showed that manganese oxides, aluminum and iron oxy-hydroxides, have high antimony removal capacity under reducing condition and at low pH values, while as the pH increases, the sorption capacity usually decreases (Leuz et al., 2006; Thanalabasingam and Pickering, 1990; Rakshit et al. 2011). In view of these studies, sorption experiments were performed using synthetic compounds of the class of layered double hydroxides (LDH). The LDH minerals are characterized by a layered structure composed of brucite-like sheets ($[M^{2+}_{1-x}M^{3+}_{x}(OH)_2]^{x+}$), superposed and positively charged, due to the partial substitution of bivalent cations (M^{2+} = Mg^{2+}, Zn^{2+}, Ca^{2+}) by trivalent cations (M^{3+} = Al^{3+}, Fe^{3+}). The positive charges are compensated by anions or anionic complexes (A^{n-} = Cl^-, NO_3^-, CO_3^{2-}) in the interlayer, where structural water can also occur (Cavani et al., 1991). These minerals have important properties as: anion exchange capacity, sorption capacity, high specific surface area, and a property called “memory effect”. This latter is the capacity of the calcined phases, that undergone to structural collapse due to the lost of interlayer water and anions, to recovery its structure when immerged in aqueous solution. Efficacy and potential of LDH in remediation of polluted waters, at circum-neutral pH values, is well-known with respect to several anionic complexes like arsenate, chromate, vanadate, etc. (Goh et al., 2008) but has not been investigated enough in antimony-polluted solutions (Kameda et al., 2011; Mitsunobu et al., 2009). Natural LDH phases, having $Sb(OH)_6^-$ as interlayer anion complex (Cualstibite group), provide an important suggestion for the choice of starting cationic composition of LDH synthesis to use in removal tests (Mills et al., 2012).

The double aim of this work is improve the knowledge of the antimony behavior in the waters draining the abandoned mine of Su Suergiu (SE Sardinia) and study the antimony removal mechanism from aqueous solutions by layered double hydroxides (LDH), to suggest a solution for removal of Sb(V) from polluted waters under the common environmental conditions of surface water, and to assess the applicability of this method.

CHAPTER 2. Investigations on the determination of Sb(III) traces in Sb(V)-rich media by ASV: tests with synthetic solutions and Sb-polluted waters

2.1 State of art

Antimony occurs naturally in the aquatic environment as a consequence of natural processes and anthropogenic activities. Typical concentrations of total antimony in unpolluted water are less than 1 μg L^{-1} but can significantly increase as a consequence of human activity. The World Health Organization (WHO, 2011) and the European Community (Directive 98/83/EC) have fixed the limit for drinking water at 20 and 5 μg L^{-1} Sb, respectively. In aquatic systems antimony is usually found in the oxidation states Sb(III) and Sb(V) that hydrolyze easily in aqueous solutions (Filella et al., 2002b). Under reducing conditions the antimonous acid [$Sb(OH)_3$] and the products of its protonation and deprotonation [$Sb(OH)_2^+$ and $Sb(OH)_4^-$, respectively] are the main Sb(III) species, whereas under oxidizing conditions Sb(V) occurs as antimonic acid [$Sb(OH)_5$] with the related aqueous species [e.g. $Sb(OH)_6^-$]. On the basis of the current knowledge, the undissociated antimonous acid prevails over the products of its deprotonation and protonation (pKa of 11.82 at 25 °C from Zakaznova-Herzog and Seward, 2006) instead the Sb(V) protonated species prevail over undissociated antimonic acid (pKa of 2.85, Accornero et al., 2008). Consequently, in natural waters it is expect that the dominant species correspondent to the oxidation states Sb(III) and Sb(V) are respectively $Sb(OH)_3$ and $Sb(OH)_6^-$. In oxidizing condition $Sb(OH)_6^-$ is stable in solution over a wide range of pH, however, thermodynamically unstable Sb(III) has been also detected under oxidizing conditions, like oxygenated marine water, surface water, groundwater and rain water; in the same way Sb(V) oxidized species has been also determined in anoxic environments (Filella et al., 2002b). Mobility, bioavailability and toxicity of antimony are related with its speciation, therefore, the determination of total antimony (Sb(tot)) is not sufficient to asses completely its environmental impact.

Several analytical techniques can be used to determine the antimony species in aqueous media, like flow injection hydride generation atomic absorption spectrometry (Cabon et al., 2004), inductively coupled plasma-mass spectrometry (ICP-MS) and inductively coupled plasma-optical emission spectrometry (ICP-OES) (Marcellino et al., 2008), total reflection X-ray spectrometry (Marguí et al., 2013) and several electrochemical methods such as anodic stripping voltammetry (ASV) and potentiometric stripping analysis (Gadhari et al., 2011; Quentel and Filella, 2002; Renedo et al., 2007, Toghill et al., 2011). A critical point in the Sb(III) determinations, consists in the necessity of sample manipulations, like separation of the species and/or pre-concentration; moreover, in natural

oxygenated water the oxidation of Sb(III) in Sb(V) could affect the speciation results, but to the best of my knowledge a method for preserving the Sb(III) in Sb-rich water is not available so far. Therefore investigations focused on the determination of a simple method for the stabilization of Sb(III) in Sb(V)-rich media were carried out. Several tests were performed with both synthetic solution and antimony polluted water and the determination of Sb(III) was performed by a polarograph with a voltammetry technique (ASV, anodic stripping voltammetry), that does not require pretreatment of the samples. Synthetic solutions were prepared in the laboratory, while the natural waters affected by antimony pollution were sampled in the abandoned antimony mine of Su Suergiu (SE Sardinia).

At Su Suergiu the ore was mined underground since 1858, and was flanked by the foundry activity in the 1892. The mineralization is hosted in Paleozoic black shales and metalimestones, and consists of stibnite, scheelite, pyrite and arsenopyrite, with quartz and calcite in the gangue (Funedda et al., 2005). Usually the mining waste and residual materials related to metallurgical activity were dumped directly on the ground. After the final closure of all activities (1987), mining waste and foundry slag were left on the ground, without actions to mitigate the environmental impact; the volume of slag heaps is estimated at about 66,000 m^3 (RAS, 2003). Waters flowing at Su Suergiu contain high antimony concentrations, mainly due to the interaction with the residues of metallurgical processes (Cidu et al., 2014). Moreover, the waters are characterized by slightly alkaline pH and oxidizing conditions, therefore they are particularly suitable for the purposes of this study.

2.2 Materials and methods

2.2.1 Reagents and standards

All synthetic solutions were prepared using ultrapure water (Millipore, Milli-Q©, 18.2 MΩ cm^{-1}). The list and characteristics of reagents are reported in table 2.1. The Sb(III) standards were prepared daily, immediately before analyses, and the other standards were prepared 24 hours before analyses. All solutions and water samples were stored at 4°C until analysed.

Table 2.1 List of reagents and standard solutions.

Reagent	Brand	Assay	matrix
Hydrochloric acid, HCl	Carlo erba, superpure	37	
Hydrochloric acid, HCl	Carlo Erba, ultrapure	37	
Nitric acid, HNO_3	Carlo erba, superpure	69	
L(+) ascorbic acid, $C_6H_8O_6$	Alpha Aesal Germany, ACS	99	
L(+) tartaric acid, $C_4H_6O_6$	Sigma-Aldrch, Uk	99	
Sb(V) solid, $K[Sb(OH)_6]$	Fluka, Sigma-Aldrich, Uk	>99	
Rhodium solution, Rh	Sigma-Aldrch, Uk	1025	HCL 5%
Sb(III) solution, Sb_2O_3	Exaxol Italia	1000	$C_4H_6O_6$ 3 % + HNO_3 1%
Sb(V) solution, $SbCl_5$	Exaxol Italia	100	HCl 25%

2.2.2 Analytical methods

The concentration of Sb(III) was determined by anodic stripping voltammetry (ASV, Metrohm 797 VA Computrace) at the hanging mercury drop electrode (HDME) following the method developed by Metrohm (Application Bulletin 74/3e). The potential values were referred to an Ag/AgCl, 3 mol L^{-1} KCl reference electrode, and a Pt wire auxiliary electrode. Measurements were made by the differential pulse (DP) mode (table 2.2). During the analysis the solution was de-aerated with an inert gas (N_2).

Table 2.2 Parameter and operating conditions used for the Sb(III) determination by ASV.

Working electrode	HDME	Post electrolysis time	20 s
Drop size	4	(Deposition time)	
Stirrer speed	2000 rpm	Equilibration time	10 s
Mode	DP	Pulse amplitude	10 mV
Purge time	300 s	Start potential	- 300 mV
Cleaning deposition potential	- 240 mV	End potential	50 mV
Cleaning deposition time	180 s	Voltage step	4 mV
Post electrolysis potential	- 110 mV	Voltage step time	0.2 s
Peak potential	- 150 mV	Sweep rate	20 mV s^{-1}

Voltammetric measurements of Sb(III) were made using 10 mL of sample plus 0.6 mL HCl and two manual additions of 1 mg L^{-1} Sb(III) standard solution, the volume of additions ranged between 25 and 100 µL depending on the intensity of the sample signal (fig.2.1).

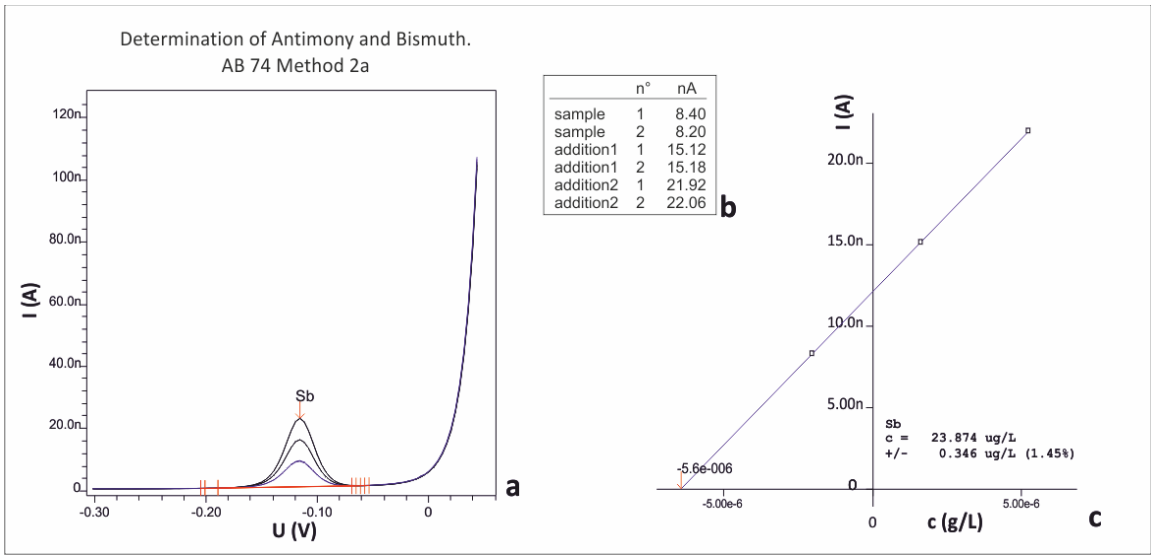

Figure 2.1 Example of Voltammetric Sb(III) determination: (**a**) curves of Sb(III), where **I(A)** indicate the current in ampere and **U(V)** indicate the potential in volts; (**b**) peak charge (nA = nanoampere); (**c**) curves and Sb(III) concentration.

Sb(tot) was determined by ICP-MS (quadrupole, Perkin–ElmerSCIEX ELAN DRC-e) using the ^{121}Sb and ^{123}Sb atomic mass units, with Rh as internal standard (10 µg L^{-1} Rh). The ICP-MS was fitted with a cross-

flow nebulizer and a Ryton Scott spray chamber. At high concentrations, Sb(tot) was also determined by ICP-OES (ARL Fisons 3520) fitted with a concentric nebulizer and a quartz, conical spray chamber. The operating parameters of the instruments were optimized daily. The working range of ICP-OES and ICP-MS were 100 to 50,000 μg L^{-1} Sb and 0.1 to 100 μg L^{-1} Sb, respectively. Concentration of Sb(V) was determined subtracting Sb(III) from Sb(tot).

2.2.3 Tests with synthetic solutions

Synthetic solutions, with nominal concentration of 10 μg L^{-1} Sb(III), were prepared by diluting the Sb(III) mother solution in Milli-Q water. The Sb(III) concentration was determined immediately and measurements were repeated after 7 and 30 days in order to assess the efficacy of stabilization during the time. The first series of preservation tests for the time stability of Sb(III) were:

a) 1% v/v HCl

b) 0.1% w/v L(+) ascorbic acid

c) 0.2% v/w L(+) tartaric acid plus 0.1% v/v HNO_3

There are not previous data relative the use of L(+) tartaric acid plus nitric acid for the Sb(III) preservation; these reagents are tested considering that are used for the Sb(III) mother solution (see table 2.1).

To evaluate if the initial Sb(III) concentration affects the efficacy of the stabilization, and to estimate the dilution effects during the determinations, further tests were performed on solutions with starting nominal concentrations equal to 5, 20 and 500 μg L^{-1} Sb(III). Determinations were repeated at a fixed time; on the basis of the first results only the stabilizations with hydrochloric acid or L(+) tartaric acid plus nitric acid were used.

These stabilizations were also tested in Sb(V)-rich media. An appropriate amount of $K[Sb(OH)_6]$ were dissolved in Milli-Q water in order to have an 10 mg L^{-1} Sb(V) solution; considering the high purity of $K[Sb(OH)_6]$ (table 1.1), concentrations of Sb(III) <0.1 mg L^{-1} were expected. Three aliquots were prepared: one was kept in Milli-Q, the other two aliquots were stabilized with suprapure HCl or L(+) tartaric acid plus nitric acid.

2.2.4 Water sampling

Tests were also carried out with the antimony polluted water collected in the abandoned antimony mine of Su Suergiu (SE Sardinia) and surroundings. The physical-chemical parameters were measured at the sampling site, water samples were filtered through 0.45 μm pore-size filters (OlimPeak, polypropylene) into pre-cleaned high-density PE bottles and stored at 4°C till the analyses. For the determination of Sb(III) an aliquot was filtered and not stabilized, other two aliquots were filtered and stabilized with HCl 1% (v/v) or L(+) tartaric acid 0.2% (w/v) plus HNO_3 1% (v/v). For analyses of Sb(tot)

by ICP-MS and/or ICP-OES another aliquot was filtered and acidified with HNO_3 1%, (v/v).

2.2.5 Standard addition tests

For this purpose, three aliquots of 50 mL samples and a fixed volume of spike (0.1 mL) having an appropriate concentrations of Sb(III) were added to each aliquot (Cidu R., 2000).

The standard addition tests were carried out with both synthetic solutions and mining-impacted water; samples stabilized with HCl 1% (v/v) or L(+) tartaric acid 0.2% (w/v) plus HNO_3 1% (v/v), and not stabilized, were tested for each solution. When the test was performed with mining-impacted water, the spikes were added at the sampling site and Sb(III) was determined in laboratory within few hours after the sampling.

The bottles used to store the stabilized aliquots of both synthetic solutions and mine water samples were pre-cleaned as follows: depending on the reagent to be used, the bottles were filled with HCl 3% (v/v) or HNO_3 3% (v/v) for 3 days, thereafter were rinsed with Milli-Q, and in laboratory or at sampling point were also rinsed with the samples before collection.

2.3 Results

The detection limits were calculated considering 10 times the standard deviation of blank solutions processed during the analyses. The detection limits of Sb(tot) were 0.1 µg L^{-1} and 50 µg L^{-1} for ICP-MS and ICP-OES, respectively. Detection limit of Sb(III) determined by ASV was 0.4 µg L^{-1}.

2.3.1 Synthetic solutions

Analyses performed on solutions containing nominal concentration of 10 µg L^{-1} showed recoveries >90% for measurements carried out within 7 days (table 2.3). After 30 days, concentrations of Sb(III) determined in the solution stabilized with L(+) tartaric acid plus nitric acid was stable, while a marked decrease was observed in the other solutions. In view of these results, the L(+) ascorbic acid was not used in subsequent tests.

Table 2.3 Results of temporal stability of Sb(III) in synthetic solution containing 10 µg L^{-1} Sb(III) stabilized with HCl 1%, 0.1 % L(+) ascorbic acid or HNO_3 1% + L(+) tartaric acid.

	Sb(III) 10 µg L^{-1}	1 d µg L^{-1}	SD	recovery* %	7 d µg L^{-1}	SD	recovery %	30 d µg L^{-1}	SD	recovery %
reagents	HCl 1%	10.4	0.1	104	9.1	0.5	91	7.6	0.2	76
	0.1 % L(+) ascorbic acid	9.8	0.3	98	9.3	0.7	93	7.0	0.3	70
	HNO_3 1% + L(+) tartaric acid	12.5	0.9	125	11.5	0.8	115	12.4	0.7	124

*recovery is calculated with respect to the nominal initial Sb(III) concentration.

Determination performed on solutions containing 5 µg L^{-1} Sb(III) showed that after 20 days the concentration of Sb(III) was stable only when the stabilization with L(+) tartaric acid plus nitric acid were used, while decreased in solution with HCl 1% (v/v) (table 2.4). Instead concentrations of Sb(III) determined in synthetic solutions with initial Sb(III) of 20 µg L^{-1} concentration resulted in stable values over 20 days for both stabilizations.

Table 2.4. Temporal stability of Sb(III) determined in sinthetic solution with initial concentrations 5 and 20 µg L^{-1} stabilized with HCl 1%or HNO_3 1% + L(+) tartaric acid.

Sb(III)	reagents	1 d		recovery	7 d		recovery	20 d		recovery
µg L^{-1}		µg L^{-1}	SD	%	µg L^{-1}	SD	%	µg L^{-1}	SD	%
5	HCl 1%	5.0	0.1	100	4.6	0.3	92	4.4	0.3	88
	HNO_3 1% + L(+) tartaric acid	5.1	0.1	102	5.3	0.2	106	5.2	0.3	104
20	HCl 1%	20.6	0.3	103	20.9	0.4	105	20.9	0.6	105
	HNO_3 1% + L(+) tartaric acid	21.5	0.4	108	21.3	0.5	107	20.6	0.2	103

* recovery is calculated with respect to the nominal Sb(III) concentration of diluted samples.

These results suggest that the efficacy of the Sb(III) stabilization with HCl is related not only with the time but also with the initial concentration of Sb(III) in solution.

The working range of ASV was 1-20 µg L^{-1}, consequently, in the analyses performed with natural solutions samples often needed to be diluted. To assess the effect of dilution during the analyses, further tests were carried out with concentrated solutions (500 µg L^{-1} Sb(III)). During analyses samples were diluted with Milli-Q containing the same reagents used for the stabilization. The recovery was in the range 96-109% with respect to the expected values (table 2.5).

Table 2.5 Temporal stability of Sb(III) determined in synthetic solution with initial concentrations 500 µg L^{-1} Sb(III) and effects of dilution during analyses on aliquots stabilized with HCl 1%or HNO_3 1% + L(+) tartaric acid.

STD Sb(III) 500 µg/L		0d		recovery*	10d		recovery	20d		recovery
reagents	dilution	µg L^{-1}	SD	%	µg L^{-1}	SD	%	µg L^{-1}	SD	%
1% HCl	1/100	5.1	0.1	101	5.0	0.1	100	5.2	0.1	103
HNO_3 1% + L(+) tartaric acid	1/100	5.1	0.1	102	5.4	0.2	107	5.3	0.1	106
1% HCl	1/25	19.1	0.3	96	20.3	0.3	101	21.4	0.4	107
HNO_3 1% + L(+) tartaric acid	1/25	21.2	0.4	106	20.8	0.4	104	21.8	0.4	109

* recovery is calculated with respect to the nominal Sb(III) concentration of diluted samples.

2.3.2 Mine water

Concentrations of both Sb(V) and Sb(III) were determined only in water samples collected in the mine area, while the Sb(III) were always below the detection limit in uncontaminated waters; therefore uncontaminated waters are not considered in this study.

The composition of water collected in the mine area is calcium and sulfate dominant, pH values were

circumneutral to slightly alkaline, Eh values and dissolved oxygen indicated oxidizing conditions (table 2.6).

Table 2.6. Chemical-physical parameters and concentrations of major anions in water sampled at Su Suergiu**.**

sample	date	flow	T water	EC	pH	Eh	O_2	Ca	Mg	Na	K	HCO_3	Cl	SO_4	Sb(tot)
		$L\ s^{-1}$	° C	$mS\ cm^{-1}$		V	$mg\ L^{-1}$								$\mu g\ L^{-1}$
SU1	09-may-12	0.05	16	0.5	7.7	0.35	4.4	306	53	44	4.1	392	50	670	4600
SU2	09-may-12	0.05	22	1.8	8.4	0.42	3.8	248	49	163	9.0	338	60	816	13,000
SU1	26-may-14	0.25	19	2.2	7.5	0.40	8.0	440	45	110	3.7	420	60	920	7600
SU1	30-jun-14	0.03	22	2.4	7.8	0.45	7.0	362	63	166	7.2	484	59	1000	9990
MU8	13-may-14	1.00	19	1.1	7.9	0.46	11.0	140	15	45	2.2	268	74	232	1800

The high concentration of Sb(tot), from 1800 to 13,000 $\mu g\ L^{-1}$, is due to the interaction of the water with the slag waste materials (§ 3). Coherently with the pH and redox conditions of water, the Sb(V) prevailed but also Sb(III), probably thermodynamically unstable, occurred (table 2.7).

Table 2.7 Concentrations of Sb(V) and Sb(III) determined in water sampled at Su Suergiu within 24 hours upon the water collection (Sb(III) analyses were run on three replicates).

SU1 09-may-12	Sb(III)						Sb(V)
	$\mu g\ L^{-1}$	SD	RSD %	mean	SD	RSD %	$\mu g\ L^{-1}$
not stabilized	27	2	7.4				
1% HCl	42	3	7.1				
HNO_3 1% + L(+) tartaric acid	25	2	8.0				
				31	8	25	4570
SU1 30-jun-14	Sb(III)						Sb(V)
	$\mu g\ L^{-1}$	SD	RSD %	mean	SD	RSD %	$\mu g\ L^{-1}$
not stabilized	152	5	3.3				
1% HCl	180	16	8.9				
HNO_3 1% + L(+) tartaric acid	110	10	9.1				
mean				147	28	19	9840
SU2 09-may-12	Sb(III)						Sb(V)
	$\mu g\ L^{-1}$	SD	RSD %	mean	SD	RSD %	$\mu g\ L^{-1}$
not stabilized	160	10	8.0				
1% HCl	150	10	9.1				
HNO_3 1% + L(+) tartaric acid	120	8	6.7				
				143	17	12	12,850

Analyses were carried out within 48 hours and showed significant differences between the three aliquots considered. The relative standard deviation (standard deviation SD/mean) was <10% for Sb(III) determined in each aliquot, while the agreement among concentrations in the different aliquots ranged between 12 and 25%.

2.3.3 Standard addition tests

In sample with low Sb(III) contents, the Sb(III) values measured in stabilized aliquots agree, while Sb(III) determined in the aliquots not stabilized decreased significantly (table 2.8). For high Sb(III) concentration the highest values were obtained in the aliquot stabilized with hydrochloric acid, the

agreement among the different aliquots fall in the same range observed in the test with synetic solutions.

Table 2.8 Concentrations of Sb(III) determined by ASV in water sampled at Su Suergiu within 24 hours upon the water collection. Concentrations of standard addition were 40, 100 and 200 µg L^{-1} Sb(III) for sample SU1 26-may-14 and 10, 20 and 40 L^{-1} Sb(III) for sample MU8 13-may-14.

						standard addition test		
sample		aliquot	Sb(III)			Sb(III)		
			µg L^{-1}	SD	RSD (%)	µg L^{-1}	SD	RSD (%)
MU8	13-may-14	not stabilized	7.5	0.4	5.3	10.5	0.5	4.8
*[Sb(tot) = 1800 µg L^{-1}]		1% HCl, suprapure	27	3.7	13.7	19	1.5	7.9
		0.2% Ac.Tart.+1% HNO_3	26	0.9	3.5	11	0.5	4.5
		mean	20	8.8	44	13.5	3.9	29
SU1	26-may-14	non stabilized	119	8.7	7.3	155	10	6.5
[Sb(tot) = 7600 µg L^{-1}]		1% HCl, suprapure	144	5.5	3.8	180	10	5.6
		0.2% Ac.Tart.+1% HNO_3	80	4.9	6.1	95	5.9	6.2
		mean	114	26	23	135	30	22

*concentrations of Sb(tot) were determined by both ICP-OES and ICP-MS.

In the synthetic solution reproducibility of Sb(tot) determined by ASV was good (<6%) in all aliquots, while it was >10% for Sb(III) in solutions kept in suprapure HCl and in Milli-Q (table 2.9). The worse recovery occurs in the Milli-Q solution so stabilization appears necessary to preserve Sb(III) into solution. Concentration of Sb(III) was high (0.305 ± 0.005 mg L^{-1}) with respect to the expected values in solution prepared using high-purity $K[Sb(OH)_6]$. A further proof, using ultrapure HCl for the stabilization of samples and in the ASV cell during the analysis, was performed to evaluate if the acid provides antimony in solution. Results showed very low difference so, a possible explanation, could be that, at high concentrations of Sb(V), the partial reduction of Sb(V) to Sb(III) might be facilitated by the N_2 flux, that is under reducing condition, and the acidity in the ASV analyses (Séby et al., 2012).

Table 2.9. Concentrations of Sb(tot) and Sb(III) determined by ASV in 10 mg L^{-1} synthetic solution prepared dissolving $K[Sb(OH)_6)]$ in Milli-Q. Concentrations of standard addition were 100, 200 and 400 µg L^{-1} Sb(III)**.**

sample	aliquot	Sb(tot), ASV			Sb(III)			standard addition test Sb(III)			
		mg L^{-1}	SD	RSD (%)	mg L^{-1}	SD	RSD (%)	mg L^{-1}	SD	RSD (%)	recovery (%)
STD Sb(tot) 10 mg L^{-1}	not stabilized	10.3	0.4	4.1	0.237	0.03	10.5	0.300	0.029	9.7	79
	1% HCl, suprapure	9.8	0.5	5.5	0.285	0.04	15.1	0.310	0.022	7.1	92
	1% HCl, ultrapure	10.3	0.3	2.9	0.270	0.01	4.4				
	0.2% Ac.Tart.+1% HNO_3	9.5	0.3	3.2	0.280	0.017	6.1	0.305	0.016	5.2	92

2.4 Summary

This study was focused on the determination of a simple method for the stabilization of Sb(III) in Sb(V)-rich media, flanked to a simple Sb(III) analytical technique which does not require particular sample manipulations. For this purpose several reagents were tested with synthetic solutions and natural waters, and the Sb(III) was analyzed by ASV. The reagents tested for the stabilizations were: 1% v/v HCl, 0.1% w/v L(+) ascorbic acid and 0.2% v/w L(+) tartaric acid plus 0.1% v/v HNO_3.

Tests carried out with synthetic solution showed that the concentration of Sb(III) decreased over time, therefore, sample stabilization is needed to avoid Sb(III) oxidation. The best reproducibility and recovery were obtained with the stabilization carried out with tartaric acid plus nitric acid.

Results related to the antimony polluted water show that the Sb(III) is a minor constituent in the antimony rich water flowing at Su Suergiu, characterized by circumneutral pH values and oxidizing conditions. Among the several reagents tested, also with natural water the tartaric acid plus nitric acid appear the most suitable stabilization but further investigations are needed to confirm this hypothesis. Speciation of antimony in aqueous solutions can be obtained with the determination of Sb(tot) either by ICP-MS or ICP-OES, and Sb(III) using ASV. The Sb(V) concentration is calculated by subtracting Sb(III) from Sb(tot). Due to the instability of Sb(III), analyses should be carried out as soon as possible upon the water collection (Cidu et al., 2015).

CHAPTER 3. Antimony contamination and dispersion in water draining the Su Suergiu abandoned mine area

3.1 State of art

Antimony can be introduced to the aquatic environment through natural processes and anthropogenic sources. In the last decades the concern of antimony like pollutant of priority interest has been growing as a consequence of increasing industrial production, its connected antimony extraction and the impact of these activities on the environment. The World Health Organization (WHO, 2011) has established a guideline value of 20 μg L^{-1} Sb for drinking water, while both the European Community (Directive 98/83/EC) and Italian Legislation (DL. vo 31/2001) indicate 5 μg L^{-1} Sb. Typical concentrations of antimony in unpolluted waters are less than 1 μg L^{-1} but can increase in areas affected by anthropogenic activities, in particular very high concentrations of Sb may occur in water draining abandoned mine sites (Asaoka et al., 2012; Casiot et al., 2007; Cidu et al., 2008a, b; Filella et al., 2002a; Ritchie et al., 2013).

At present, the hydrogeochemistry of antimony is not completely understood. The most common oxidation states of this element in the environment are Sb(III) and Sb(V), and both hydrolyze easily in aqueous solutions (Filella et al., 2002b). The Sb(V) prevails in oxygenated water as $Sb(OH)_6^-$ while under reducing condition Sb(III) is more stable as aqueous $Sb(OH)_3$, but significant concentration of Sb(III) are found in oxic waters as well as oxidizing species have been determined in anoxic waters (Accornero et al., 2008; Filella et al., 2002a).

It has been recognized that the fate and impact of antimony (mobility, bioavailability then toxicity) on the environment are related to its speciation (Filella et al., 2002b; Wilson et al., 2010). Mobility of antimony in solution and its impact on the environment depend on several factors, such as antimony speciation, chemistry of solutions, pH and redox conditions. Amorphous iron and manganese oxyhydroxides present in natural waters may play a dual effect by absorbing and oxidizing the more toxic Sb(III) into Sb(V) (Belzile et al., 2001). Natural attenuation of antimony may occur also through sorption onto manganese and iron oxides (Filella et al., 2009; Wang et al., 2011) or by the precipitation of Sb-bearing solids (Mitsunobu et al., 2010, Roper et al., 2012). In other cases antimony persists in solution at long distance from the source of contamination (Ashley et al., 2003; Cidu et a., 2008a, b, Wilson and Webster-Brown, 2009). In this context, the kinetics of redox reactions and the affinity with potential ligands in forming aqueous complexes under environmental pH and oxidizing conditions play a significant role, but unfortunately there is still lack of information in this sense (Accornero et al., 2008; Filella et al., 2009; Quentel et al., 2004).

The present work is part of a larger project (PRIN 2009), that studied antimony geochemistry and the processes of its transfer toward the system water-soil-plant, aimed to better understand the processes and the factors that govern the dispersion of antimony so that more effective remedial action might reduce antimony contamination (Cidu et al., 2014).

This study has been focused on the antimony contaminated water draining the abandoned mine of Su Suergiu (SE Sardinia, Italy), an area which is considered a priority in the regional remediation plan for contaminated sites. Antimony polluted water draining the abandoned mine, impact the main river of south Sardinia, the Flumendosa River, that supplies water for domestic and agriculture uses. Previous studies carried out in the area have established that the contamination continued several kilometer downstream the confluence of the polluted water into the Flumendosa River (Cidu et al., 2008a, b).

3.2 Study area and mining history

The study area is located in the south-east of Sardinia, in the mining district of the Sarrabus-Gerrei. Geology of the area consists of low-grade metamorphic rocks belonging to allocthonous units of External Nappes zone, set in place during the Hercynian orogenesis (Carmignani et al., 1986). Schematic geological setting of the area is show in figure 3.1. From the bottom to top the outcropping succession consists of the Cambrian to Lower Ordovician siliciclastic deposits, mainly micaceous metasandstones and quartzite, followed by intermediated-acid metavolcanic rocks (Middle Ordovician), sediments of pelagic deposition system constituted by black shales, metalimestones and quartzites (Silurian - Middle Devonian), Middle Devonian - Lower Carboniferous metalimestones, and Lower Carboniferous syntectonic deposits of the Culm type. The emplacement of the ore is linked to magmatic-hydrothermal activity contemporary to the main Hercynian deformation phases. The mineralization at Su Suergiu consists of stibnite (Sb_2S_3), scheelite ($CaWO_4$), arsenopyrite (FeAsS), pyrite (FeS_2) and gold, with calcite and quartz in the gangue; it is made up of lenses arranged parallel to the foliation of highly deformed black shales (Silurian - Middle Devonian) and metalimestone (Middle Devonian - Lower Carboniferous) belonging the cataclastic belt of Villasalto Fault (Funedda et al., 2005).

At Su Suergiu mine activity was developed underground from 1858 to 1960, with exploitation peaks in the 1920-1930's. From 1882 the mining activity was flanked by metallurgical activity. In the smelter, ores were processed to obtain antimony sulfides and oxides and from the first years of 1900 the foundry began also the production of metallic antimony from the oxides. During the reduction processes the oxides were mixed with charcoal, and sodium carbonate was added in order to obtain a better fluidity (Secchi and Lorrai, 2001).

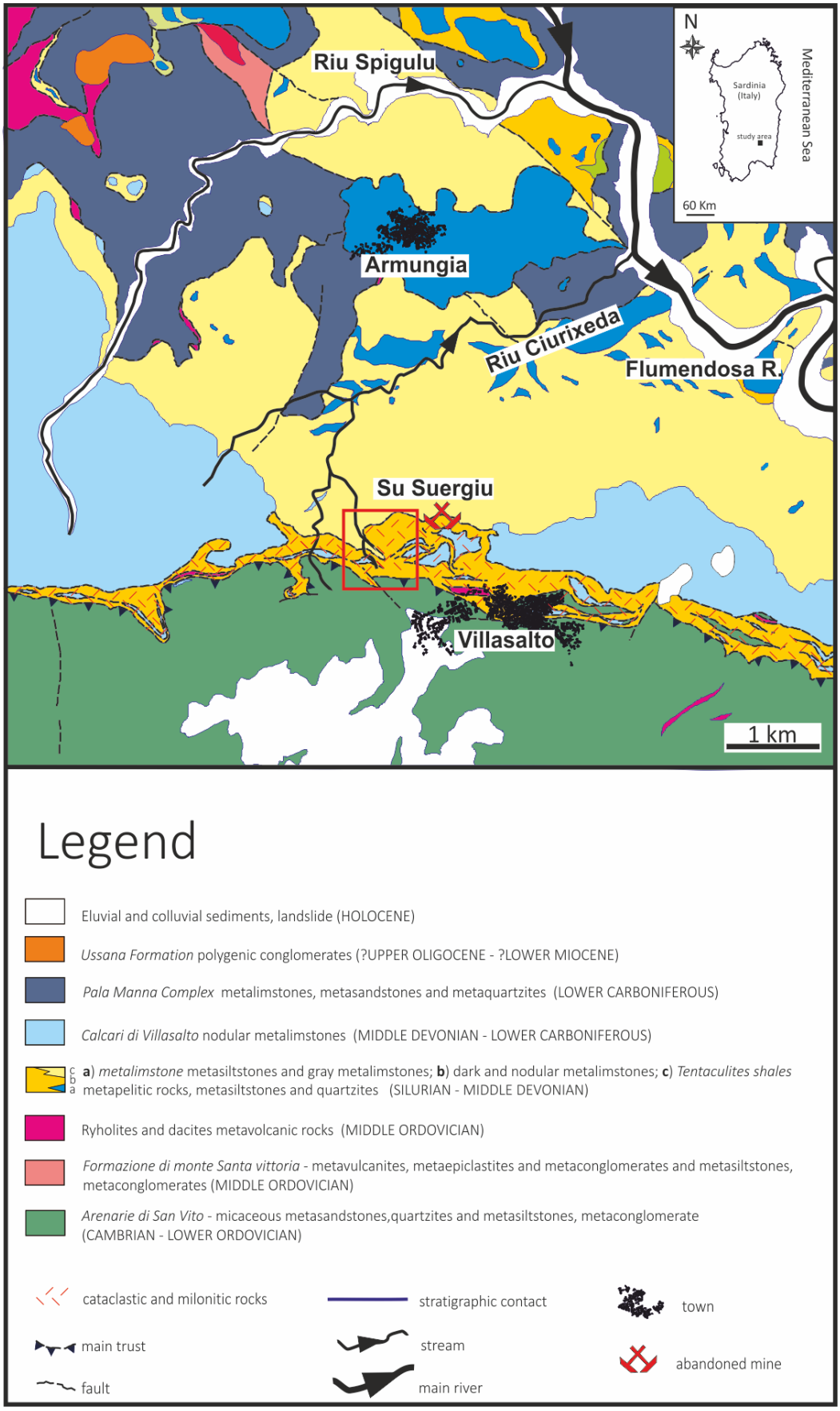

Figure 3.1 Schematic geological map of the study area (RAS, 2013, modified).

The other reagents used in the smelter processes were coke, caustic soda and fuel oil. After the end of mining at Su Suergiu, ore coming from other areas of Italy, Turkey and China was processed in the foundry.

In 1987 the metallurgical plant was finally closed and both mining residues and slag heaps were left on the surface. Landfills of mining residues are mainly constituted by fine materials, most of them are completely vegetated or nearly so and only the bodies situated near the stream beds show evidence of erosion processes. The foundry slags, consisting of residues of several metallurgical processes are dumped in two bodies (about 66,000 m^3; RAS, 2003) in front of the foundry plant (fig.3.2) and are affected by significant erosion from storm runoff.

Figure 3.2 The heaps of foundry slag in front of the foundry plant.

At present, the only environmental mitigation consists of a retaining wall built on the edge of the slag heap to divert runoff and minimize the slag heap erosion processes. However, after storm events the wall was damaged and foundry wastes were transported by runoff for a long distance downstream from the dump (fig.3.3 and 3.4).

The area under investigation comprises the Su Suergiu abandoned mine, the Riu Ciurixeda catchment and a portion of the Flumendosa River. Climate of the area is semi-humid, characterized by dry summer and rainfall variable from year to year, mostly occurring from October to April. Data collected from 1955 to 1992 at stations located in the area show mean annual precipitation of 670 mm, and mean annual temperature of 16.2 °C (RAS, 1998).

Most rocks are characterized by permeability in the range of 10^{-4} to 10^{-7} cm s^{-1} (IGEA, 2009). Metalimestones show permeability in the range of 10^{-2} to 10^{-4} cm s^{-1} (IGEA, 2009), mainly due to fractures, but their relevance is negligible due to small outcrops.

Figure 3.3 Erosion of slag waste after summer storms (date: 30.07.2014).

Figure 3.4 Foundry waste carried downstream from the dump (date: 26.05.2014).

Morphology in the catchment is characterized by steep slopes (up to 60%) covered by degraded Mediterranean *maquis*. The springs are scanty, and usually show little flow (<0.1 L s^{-1} under high flow condition). Waters flowing at Su Suergiu are mainly streams whose flow conditions are dependent on the rainfall seasonal trend and that often flown underground. The Riu Ciurixeda stream collects the untreated drainage from Su Suergiu and flows directly into the Flumendosa River, the main river in south Sardinia.

3.3 Water sampling and analyses

Several sampling surveys were carried out under different seasonal conditions, from May 2012 to July 2014, in the mine area and surroundings. Waters collected in the mine area consist of waters flowing out of adits, waters draining the mining and foundry slag, and streams. Upstream from the mine area, unpolluted water of spring, streams and the Flumendosa River before the Riu Ciurixeda confluence was sampled; water sampled downstream the mine area were collected in the Riu Ciurixeda which receives all mine drainages and the Flumendosa River after the confluence of polluted waters (fig.3.5).

Physical-chemical parameters, such as temperature, electrical conductivity (EC), redox potential (Eh) and pH were measured at the sampling site. The Eh was measured with a platinum electrode, and values were corrected against ZoBell's solution (Nordstrom, 1977). Alkalinity was measured both in the field and in the laboratory using the methyl-orange titration method with hydrochloric acid and the Gran function plot method, respectively. Alkalinity was chiefly attributed to the HCO_3^- ion, the CO_3^{-2} ion being always undetectable, and the contribution of non-carbonate species being negligible. At sampling sites, an aliquot of water was filtered through 0.45 µm pore-size filters (OlimPeak, polypropylene) and stored in HDPE (polyethylene high-density) bottle for ions analyses by ion chromatography; another aliquot was filtered into preconditioned HDPE and acidified with 1% v/v HNO_3 for ICP-OES and ICP-MS analyses. At selected sites a further aliquot was filtered and stabilized with 1% v/v HNO_3 + 0.2%, w/v L(+) tartaric acid, for Sb(III) analyses by anodic stripping voltammetry (ASV, Metrohm 797 VA Computrace) at the hanging mercury drop electrode (table 3.1).

Total antimony, Sb(tot), was determined by ICP-MS (Sb(tot) <50 µg L^{-1}) or ICP-OES (Sb(tot) >50 µg L^{-1}). During trace elements analyses with ICP-MS, Rh was used as internal standard. The reference solutions SRM1643e supplied by the US National Institute of Standard & Technology (Gaithersburg, Maryland), and EnviroMAT ES-L-2 and EP-H-3 supplied by SCP Science (St. Laurent, Quebec) were used during ICP-OES and ICP-MS analyses to evaluate analytical errors.

Saturation index (SI) of gypsum and calcites were determined by WATEQ4F 4.00 source code (Ball and Nordstrom, 1991 and updates), saturation index is calculated as SI = log (IAP/K_{sp}), where IAP is the ionic activity product and K_{sp} is the solubility-product constant.

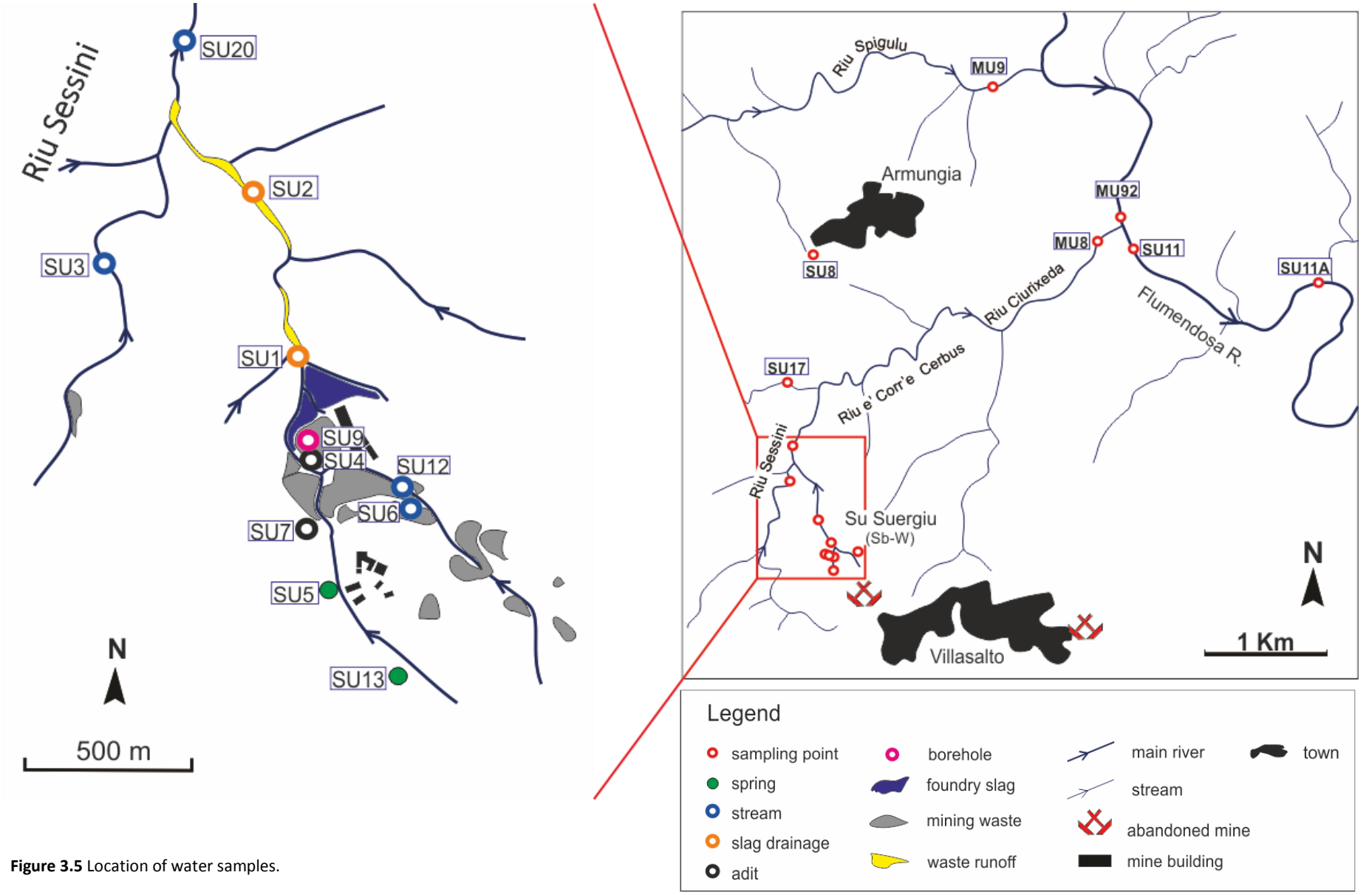

Figure 3.5 Location of water samples.

Table 3.1 Sample stabilization and analytical techniques.

Sample stabilization	Elements	Analytical method
none	Cl, F, SO_4,NO_3,Br, Ca, Mg, K, Na	*ion chromatography*, IC (Dionex ICS3000)
suprapure HNO_3 1% (v/v)	Ca, Mg, Na, K, S(tot), Si, B, Sb(tot)	*inductively-coupled plasma optical-emission spectrometry*, ICP-OES (ARL Fisons 3520)
	Li, Be, B, Al, V, Cr, Mn, Ni, Co, Cu, Zn, Ga, As, Se, Rb, Mo, Ag, Sr, Ba, Fe, Cd, Sb(tot), Te, Tl, Pb, U	*inductively-coupled plasma mass spectrometry*, ICP-MS (Perkin-ElmerSCIEX ELAN DRC-e)
suprapure HNO_3 1% (v/v) + tartaric L (+) acid 0.2% (w/v)	Sb(III)	*anodic stripping voltammetry*, ASV (Metrohom 797 VA Computrace; app. bulletin 74/3 b)

3.4 Results

The ionic balance was always less than ±6%. The reproducibility of Sb(tot) expressed as relative standard deviation, and the recovery were in the range of 2.9-9.7% and 98-105 %, respectively (table 3.2).

Table 3.2 Concentration of Sb(tot) determined in reference solutions.

Reference solution	Certified value		Measured value				recovery	Technique
	µg L^{-1}	SD	µg L^{-1}	SD	RSD %	n°	%	
SRM1643e	58.3	0.61	57.1	4.1	7.2	9	98	ICP-MS
ES-L-2/100	10	0.5	10	0.96	9.7	9	99	ICP-MS
EP-H-3/10	505	16	530	16.4	2.9	6	105	ICP-OES

Values of pH, Eh and EC of all samples collected from 2012 to 2014 are summarized in table 3.3. All samples showed Eh and pH values indicating respectively oxidizing and neutral or slightly alkaline conditions; EC values of waters collected in the mine area increased significantly with the increase of sulfate and calcium concentrations, and also sodium in slag drainage (fig.3.6). Considering the relative abundance of major ions and the concentration of antimony in solution it is possible to group the samples in: upstream waters in which are included spring, surface waters collected out of the mine area, and the samples of Flumendosa River upstream from the confluence of the Riu Ciurixeda; water collected in the mine area that grouped slag drainage, surface waters and water collected from adits and borehole; finally, the downstream water group comprises samples of Riu Ciurixeda and Flumendosa River downstream from the confluence (table 3.4).

Composition of samples collected in the mine area was Ca-(Na)-sulfate dominant, the very high concentration of sulfate, up to 1800 mg L^{-1} and median 925 mg L^{-1}, is attributable to the oxidation of sulfide minerals. Water flowing immediately downstream from the slag wastes (samples SU1 and SU2) often resulted in sodium enrichmen as a consequence of the dissolution of sodium carbonate contained in the slag heap.

Samples of Rio Ciurixeda showed Ca-sulfate composition reflecting the influence of mine drainage, whereas waters of Flumendosa River are Ca-bicarbonate(sulfate) dominant and the relative abundances of major anions did not vary significantly before and after the confluence of Rio Ciurixeda (fig.3.6).

Table 3.3 Value of pH, Eh and EC determined in water samples (complete datas are reported in appendix I).

		upstream			n = 13	mine area			n = 27	downstream			n = 13
	units	min	max	median	mean ± σ	min	max	median	mean ± σ	min	max	median	mean ± σ
pH		6.1	8.2	7.7	7.6 ± 0.6	7.0	8.5	7.8	7.9 ± 0.4	7.6	8.3	7.9	7.9 ± 0.2
Eh	V	0.38	0.51	0.45	0.45 ± 0.04	0.34	0.43	0.46	0.44 ± 0.05	0.37	0.50	0.46	0.45 ± 0.04
EC	mS/cm	0.19	0.81	0.41	0.43 ± 0.16	0.41	3.75	2.03	1.88 ± 0.91	0.41	1.20	0.78	0.79 ± 0.27

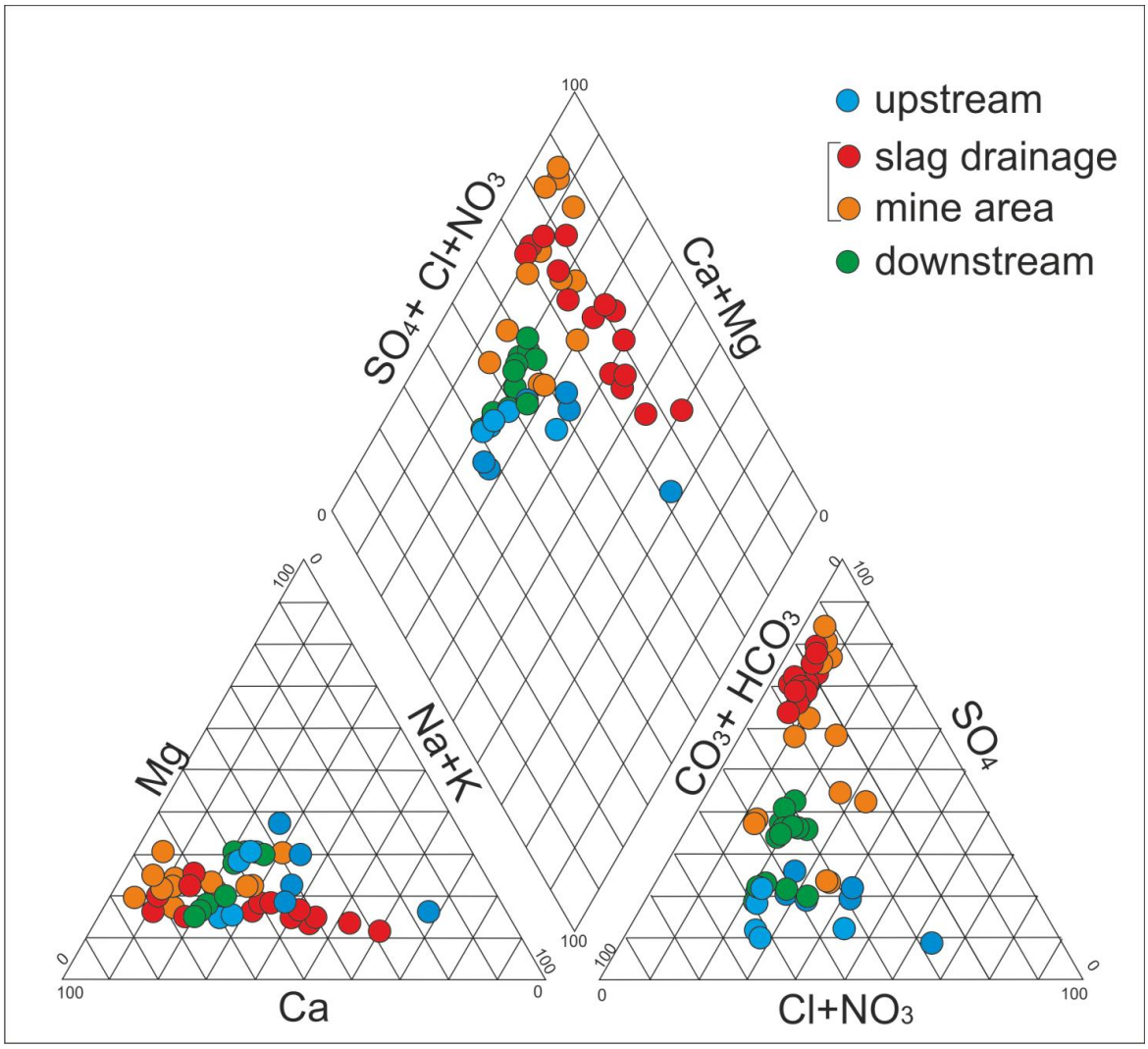

Figure 3.6 Piper diagram showing the chemistry of solution.

Table 3.4 Values of flow, temperature, pH and dissolved oxygen determined at the sampling sites, and concentrations of major anions, Sb(tot) and Sb(III) determined in water samples. Label of sample are referred to fig.3.5.

Sample	Tipe[a]	Date	T w (°C)	Flow L s^{-1}	pH	O_2 mg L^{-1}	Ca	Mg	Na	K	HCO_3	Cl	SO_4	NO_3	Sb	Sb(III)
							mg L^{-1}				mg L^{-1}				µg L^{-1}	
upstream																
SU8	sp	09.05.12	16	0.03	7.6	8.4	30	10	30	0.8	93	57	36	0.59	0.98	<dl[c]
SU15	sp	13.06.12	18	<0.1	6.1	n.a.[b]	7	4	31	1.7	34	45	8	<0.1	0.47	<dl
MU9	st	02.05.12	17	50	7.8	6.0	49	8	26	1.8	162	39	24	0.04	0.45	n.a.
MU9	st	28.02.13	8	250	8.2	10.2	24	6	22	1.5	77	42	17	5.01	0.50	n.a.
MU9	st	20.06.13	18	1	7.5	7.4	69	11	33	1.7	222	57	27	< dl	0.43	n.a.
MU92	ri	23.05.12	17	1000	8.0	7.0	66	23	33	2.2	227	53	72	0.28	3.9	<dl
MU92	ri	28.02.13	8	3000	7.8	10.2	37	15	25	1.8	128	48	40	5.14	1.9	n.a.
MU92	ri	23.07.13	26	1000	7.7	5.8	61	24	31	2.4	218	47	63	< dl	4.5	<dl
MU92	ri	09.01.14	10	4000	7.7	8.6	46	19	28	1.8	170	51	53	3.14	2.1	<dl
MU92	ri	20.06.13	24	1000	8.1	7.0	55	21	27	1.9	215	48	51	< dl	5.35	<dl
SU5	sp	09.05.12	13	<0.1	7.4	7.0	26	13	27	1.5	85	52	39	3.12	4.20	<dl
SU13	sp	13.06.12	15	<0.05	7.0	n.a.	31	19	25	1.4	115	38	49	<0.1	1.37	<dl
SU17	st	28.02.13	8	8	8.2	8.8	107	28	30	0.6	248	68	173	1.34	3.3	n.a.
mine area																
SU3	st	09.05.12	15	0.5	7.8	3.8	165	38	33	3.0	214	55	400	<0.1	330	2
SU3	st	11.12.12	8	20	8.2	n.a.	99	25	37	2.7	137	78	185	51.3	204	n.a.
SU3	st	28.02.13	8	80	8.1	12.6	41	11	26	2.4	108	49	48	7.1	48.1	n.a.
SU3	st	20.06.13	19	0.05	7.6	4.2	422	92	46	3.2	277	71	1280	< dl	315.5	n.a.
SU1	sl	02.05.12	18	0.05	7.9	8.0	310	57	48	4.1	342	52	663	<0.1	4400	n.a.
SU1	sl	09.05.12	16	0.05	7.7	4.4	306	53	44	4.1	392	50	669	0.99	4600	28
SU1	sl	30.10.12	10	0.04	7.8	8.4	350	82	383	8.8	651	58	1370	<0.1	13,000	230
SU1	sl	28.02.13	13	0.3	7.6	8.8	339	75	94	4.2	320	56	1007	< dl	6700	n.a.
SU1	sl	01.07.13	22	0.1	8.1	7.0	270	64	470	21	558	55	1340	< dl	16,400	27
SU1	sl	20.06.13	22	0.01	8.2	7.2	267	52	311	16	508	55	1200	5.6	15,000	n.a.
SU1	sl	23.07.13	20	0.07	8.0	7.8	286	65	360	14	540	52	1170	< dl	13,000	60
SU1	sl	26.05.14	19	0.25	7.5	8.0	370	51	112	4.7	415	60	925	2.00	7600	135
SU1	sl	09.01.14	14	0.4	7.1	8.8	337	47	56	2.2	351	61	801	6.05	6000	40
SU1	sl	30.06.14	22	0.03	7.8	7.0	354	63	158	6.7	484	59	1000	0.58	9990	147
SU2	sl	02.05.12	22	0.07	8.4	7.2	243	54	171	8.8	264	64	789	<0.1	12,800	55
SU2	sl	09.05.12	22	0.05	8.4	3.8	248	49	163	9.0	338	60	816	<0.1	13,000	140
SU2	sl	30.10.12	16	0.1	8.5	10.4	256	61	600	15	458	76	1800	<0.1	30,000	760
SU2	sl	28.02.13	9	0.05	8.5	12	353	84	286	11	387	63	1310	< dl	14,000	n.a.
SU2	sl	20.06.13	25	0.01	8.3	7.0	283	55	278	12	400	60	1238	2.91	22,000	n.a.
SU12	st	13.06.12	19	0.01	8.1	n.a.	540	158	52	6.0	296	54	1644	<0.1	890	1
SU20	st	11.12.12	11	5	7.6	n.a.	177	39	76	3.8	208	76	420	44.4	4020	n.a.
SU20	st	30.10.12	16	0.1	7.4	5.8	401	90	95	6.0	298	96	1280	20.9	4000	150
SU20	st	28.02.13	8	30	8.0	12	43	11	26	2.2	115	51	51	7.86	90	n.a.
SU4	ad	09.05.12	14	0.1	7.1	1.8	138	21	33	1.5	305	46	180	<0.1	490	1
SU6	st	09.05.12	13	0.05	7.8	8.0	158	32	31	3.1	212	43	309	<0.1	850	6
SU7	ad	09.05.12	12	0.01	7.8	8.4	42	19	36	2.2	98	50	120	5.85	225	3
SU9	bh	23.05.12	18	0.01	7.0	3.2	500	80	40	1.5	352	89	1200	<0.1	99	1
downstream																
MU8	st	02.05.12	17	50	8.3	8.0	124	21	44	3.9	254	60	193	<0.1	1500	n.a.
MU8	st	23.05.12	17	40	7.9	5.6	138	23	49	3.9	284	75	193	0.63	1540	2
MU8	st	28.02.13	8	50	8.0	10.2	82	18	37	3.7	186	61	133	8.76	1600	n.a.
MU8	st	20.06.13	19	0.25	7.7	5.4	160	27	58	4.1	365	99	235	< dl	1100	70
MU8	st	01.07.13	20	0.15	7.7	5.2	176	30	65	4.5	415	106	250	< dl	1060	35
MU8	st	23.07.13	22	0.2	7.6	2.2	166	29	69	5.4	380	93	204	0.54	1340	50
MU8	st	09.01.14	11	120	7.8	11	99	18	37	3.4	219	65	152	6.55	1600	5
MU8	st	13.05.14	19	1	7.9	11	137	20	46	3.3	268	74	230	0.08	1800	13
SU11 A	ri	23.05.12	18	1000	8.0	6.6	66	23	32	2.2	227	53	75	<0.1	29	<dl
SU11	ri	28.02.13	8	3000	8.0	10.6	39	16	26	1.9	129	48	43	5.52	19	n.a.
SU11	ri	20.06.13	24	200	8.1	7.0	57	22	27	1.9	223	48	56	0.21	18	n.a.
SU11	ri	23.07.13	27	200	7.8	5.8	63	24	32	2.5	218	48	69	0.31	22	<dl
SU11	ri	09.01.14	11	4000	7.7	8.8	47	20	28	1.9	171	51	58	3.1	51	<dl

[a] sp = spring; st = stream; ri = river; sl = slag drainage; ad = adit; bh = borehole.
[b] n.a = not analized
[c] dl = detection limit

The median concentrations of antimony in uncontaminated Sardinian surface and ground waters were estimated at 0.3 µg L^{-1} (Cidu and Frau, 2009) and 0.5 µg L^{-1} Sb (Biddau, 2012) respectively.

The median concentration of Sb(tot) determined in waters upstream from the mine area was below the limits established for drinking water, but relatively high (1.9 µg L^{-1}) suggesting that the concentration of antimony in unpolluted water reflects high values of local background due to the geological setting of the Sarrabus-Gerrei mining district.

Waters collected in the mine area were characterized by high antimony concentrations, but it is possible to note certain variability among them (fig.3.7).

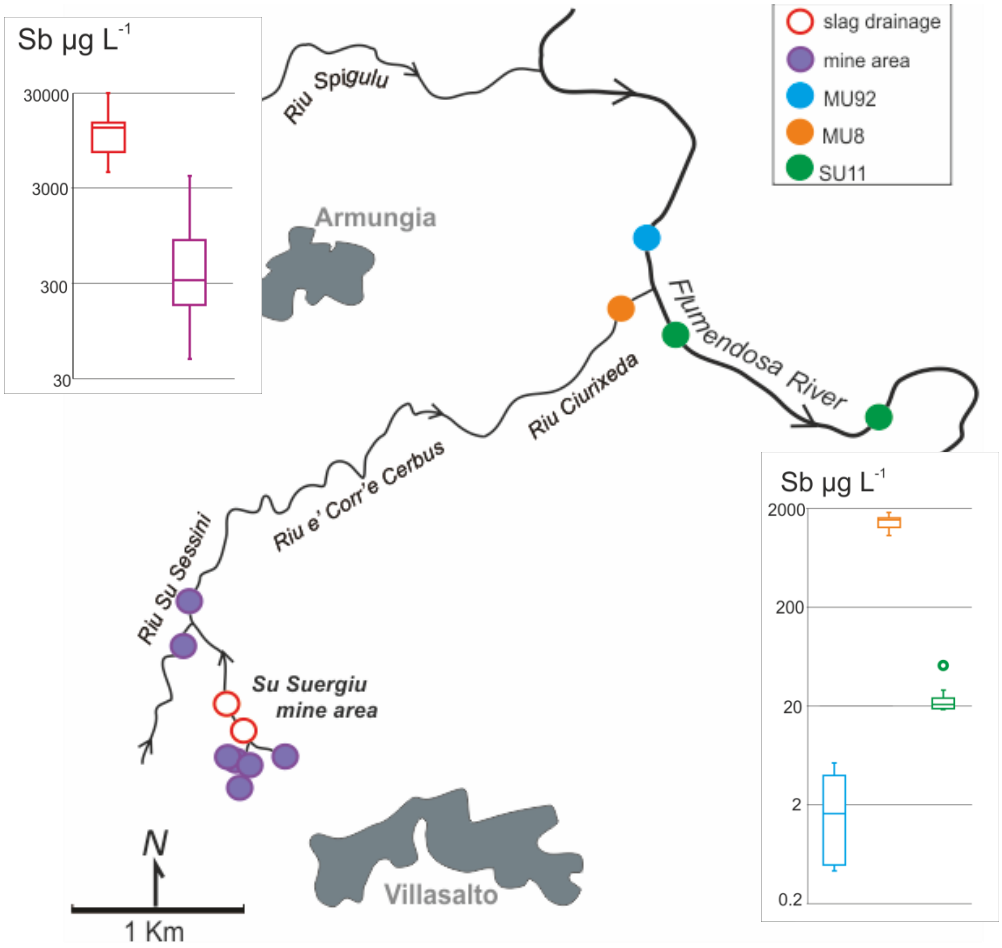

Figure 3.7 Box plot of Sb(tot) concentrations in the water sampled in the mine area, in the Riu Cirixeda and in Flumensosa River before and after the confluence of polluted water.

The slag drainage (samples SU1 and SU2), showed the highest concentrations, up to 30,000 µg L^{-1} Sb(tot) (median value 13,000 µg L^{-1} Sb(tot)). Concentration of total antimony ranged between 48 – 4020 µg L^{-1} (median: 323 µg L^{-1}) in the other samples of the mine area. The adit drainages contain relatively low antimony concentrations, whereas the content of antimony in streams is conditioned by the flow

conditions. The Riu Ciurixeda catchment collects water from the mine area and flows into the Flumendosa River with 10^3 µg L^{-1} Sb(tot) (median: 1520 µg L^{-1}). The impact of Riu Ciurixeda on the Flumendosa River is clearly shown in fig.3.7. Despite the effect of dilution, the water flowing downstream the confluence showed a significantly increase of antimony concentration, up to 51 µg L^{-1} (median Sb(tot) = 22 µg L^{-1}) under extremely high flow condition, and exceeded the drinking water limit established by the WHO (20 µg L^{-1}) and EU (5 µg L^{-1}).

The highest concentrations of Sb(III) were determined in the slag drainage where content of total antimony is maximum, and Sb(III) reached the 6% of Sb(tot); when Sb(III) was analyzed in water of Flumendosa River it was always under the detection limits (table 3.4). Speciation modeled by Visual MINTEQ showed that Sb(V) and Sb(III), respectively occur as $Sb(OH)_6^-$ (100%) and $Sb(OH)_3$ (99.9%) aqueous species.

3.5 Discussion

The oxidation reaction of stibnite, pyrite and arsenopyrite decreases the pH values, consequently, acid pH should be expected in water flowing at Su Suergiu, especially in the slag drainage. However these waters showed neural or slightly alkaline conditions from the buffer effect by carbonate minerals. In particular, the strong enrichment of sodium in the slag drainage (fig.3.8) indicates the dissolution of sodium carbonate that has been used in the ore processing.

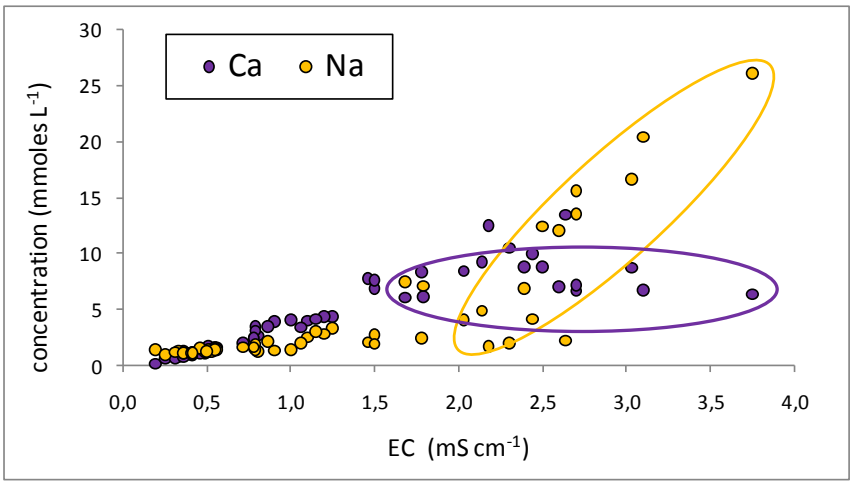

Figure 3.8 Concentrations of Ca and Na vs EC; the circles indicate the slag drainage.

High availability of dissolved bicarbonate promotes the precipitation of calcite (fig.3.9) which reaches saturation more easily than gypsum, so the calcium in solution is limited by calcite solubility equilibrium. Gypsum saturation was never reached but it is possible that at extremely low flow condition gypsum also precipitates, especially in water draining the mine area.

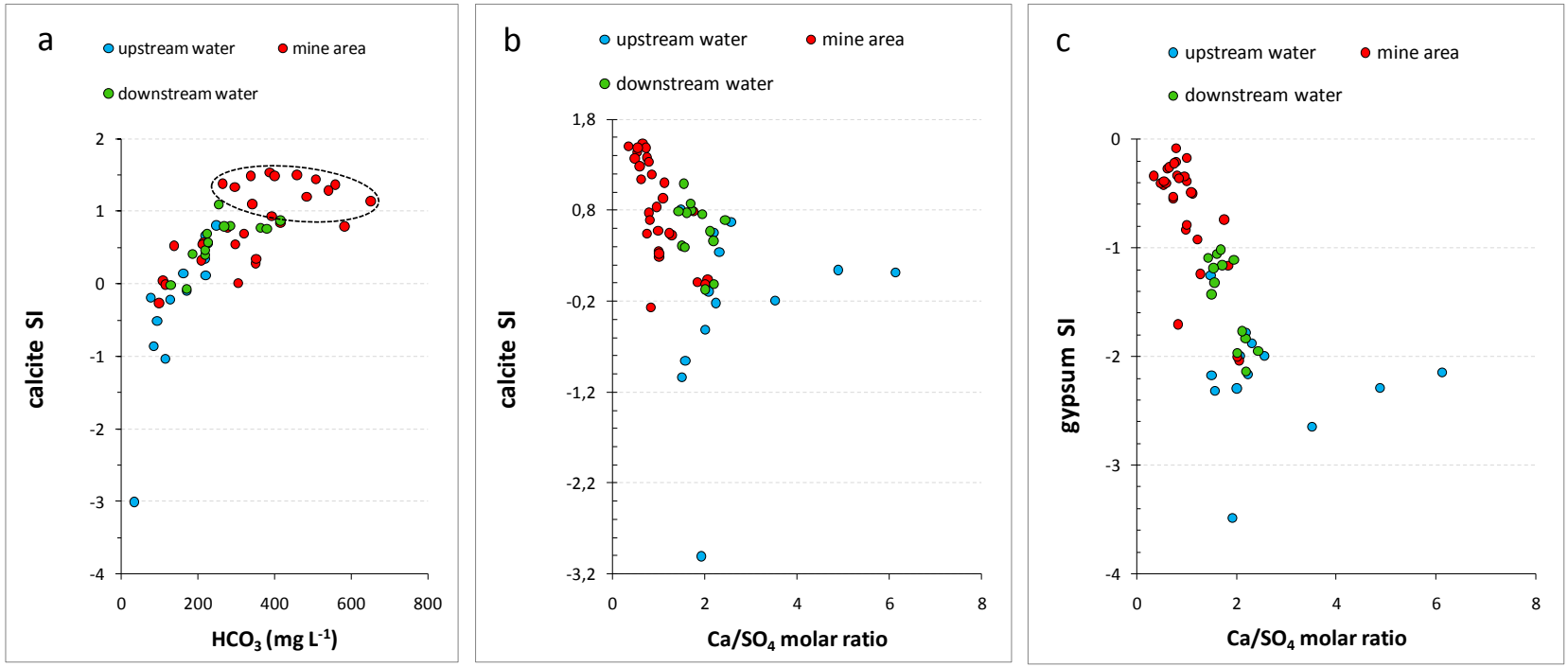

Figure 3.9 (**a**) Plot of calcite Saturation Index (SI) vs HCO_3 concentration, the dashed line indicates the slag drainage; (**b**) plot of calcite Saturation Index (SI) vs Ca/SO_4 molar ratio; (**c**) plot of gypsum Saturation Index (SI) vs Ca/SO_4 molar ratio

Data collected from 2012 to 2014 agree with previous studies (Cidu et al. 2008b): the main source of antimony contamination of the water system at Su Suergiu is represented by the interaction between water and materials hosted in the slag heaps (fig.3.10), while water collected out of adits or in the streams that interact with the other mining residues showed relatively low antimony concentrations. It is noteworthy that waste materials eroded from the slag heaps are transported by the surface runoff and widely dispersed through the area, until the confluence of Riu Ciurixeda with the Flumendosa River. It is expected that, especially under high flow conditions when the stream waters flow mainly on the surface, the interaction between water and foundry slag continues also downstream the mine area and contributes to increase the antimony concentration in the Riu Ciurixeda. It could explain the relatively low variability of antimony concentration determined in the Riu Ciurixeda samples (MU8) as compared to the high variability of flow conditions. For example, considering the MU8 samples with the highest (120 L s^{-1}) and the lowest (0.2 L s^{-1}) flow values (table 3.4), respectively collected in 09.01.14 and 23.07.13, the Sb(tot) vary slightly, from 1340 to 1600 µg L^{-1}.

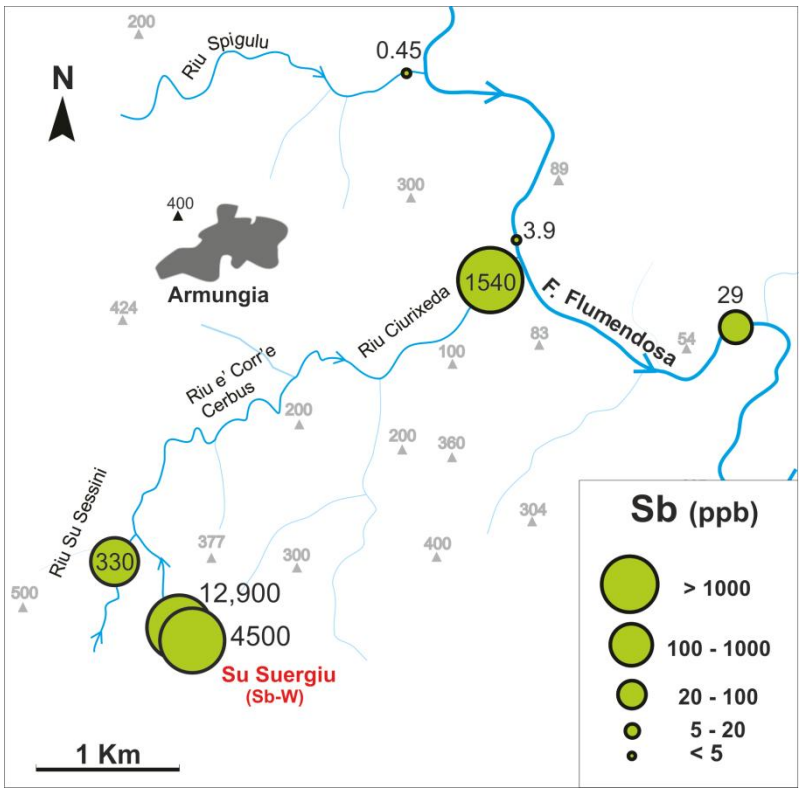

Figure 3.10 Concentration of Sb(tot) determined in water sampled on May 2012.

This result could be explained as follows: under low-flow condition, even at low inputs of water from the mine area, the high Sb(tot) content might be due to the concentration subsequent to the evaporation, while under high flow condition the effect of dilution might be partly compensated by the interaction between water and waste materials dispersed downstream the mine area.

Total dissolved antimony increased with increasing SO_4^{-2} concentrations (fig.3.11). Antimony may come in solution through the oxidative dissolution of stibnite that could be represented by the reaction [1]:

$$Sb_2S_3 + 7O_2 + 8H_2O \longleftrightarrow 2Sb(OH)_5 + 3SO_4^{2-} + 6H^+ \qquad [1]$$

and $Sb(OH)_5$ become stable in solution as anionic complex as indicated by the reaction [2](Leveret et al., 2012 and reference therein):

$$Sb(OH)_5 + H_2O \longleftrightarrow Sb(OH)_6^- + H^+ \qquad \lg K(298.15\ K) = -2.848 \qquad [2]$$

The Sb/SO_4^{-2} molar ratio from reaction [1] is 0.667 while waters collected in the mine area ranged between ~0.015-0.0001. This difference could mean that stibnite is not the principal source of sulfate, that it may also be derived from dissolution of other sulfide minerals, such as pyrite and arsenopyrite. Alternatively, antimony might be released also by dissolution of other Sb-bearing solid phases, like Sb-oxides such as valentinite, Sb_2O_3, and tripuhyite, a ferric antimonite, contained in the residues of the metallurgical wastes. A third alternative is that after stibnite oxidizes, the antimony reprecipitates as a secondary mineral such as tripuhyite while the sulfate is still soluble and mobile. If this last alternative is the main reason for Sb/SO_4 ratios, being so different from that of stibnite, then the greatest attenuation of Sb is occurring at the source.

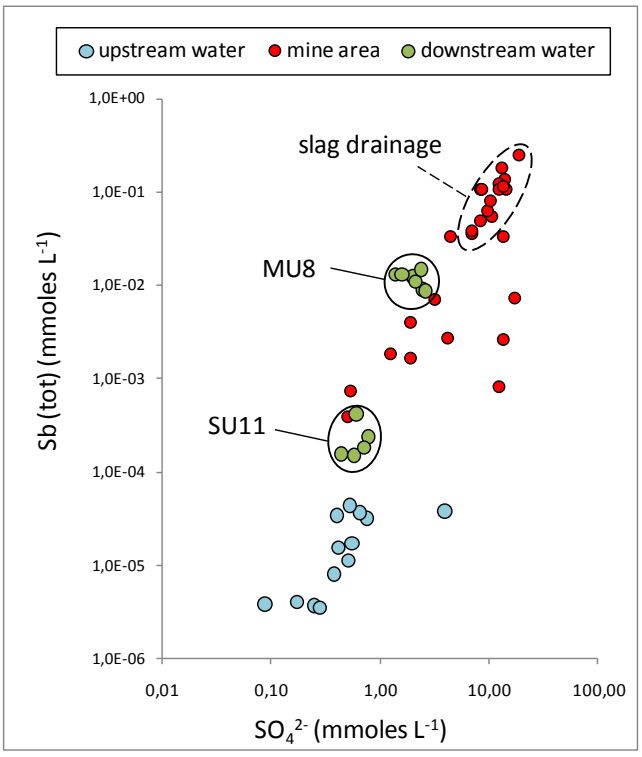

Figure 3.11 Concentration of Sb(tot) vs SO_4^{2-}.

To indentify possible attenuation processes, such as precipitation of Sb-bearing solid phases or adsorption on particulate phases, the species calculation was performed on the slag drainage sample (SU2 30-oct-12) that showed the highest contents of Sb(tot), Sb(III), SO_4^{-2}, and Na (Cidu et al., 2014). The results indicate undersaturation with respect to several antimony solid phases. Being Fe concentration under the detection limit (< 20 $\mu g\ L^{-1}$), it is not possible to determine the saturation of tripuhyte, that can precipitate even at very low Fe concentration (Cidu et al., 2014). The Sb(V) attenuation through the tripuhyte precipitation (especially near the source of contamination) it is not excluded so further studies are needed to constrain this hypothesis. Considering the results of the species calculation on the slag drainage sample (SU2 30-oct-12), it is reasonable to suppose undersaturation conditions also in the other samples.

At the state of current knowledge, dilution appears to be the main way for the natural decrease of antimony concentrations. The Sb/SO_4^{-2} molar ratios of water sampled in the Flumendosa River downstream the confluence of Riu Ciurixeda falls within the same range of samples collected in the mine area. With the cautions due to the uncertainties derived from the estimate of the flow, and considering only samples collected under high flow conditions, the dilution effect evaluated through the molar ratios of Sb/Cl^- and Sb/Na between the Riu Ciurixeda (MU8) and the mixing (SU11) waters, suggests a conservative behavior for antimony (table 3.5).

Table 3.5 Dilution factor between the Riu Ciurixeda (MU8) and the Flumendosa River downstream from the confluence (only high-flow conditions are represented in that often under-low flow conditions the Riu Ciurixeda flows underground).

Date	MU8	SU11	dilution	MU8/SU11	MU8/SU11
	flow ($L\ s^{-1}$)		factor	$Sb/Cl\ 10^{-3}$	$Sb/Na\ 10^{-3}$
23.05.12	40	1000	25	38	35
28.02.13	50	3000	60	66	59
09.01.14	120	4000	33	25	24

Comparing the load of conservative elements and Sb in Flumendosa River before and after the Riu Ciurixeda confluence (table 3.6), the ratios between the sum of loads of Riu Ciurixeda plus Flumendosa River before the confluence (MU92+MU8), and the Flumendosa River after the confluence (SU11), a conservative behavior of Sb as well chlorine, sulfate and sodium, is observed suggesting that downstream the mine area the main abatement of Sb concentration in solution is due to dilution.

The Sb(III) has higher affinity with particulate phase than Sb(V) (Wu et al., 2011, Leuz et. al, 2006, Thanabalasingam and Pickering, 1990), consequently the dominance of Sb(V) due to the pH and oxidizing conditions of water under study, can explain the conservative behavior of antimony and the dispersion for a long distance downstream from the source of contamination. Also, the high bicarbonate concentrations would be highly competitive for sorption sites and tend to prevent

antimony from easily sorbing onto sediment surfaces.

Table 3.6 Comparison of load of Sb, Cl- ,SO_4^{2-} and Na in Flumendosa River before and after the Riu Ciurixeda confluence.

samples **09.01.14**	flow	Sb	Cl^-	SO_4^{2-}	Na
	L/s	μg s^{-1}	mg s^{-1}	mg s^{-1}	mg s^{-1}
MU92	4000	8400	204000	212000	112000
MU8	120	192000	7800	18240	4440
MU92+MU8	4120	200400	211800	230240	116440
SU11	4000	204000	204000	232000	112000
(MU92+MU8)/SU11	1.03	0.98	1.04	0.99	1.04

It is necessary to underline that the geochemistry of water flowing at Su Suergiu, as well as the antimony contamination and the subsequent impact on the Flumendosa River, do not show significant variations since the first survey carried out in the area in the 2005 (table 3.7), and the recent actions aimed to retain the runoff of water appear insufficient to mitigate the impact of the contaminated water flowing from Su Suergiu.

Table 3.7 Load of Sb determined in the Riu Ciurixeda waters under high flow conditions.

sample	date	Flow	Sb	load
		L s^{-1}	μg L^{-1}	Kg day^{-1}
MU8	08.04.05	400	800	27.6
MU8	02.05.12	50	1500	6.5
MU8	23.05.12	40	1540	5.3
MU8	28.02.13	50	1600	6.9
MU8	09.01.14	120	1600	16.6

3.6 Summary

As a consequence of past mining activities, antimony dissolved reaches extremely high concentrations in water draining Su Suergiu mine, and the water contamination is extended several kilometers downstream the mine area.

Results of recent study, in agreement with previous surveys, observed that the antimony contamination of water system is mainly due to the interaction of water with the foundry slag, while waters flowing out of adits appear a minor source of contamination. Highest antimony concentrations were detected in the water flowing out of the foundry slag dump; the slightly alkaline pH and oxidizing condition of slag drainages, favor the prevalence of Sb(V), less toxic but more mobile, than the Sb(III) form.

There is no evidence of natural attenuation processes like precipitation of Sb-bearing phases or sorption on particulate phase, but it is not possible exclude them, especially near the source of

contamination, while downstream the mine area the main natural abatement of antimony concentration in solution can be represented by the dilution process.

The Riu Ciurixeda collects all mine drainages, and about 3 kilometers down the mine area flows into the Flumendosa River, the most important water body of south Sardinia that provides water for both agricultural and domestics uses.

Antimony concentration in water downstream the Su Suergiu decreases with the distance, however, despite the dilution effect due to the increase of the flow, the Riu Ciurixeda water has substantial antimony contamination. This result is the consequence of the strong contamination of the water draining Su Suergiu, the conservative behavior of antimony in solution and the interaction, downstream the mine area, of surface water with the slag waste widely dispersed till the confluence of Riu Ciurixeda into the Flumendosa River. After the confluence of Riu Ciurixeda into the Flumendosa River the antimony concentration decreases significantly due to the further dilution by uncontaminated tributaries, however, dissolved antimony exceeds the drinking water limit of both WHO (20 μg L^{-1}) and EC (5 μg L^{-1}), especially under high-flow condition (up to 51 μg L^{-1}).

On the basis of these results, appropriate actions aimed to mitigate the antimony contamination in the water system, should be addressed directly on the primary source of contamination at Su Suergiu, the slag heaps, in order to limit the interaction between the water and the slag waste, and to stop the dispersion of the slag waste downstream the mine area. Eventually, actions addressed on the mitigation of antimony directly through the treatment of the contaminated waters, should be carried out by means of sorbents having high affinity for Sb(V) and able to remove anions under slightly alkaline pH and oxidizing conditions.

CHAPTER 4. Study of Sb(V) removal from aqueous solution by layered double hydroxides (LDH)

4.1 State of art

With the growing concern of antimony as pollutant of priority interest, several studies were carried out with a large suite of sorbents in order to better understand the antimony sorption mechanisms and find solutions for the purification of antimony contaminated waters.

The affinity of antimony for the sorbents depends on its aqueous speciation, the pH and redox conditions of solutions, as well as the physical-chemical characteristics of the solid surfaces. In general it was observed that the antimony sorption capacity of manganese oxides and iron oxy-hydroxides increases as the pH decreases (Ambe, 1987; Leuz et al., 2006; Thanalabasingam and Pickering, 1990). Guo et al. (2014) reported that adsorption of Sb(V) onto the iron oxides was favored at acidic conditions, while the Sb(III) adsorption is constant in a broad range of pH. Rakshit et al. (2011) found that gibbsite is able to sorb Sb(V), but the increment of pH from 5 to 7 can decrease significantly (40%) the Sb(V) retention capacity in gibbsite-dominated soil. Also activate alumina (Xu et al., 2001) show high Sb(V) sorption capacity at low pH values. A recent study was performed with chitosan-nano-titania composite sorbents (TA-chitosan); these compounds were able to sorb both Sb(V) and Sb(III) but showed the highest sorption capacity under reducing conditions, where Sb(III) is the prevalent form (Nishad et. al., 2014).

All sorbents cited above showed more affinity for Sb(III) than Sb(V) and maximum sorption capacity at low pH, while as the pH increases the removal capacity decreases. The minerals belonging to the class of layered double hydroxides could represent an alternative for Sb(V) removal from aqueous solution under neutral or slightly alkaline conditions. Layered double hydroxides (LDH), also known as anionic clays or hydrotalcite-like compounds, are a class of natural and synthetic layered materials, described by the general formula:

$$[M^{2+}_{(1-x)}M^{3+}_{x}(OH)_2]^{x+}(A^{n-})_{x/n}\cdot mH_2O$$

where M^{2+} are divalent cations (Mg^{2+}, Zn^{2+}, Ca^{2+}, Fe^{2+}, etc.), M^{3+} are trivalent cations (Al^{3+}, Fe^{3+}, Cr^{3+}, etc.), A^{n-} indicates anionic species with the valence n (CO_3^{2-}, SO_4^{2-}, Cl^-, NO_3^-, etc.), and the value x indicates the molar ratio $M^{3+}/(M^{2+}+M^{3+})$. LDH exist naturally in the environment and the synthetic terms can be produced, in a wide range of compositions, through simply and relatively low expensive processes. Due to their high specific surface and anion exchange capacity these minerals can be used in a wide range of industrial sectors such as catalysis, polymerization, pharmaceutical industry (as drug

carriers), etc. (Goh et al., 2008). From the environmental point of view, LDH show the advantage that can be used at pH conditions at which some pollutants are most commonly found in the environment. Several studies showed that calcined and uncalcined LDH have a potential use as adsorbents for several toxic elements that are stable in aqueous solutions at circumneutral pH as oxyanions, such as arsenate, arsenite, selenate, selenite, chromate, vanadate etc. (Carriazo et al., 2007; Rojas Delgado et al., 2008; Goh et al., 2008 and reference therein). At oxidizing conditions of natural waters, the Sb(V) prevails on the Sb(III), and is stable in solution in a wide range of pH as $Sb(OH)_6^-$ (Filella et al., 2002a). At the present time few studies have been carried out on the LDH antimony removal capacity from solutions (Mitsunobu et al., 2009; Kameda et al., 2011).

This work was aimed to find suitable solutions for the remediation of antimony at pH and redox conditions usually occurring in natural waters. For this purpose, the $Sb(OH)_6^-$ removal capacity of LDH with several compositions was investigated. The LDH were tested through sorption experiments performed with synthetic solutions containing $Sb(OH)_6^-$. The removal processes were also studied by ATR-IR and finally, the sorbents that showed the most promising results were tested with the antimony polluted water collected in the Su Suergiu mine area (§ 3).

4.1.1 Structure and properties of LDH

The LDH are characterized by a layered structure that consists of positive hydroxide layers $[M^{2+}_{(1-x)}M^{3+}_x(OH)_2]^{x+}$ stacked along the *c* axis, with anions and water molecules in the interlayers $[(A^{n-})_{x/n}\cdot mH_2O]^{x-}$. The hydroxide layers have a structure similar to that of brucite $[Mg(OH)_2]$ and are composed by octahedral units of divalent cations (M^{2+}) coordinate by sixfold OH^-, that share the edges in order to form infinite sheets (Goh et al., 2008). The brucite-like sheets result positively charged as a consequence of the isomorphous substitution of divalent cations to trivalent cations. For pure phases (i.e. without the precipitation of secondary phases) the molar ratio $x = M^{+3}/(M^{2+}+M^{3+})$ is comprised in the range $0.20 \leq x \leq 0.34$ (Cavani et al., 1991; Vaccari 1998). The excess of positive charges is compensated by anionic species intercalated in the interlayer region, which can contain also a variable quantity of water molecules (fig.4.1). The interactions in the interlayer region consist of: Coulombic forces between the positively charged sheets and the anions in the interlayer, hydrogen bonding between the hydroxyl groups of the positive sheets and the interlayer anions, and hydrogen bonding between the hydroxyl groups and the water molecules; in addition the water molecules are connected through extensive hydrogen bonding to the hydroxyl groups of the metal sheets and the interlayer anions (Palmer et al., 2010).

Both natural and synthetic LDH present several polytypes mainly belonging to the dimetric crystallographic group. The basal spacing *c'* indicates the thickness of the brucite-like sheet and the

interlayer (fig.4.1), it can be calculated through the XRD basal reflection (003) as $c' = 3d_{(003)}$. The thickness of the interlayer region depends on the dimension of the anionic species, on their orientation and on the water content. The lattice parameter a corresponds to the distance between two OH^- neighbors in the same side of the brucite-like sheet or between two nearest metal cations. The value of a is obtained directly by the XRD reflection (110) as $a = 2d_{(110)}$ (Cavani et al., 1991; Mills et al., 2012), it depends on the type of cations constituent the sheet, on their ionic radii and the M^{2+}/M^{3+} molar ratio.

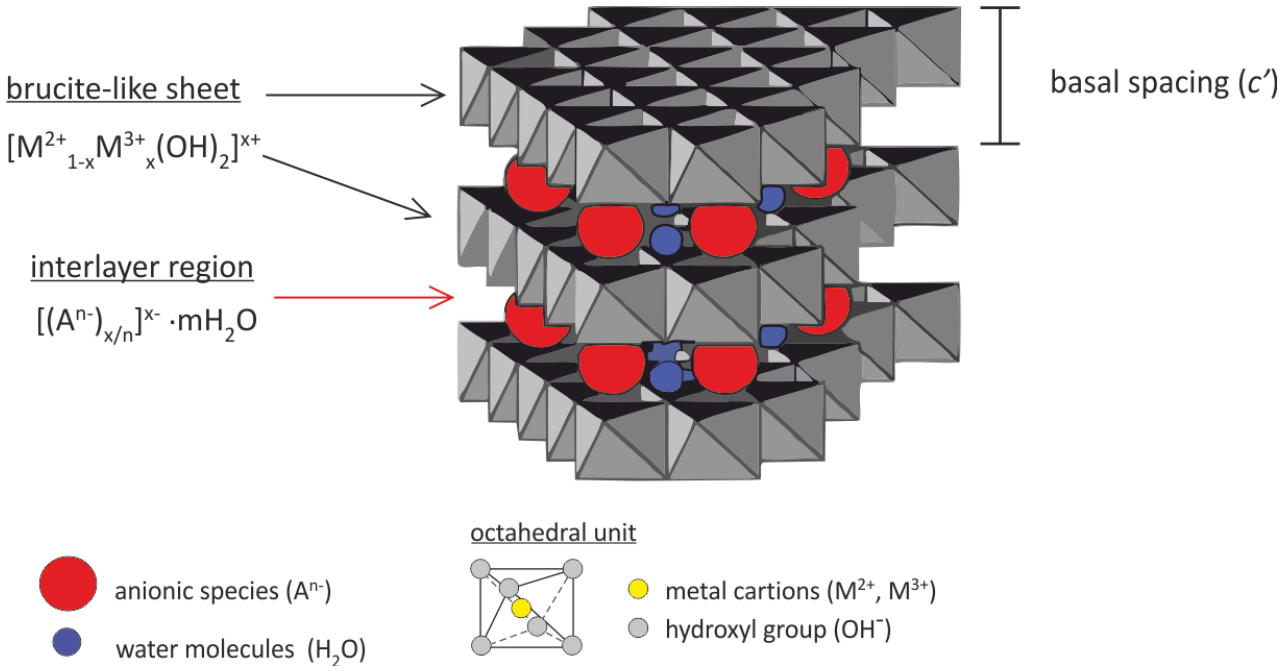

Figure 4.1 Structure of LDH (Goh et al., 2008, modified).

The layered structure confers to LDH high specific surface, adsorption capacity on the external surface and anions exchange capacity in the interlayer.

The anion exchange capacity depends on the charge of the brucite-like sheets (i.e. M^{2+}/M^{3+} molar ratio) and on the specific charge (i.e. negative charge/ionic radius) of the anionic species in the interlayer. When the M^{2+}/M^{3+} ratio is low, the positive charge of the brucite-like sheets is high and the amount of anions required to neutralize the structure increases. In this case the thickness of the interlayer depends on the strong interactions between the positive sheets and the anions in the interlayer, and on the repulsion between two nearest positive sheets. When the M^{2+}/M^{3+} ratio is high the interactions between the interlayer anions and the positive sheets are labile and the anions in the interlayer can be more easily exchanged with anions in solution, however the low positive charge can decrease the

sorption capacity. A fundamental factor is the affinity between the anionic species and the brucite-like sheets. In general LDH have high affinity with anionic species with high charge density, such as carbonates that are preferentially intercalated in LDH and can avoid a further exchange. Usually the selectivity for the interlayer anions follows the order: CO_3^{2-} > HPO_4^{2-} > $HAsO_4^{2-}$ > CrO_4^{2-} > OH^- > F^- > Cl^- > NO_3^- (Braterman et al., 2004).

The anion exchange occurs spontaneously when the anionic species contained in the interlayer has less affinity with the brucite-like sheets with respect to the anions dissolved in solution; this process is particularly useful to remove toxic elements forming anionic complexes in solution ($HAsO_4^{2-}$, AsO_4^{3-}, CrO_4^{2-}, SeO_4^{2-}, etc.). The reconstruction process (memory effect) is another very effective method that can be used to uptake the anions from solution (fig.4.2), in fact the mixed metal oxides derived from LDH calcination are able, when placed in contact with an aqueous solution, to reconstruct the layered structure by rehydration and intercalation of anionic species sorbed from solution (Palmer et al., 2009).

These properties, together with the high sorption capacity at neutral or slightly alkaline conditions, make the LDH particularly suitable to purification of surface waters polluted by toxic anions.

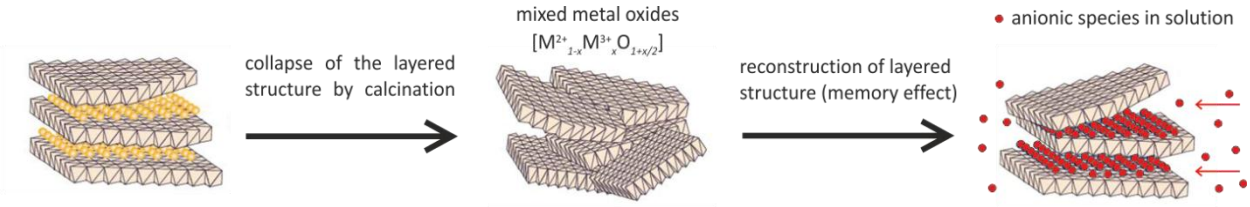

Figure 4.2 Rehydration process of mixed metal oxides derived from calcination of LDH (Li, 2005, modified).

4.2 LDH: synthesis and characterization

The Sb(V) under pH and redox conditions usually found in the environment is stable in solution as $Sb(OH)_6^-$, an anionic specie with high ionic radius and low charge, therefore with low specific charge. Despite the low specific charge of $Sb(OH)_6^-$, previous studies showed the potential of LDH for $Sb(OH)_6^-$ removal from solution and encourage further investigations; in this work the $Sb(OH)_6^-$ sorption capacity of both nitrate and calcined LDH were tested. Mitsunobu et al. (2009) reported that the LDH named Green Rust ($[Fe^{2+}_4Fe^{3+}_2(OH)_2]^{2+}[SO_4 \cdot mH_2O]^{2-}$) are able to incorporate the $Sb(OH)_6^-$ present in solution by means of the formation of inner-sphere complex on the edge sites and the formation of outer-sphere complex in the interlayer surface. Kameda et al. (2011) reported that the mixed oxides derived from the calcination of hydrotalcite-like compounds ($Mg_6Al_2(OH)_{16}CO_3 \cdot 4H_2O$) removed efficiently the $Sb(OH)_6^-$ by means of the formation of a secondary phase (brandholzite).

Nitrate LDH (LDH-NO_3) were used in order to verify the effectiveness of both anion exchange and adsorption processes for the $Sb(OH)_6^-$ removal. For this purpose LDH-NO_3 with MgAl and MgFe cationic

compositions, and different M^{2+}/M^{3+} molar ratio, were synthesized. The MgAl-NO_3 LDH easily release the NO_3^- contained in the interlayer and are able to remove anions from solution through both anion exchange and adsorption processes (Kentjono et al., 2012; Nedim et al., 2010). The MgFe-NO_3 LDH are less effective than MgAl-NO_3 LDH because remove anions from solution mainly by adsorption (Ferreira et al., 2006; Manohara et al., 2011). In this study the MgFe-NO_3 LDH were adopted taking into account the high affinity between $Sb(OH)_6^-$ and the iron hydroxides.

To produce the calcined LDH, carbonate phases like hydrotalcite ($Mg_6Al_2(OH)_{16}CO_3{\cdot}4H_2O$) and zaccagnaite ($Zn_4Al_2(OH)_{12}CO_3{\cdot}3H_2O$) were synthesized. The cationic composition of the hydrotalcite-like compounds were modified through the partial substitution of Al with Fe, while the zaccagnaite-like compounds where synthesized varying the M^{2+}/M^{3+} molar ratio. The mixed oxides derived from the calcination of the zaccagnaite-like compounds were used with the aim of reconstructing the structure of a compound like zincalstibite ($Zn_2Al(OH)_6[Sb(OH)_6]$), a LDH belonging to the cualstibite group (Mills et al., 2012) and containing the $Sb(OH)_6^-$ in the interlayer.

4.2.1 Materials and methods

4.2.1.1 Synthesis of LDH-NO_3

Synthetic LDH were prepared by a coprecipitation method. Cationic solutions (0.2 mM) were prepared dissolving $Mg(NO_3)_2{\cdot}6H_2O$ and $Al(NO_3)_3{\cdot}9H_2O$ (or $Fe(NO_3)_3{\cdot}9H_2O$) in ultrapure water (Millipore, Milli-Q©, 18.2 MΩ cm^{-1}), in order to obtain established molar ratios M^{2+}/M^{3+}= 2, 3 and 4. Nitrate solutions were dropped, by a peristaltic pump, into a reactor containing 200 mL of ultrapure water under stirring (500 rpm), and the precipitation was induced at pH 10.5±0.2 adding dropwise a NaOH solution (0.5 mM). During the synthesis, the atmosphere inside the reactor was controlled with a constant flux of Ar in order to prevent the presence of CO_2 and, thus, the possible entrance of carbonate groups into the interlayer. After 24 hours of aging at 65°C, the precipitates were washed with deionised water and recovered by a filtration system (filter Nuclepore polycarbonate, pore-size 0.45 µm) connected to a vacuum pump. Solids recovered were dried at room temperature.

4.2.1.2 Synthesis of LDH-CO_3

Cationic solutions (0.2 mM) for hydrotalcite-like phases were obtained dissolving the nitrate salts in ultrapure water. The molar ratio (M^{2+}/M^{3+} = 3) of the natural phase hydrotalcite was used, while the M^{3+} was modified as follows: Mg^{2+}/Al^{3+} = 3, Mg^{2+}/Fe^{3+} = 3 and $Mg^{2+}/(Fe^{3+}+Al^{3+})$ = 3/(0.5 + 0.5). Cationic solutions (0.2 mM) for zaccagnaite-like phases were prepared dissolving $Zn(NO_3)_2{\cdot}6H_2O$ and $Al(NO_3)_3{\cdot}9H_2O$ with the molar ratios Zn^{2+}/Al^{3+}= 2 or 3. The carbonate solution (0.05 mM) were obtained dissolving Na_2CO_3 in ultrapure water.

The saline solutions were dropped by a peristaltic pump into a reactor containing 200 mL under stirring

(500 rpm). Precipitation was induced at pH 10±0.2 and 9.5±0.2 for hydrotalcite-like and zaccagnaite-like, respectively, by dropping a 0.5 mM NaOH solution (fig.4.3). The precipitates were aged at 65°C for 24 hours, after that were washed with abundant deionised water and recovered using a Büchner funnel (filter Whatman N° 54, cellulose) connected to a vacuum pump. Solids recovered were dried at room temperature and successively were calcined at 450°C for 4 hours.

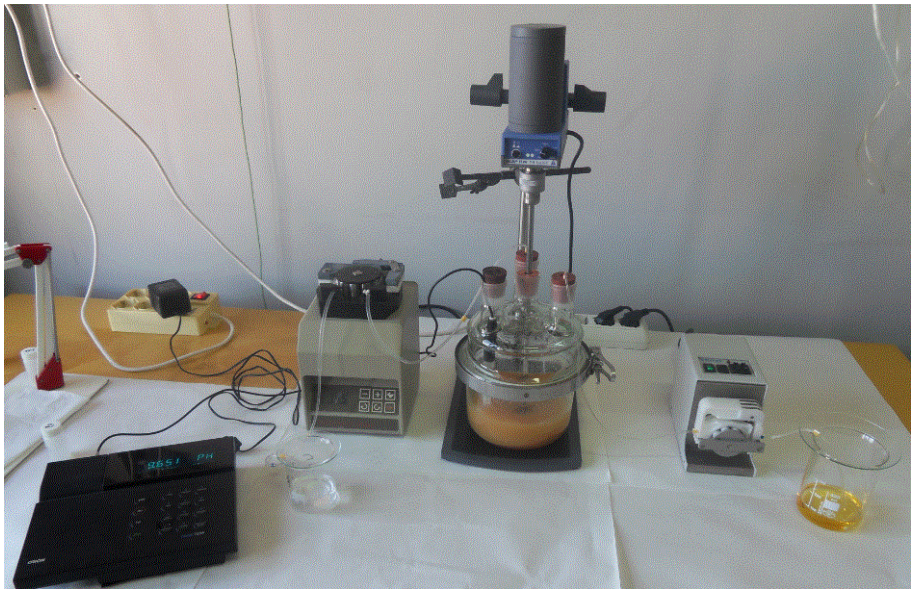

Figure 4.3 Synthesis of LDH.

4.2.1.3 Chemical and mineralogical characterizations

For chemical analyses a portion of all LDH-NO_3 was dissolved in 5% v/v H_2SO_4, while LDH-CO_3 and their calcined products were dissolved in 10% v/v HNO_3. When solids were completely dissolved, acid solution were diluted with ultrapure water for cation analyses (Mg, Zn, Al and Fe) by inductively coupled plasma optical emission spectroscopy (ICP-OES, ARL Fisons 3520), whereas NO_3^- was analysed by ion chromatography (IC, Dionex ICS3000). Mineralogical analyses were carried out by powder X-ray diffraction (XRD) using an automated Panalytical X'pert Pro diffractometer, with Ni-filter Cu-$K\alpha_1$ radiation (λ=1.54060 Å), operating at 40kV and 40mA, with the X'Celerator detector.

4.2.2 Results

Samples are marked with the chemical symbol of the cation constituent the brucite-like sheets, followed by NO_3 or CO_3 to indicate the anion in the interlayer, or "c" for the calcined phases. For LDH with the same cationic composition but different molar ratios, the number before the label indicates the M^{2+}/M^{3+} value.

4.2.2.1 LDH-NO_3

The final products show different characteristics: 2MgAl-NO_3 was a soft loose powder, while the other MgAl-NO_3 and the MgFe-NO_3 were hard. XRD patterns of both cationic compositions MgAl/MgFe-NO_3 showed the typical basal reflections (003) and (006) ascribable to the layered phases (Wang et al., 2009) (fig.4.4). The lattice parameters *c* and *a* were calculated respectively on the basis of the 2θ° angular positions of (003) and (110) reflections (table 4.1). The influence of the M^{2+}/M^{3+} molar ratio on the structure of the solids is mainly evident in the MgAl-NO_3. As the M^{2+}/M^{3+} molar ratio decreases the basal spacing increases, whereas the values of the *a* parameter decrease gradually. The difference observed in the basal spacing can be attributable to the different orientation of the nitrate groups in the interlayer.

Wang and Wang (2007), on the basis of the XRD and ATR-FTIR data, suggested that as the Mg/Al molar ratio decreases the nitrate orientations in the interlayer change from flat (Mg/Al = 4) to perpendicular (Mg/Al = 2) orientation. This hypothesis is in agreement with the consideration that the increasing of positive charge in the brucite-like sheet requires an increase of nitrate in the interlayer, which can be better arranged in perpendicular position with respect to brucite-like sheets. In addition, the increase of the basal spacing tends to minimize the electrostatic repulsions between the positive layers and confers good anion exchange capacity due to the increase of the external and interlayer surface (Wang et al., 2009).

Results of chemical analyses showed a correspondence between the Mg/Al molar ratio of the synthetic products and that of the starting solutions, while the NO_3 content suggests the presence of CO_3 in the interlayer of 2MgAl-NO_3 and 3MgAl-NO_3. This can explain the broad shoulder in the right corner of the (006) basal reflection observed in the XRD pattern of 2MgAl-NO_3.

Manohara et al. (2011) reported that the optimal Mg^{2+}/Fe^{3+} molar ratio in the MgFe-NO_3 is closed to 4/1, and for lower molar ratios the Fe^{3+} in excess precipitates as amorphous hydroxides; however other authors (Ferreira et al., 2006) obtained well crystalline 2MgFe-NO_3. These differences can be attributed to the different synthesis condition adopted. The values of the lattice parameter *a* are very closed between the MgFe-NO_3 samples with different Mg^{2+}/Fe^{3+} molar ratio (fig.4.4); varying the Mg^{2+}/Fe^{3+} molar ratio the value of *a* parameter should change, therefore these similarity probably means that the relative abundances of M^{2+} and M^{3+} in the brucite-like sheet varied slightly between the different solids synthesized. The content of NO_3^- measured in the MgFe-NO_3 samples with molar ratio Mg^{2+}/Fe^{3+} = 2 and 3 was lower than the content of Fe^{3+} (table 4.1); this means that the real M^{2+}/M^{3+} molar ratios in the final products differ from the nominal M^{2+}/M^{3+} molar ratios of the starting solutions, and indicates that the Fe^{3+} can be partially precipitated as amorphous hydroxides.

Table 4.1 Chemical compositions and structural parameters of synthesized LDH-NO_3.

sample	Mg/Al starting solution	Mg	$^{a}M^{3+}$	NO_3	Mg/Al synthetic solid	Empirical formula	(003)	d	^{b}c	(100)	d	a^{c}
	molar ratio	mmoles/g			molar ratio		°2θ	Å	Å	°2θ	Å	Å
2MgAl-NO_3	2	7.7	3.8	2.4	2.0	$[Mg_{0.67}Al_{0.33}(OH)](NO_3)_{0.21}(CO_3)_{0.06}\cdot mH_2O$ (*)	10.077	8.771	26.314	60.775	1.523	3.046
3MgAl-NO_3	3	9.0	3.0	1.8	3.0	$[Mg_{0.75}Al_{0.25}(OH)](NO_3)_{0.15}(CO_3)_{0.05}\cdot mH_2O$ (*)	11.216	7.883	23.649	60.376	1.532	3.064
4MgAl-NO_3	4	9.4	2.4	2.3	3.9	$[Mg_{0.79}Al_{0.21}(OH)](NO_3)_{0.20}\cdot mH_2O$	11.127	7.945	23.836	60.104	1.538	3.076
2MgFe-NO_3	2	7.5	3.6	0.89	2.1		11.130	7.943	23.830	59.348	1.556	3.112
3MgFe-NO_3	3	8.8	2.9	1.7	3.0		11.127	7.946	23.837	59.215	1.559	3.118
4MgFe-NO_3	4	8.5	2.1	2.3	4.1	$[Mg_{0.80}Fe_{0.20}(OH)](NO_3)_{0.22}\cdot mH_2O$	11.034	8.012	24.036	59.196	1.560	3.119

(*) content of CO_3 in the solids was estimated on the basis of NO_3 contents in order to balance the positive charges; $^{a}M^{3+}$ = Al^{3+} or Fe^{3+}; $^{b}c = 3d_{(003)}$; $^{c}a = 2d_{(110)}$

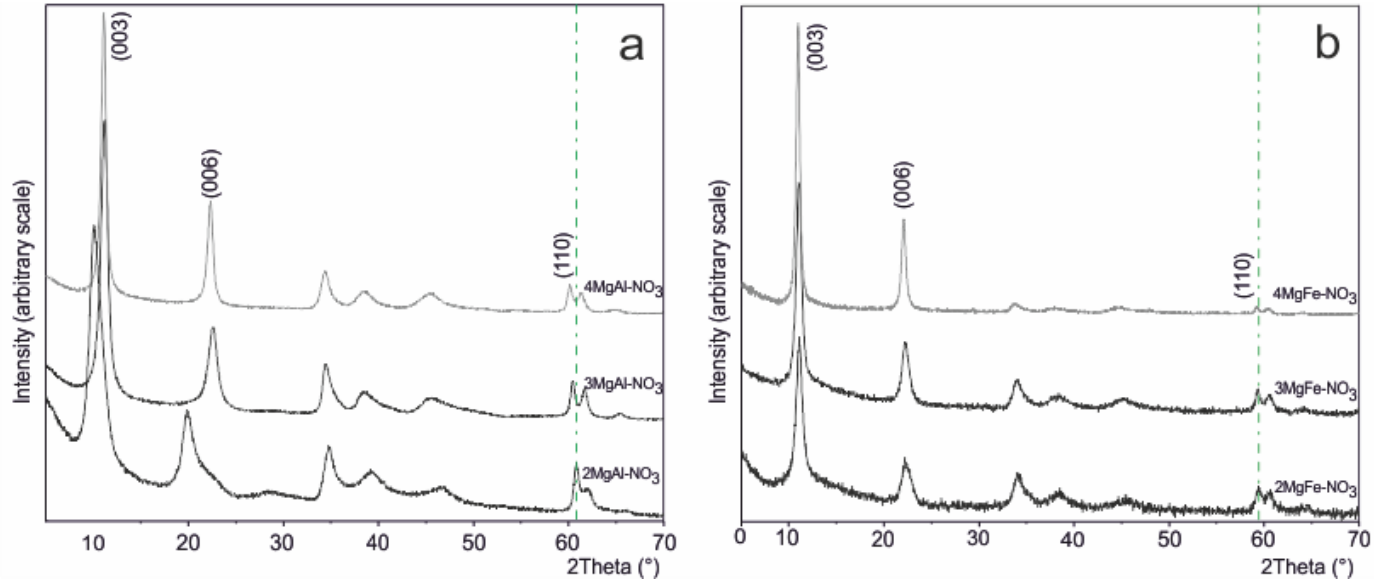

Figure 4.4 XRD patterns of (a) MgAl-NO_3 and (b) MgFe-NO_3;

4.2.2.2 LDH-CO_3

Chemical data showed that the M^{2+}/M^{3+} of synthetic products reflect the compositions of starting solutions (table 4.2). Both hydrotalcite-like and zaccagnaite-like solids appeared as white soft loose powders, the color of samples with Fe^{3+} was lightly orange (fig. 4.5).

Table 4.2 Chemical analyses of LDH-CO_3 and their calcined products.

sample	M^{2+}/M^{3} starting solution	Mg	Al	Fe	M^{2+}/M^{3+} synthetic solid	calcined sample	Mg	Al	Fe	M^{2+}/M^{3+} synthetic solid
	molar ratio	mmoles/g			molar ratio		mmoles/g			molra ratio
MgAl-CO_3	3	8.7	3.0	0	2.9	MgAl-c	12.6	4.4	0	2.8
MgFe-CO_3	3	8.6	0	2.9	2.9	MgFe-c	12.0	0	4.5	2.7
Mg(AlFe)-CO_3	3	7.9	1.4	1.4	2.8	Mg(AlFe)-c	12.4	2.2	2.3	2.8
sample	M^{2+}/M^{3} starting solution	Zn	Al		M^{2+}/M^{3+} synthetic solid	calcined sample	Zn	Al		M^{2+}/M^{3+} synthetic solid
	molar ratio	mmoles/g			molar ratio		mmoles/g			molra ratio
2ZnAl-CO_3	2	6.73	3.09		2.19	2ZnAl-c	8.70	3.98		2.19
3ZnAl-CO_3	3	7.13	2.25		3.17	3ZnAl-c	9.24	2.78		3.32

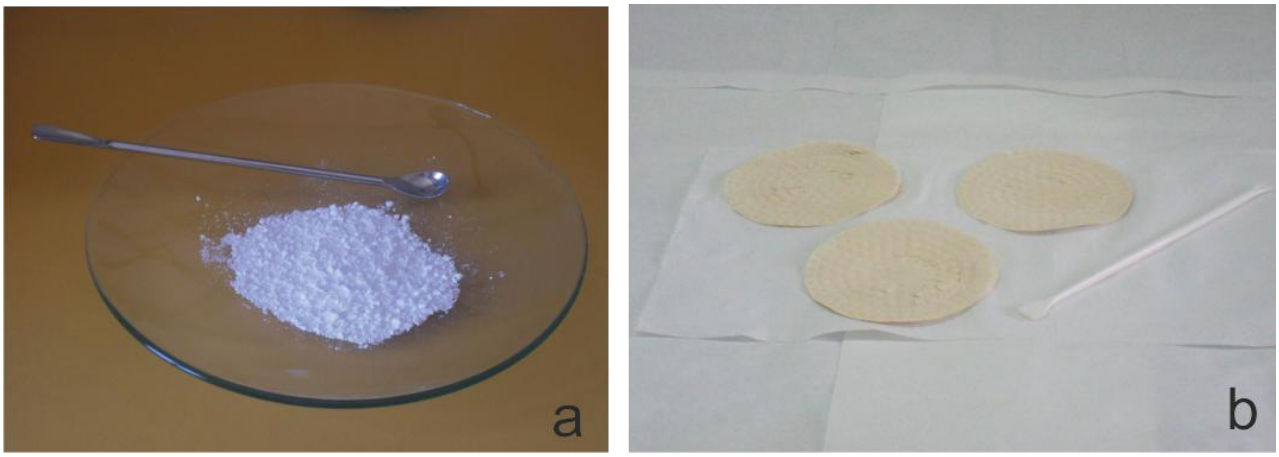

Figure 4.5. (**a**) MgAl-CO_3 and (**b**) Mg(AlFe)CO_3 dried samples.

Synthetic hydrotalcite-like samples showed the typical XRD patterns of hydrotalcite (Carriazo et al., 2007; Yang et al., 2012). As the content of M^{3+} changes from Al^{3+} to Fe^{3+} the (110) reflection shifts toward lower 2θ° values indicating a change in the dimensions of the brucite-like sheets due to the different chemical compositions (fig.4.6). The figure 4.7 shows an example of carbonate Mg(AlFe)-CO_3 LDH with its calcined product: the absence of the basal reflections in the XRD pattern of Mg(AlFe)-c confirmed the collapse of the structure, the two broad peaks at angular positions 2θ ~43° and ~62° are compatible with a disordered periclase MgO. The M^{3+} cations are probably dispersed in the structure (Kameda et al., 2011).

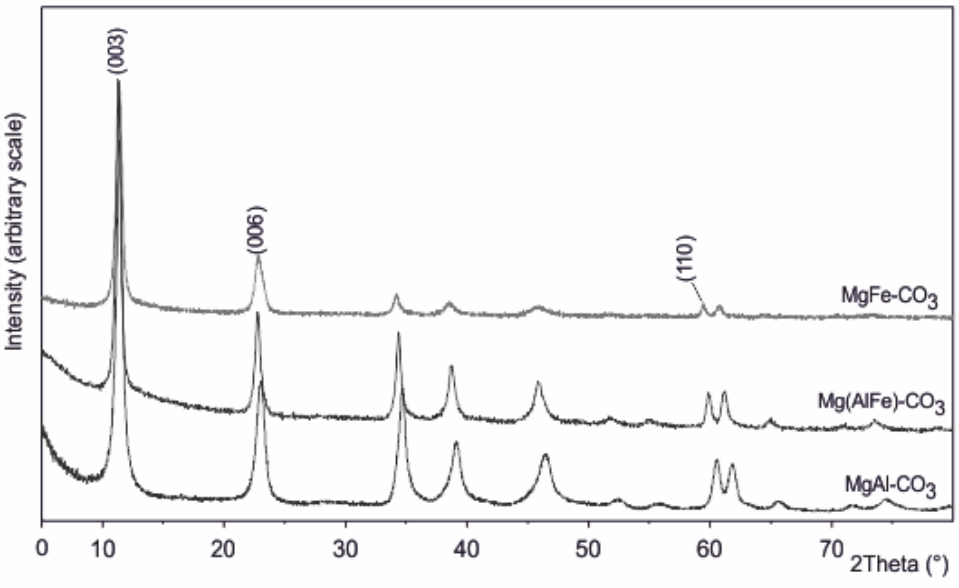

Figure 4.6 XRD patterns of synthetic hydrotalcite-like compounds with different Al^{3+} and Fe^{3+} contents.

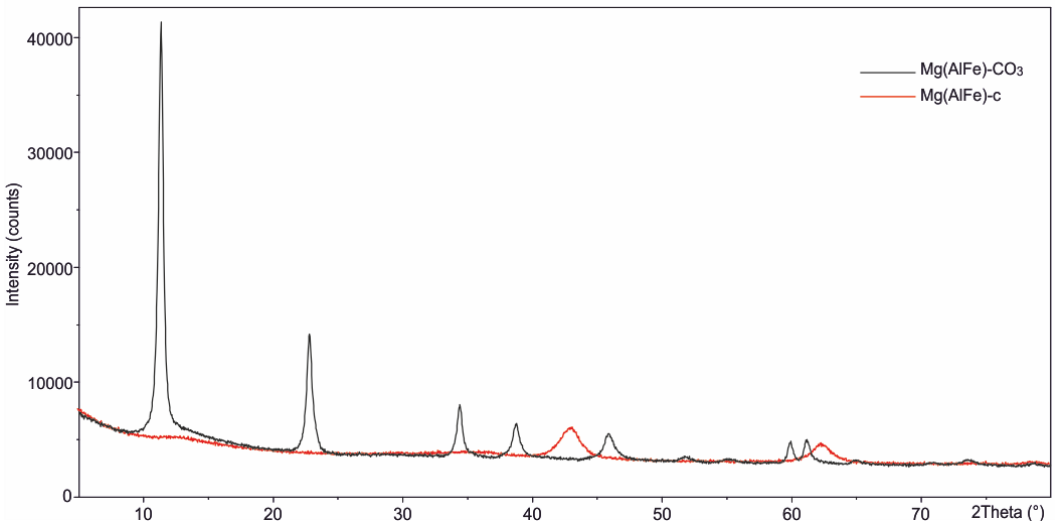

Figure 4.7 XRD patterns of the Mg(AlFe)-CO_3 and its relative calcined phase Mg(AlFe)-c.

XRD patterns of zaccagnaite-like solids are compatible with that of zaccagnaite (Lozano et al., 2012), the (110) reflection shifts gradually for different M^{2+}/M^{3+} molar ratios (fig.4.8). The XRD pattern of the calcined phase can be assigned to a highly disordered zincite ZnO (fig.4.9), while peaks of secondary Al-bearing phases were not detected, thus the Al^{3+} cations are probably dispersed in the structure as impurity (Zhang and Li, 2014).

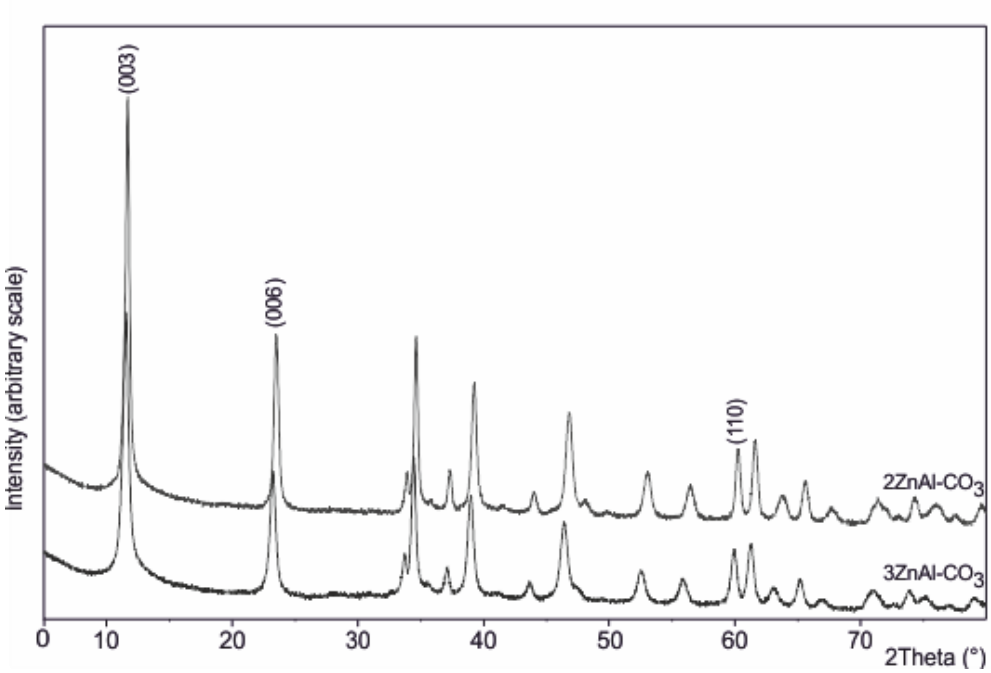

Figure 4.8 XRD patterns of synthetic zaccagnaite-like compounds with different M^{3+}/M^{3+} molar ratio.

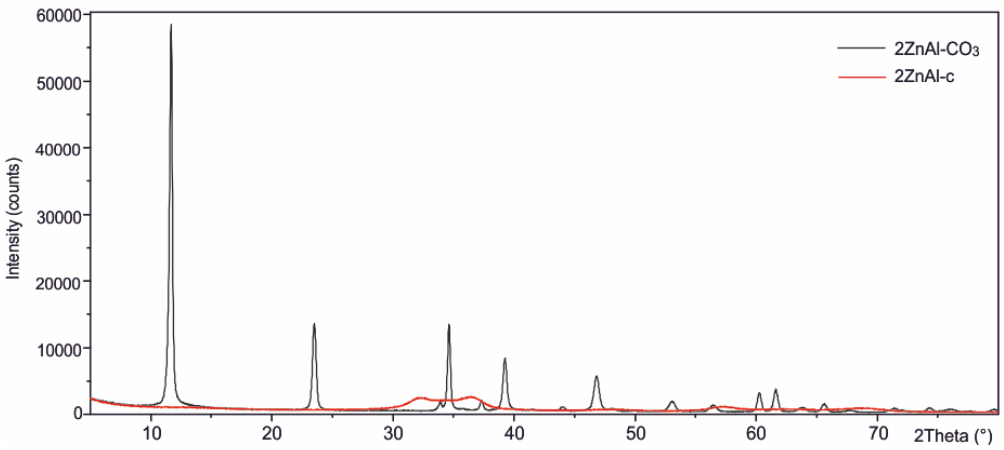

Figure 4.9 XRD patterns of the 2ZnAl-CO_3 and its relative calcined phase 2ZnAl-c.

4.3 Removal of Sb(V) by LDH: laboratory test with synthetic solutions

Sorption experiments were performed with high initial concentration of Sb(V) in solution, in order to estimate the removal capacity of sorbents and to identify the removal processes.

First of all, speedy tests were carried out with LDH-NO_3; afterward the most effective LDH-NO_3 and calcined LDH-CO_3 were used in preliminary sorption experiments. On the basis of results, selected sorbents were successively used to perform:

- experiments with initial circumneutral pH;
- experiments with different initial concentrations of Sb(V) in solution;
- experiments with coexistent oxyanions in solution as possible competitors for Sb(V).

4.3.1 Sorption Experiments

The solutions for the sorption experiments were prepared dissolving an appropriate amount of $KSb(OH)_6$ (Fluka, Sigma-Aldrich, UK) in ultrapure water (Millipore, Milli-Q©, 18.2 MΩ cm^{-1}).

4.3.1.1 LDH-NO_3 speedy tests

Batch experiments were performed by suspending, under stirring, 0.5 g of LDH-NO_3 in 200 ml of 10 mM $Sb(OH)_6^-$ solution. Time of reaction was 5 hours, in ambient atmosphere at room temperature (~25°C). The pH of solutions was measured (ORION® pHMeter and ORION Ross® electrode) before adding the sorbents and at fixed times (1, 2, 3 and 5 hours); at the same times, small volumes of solutions were sampled, filtered at 0.45 µm (filter OlimPeak, polycarbonate) and acidified (0.5% v/v H_2SO_4 suprapure) for chemical analyses by ICP-OES.

4.3.1.2 Preliminary sorption experiments

Were used the sorbents: 2MgAl-NO_3, calcined 2ZnAl-c and 3ZnAl-c, calcined MgAl-c, MgFe-c and Mg(AlFe)-c. Experiments were carried out suspending, under stirring, 0.5 g of sorbents in 200 ml of 10 mM $Sb(OH)_6^-$ solution for 48 hours, in ambient atmosphere at room temperature (fig.4.10). During the experiments pH of solutions was monitored (0, 0.5, 1, 3, 6, 24 and 48 hours) and small amounts of solution were sampled, filtered through 0.45 µm and acidified with 1% v/v HNO_3 suprapure for chemical analyses by ICP-OES.

In order to verify if the initial low pH (~5) of $Sb(OH)_6^-$ solutions affected the removal processes, further experiments at initial circumneutral pH were performed with 2ZnAl-c and Mg(AlFe)-c. Initial pH was increased by adding NaOH 0.5 M.

4.3.1.3 Sorption experiments with different initial concentrations of $Sb(OH)_6^-$ in solution

Selected sorbents, 2ZnAl-c and Mg(AlFe)-c, were used to perform further experiments in the same

modality of preliminary sorption experiments, but with initial concentration of $Sb(OH)_6^-$ in solution equals to: 1, 2.5, 5, and 12.5 mM.

Figure 4.10 Batch experiments.

At the end of all experiments, solid sorbents were collected from the reactor, washed with distilled water and recovered by filtering at 0.45 µm (filters Nuclepore, polycarbonate) with a filtration system connected to a vacuum pump. After filtration, samples were dried at room temperature.

4.3.1.4 Chemical analysis and mineralogical characterization

Concentrations of Sb, Mg, Fe, Zn and Al in solution were analyzed by ICP-OES, NO_3^- was analysed by ion cromatography (IC, Dionex ICS3000). The uncertainties during ICP-OES analyses were evaluate through the reference solutions EP-H-3 and EP-L-3 (SCP Science, Quebec).

Mineralogical analyses of sorbents, before and after experiments, were carried out by XRD. XRD patterns were collected in the 5-80° 2θ angular range on an automated Panalytical X'pert Pro diffractometer, with Ni-filter Cu-kα_1 radiation (λ=1.54060 Å), operating at 40kV and 40mA, using the X'Celerator detector.

4.3.2 Results and discussion

The analytical precision, calculated as % RSD = 100*SD/mean (where RSD is the relative standard deviation, SD is the standard deviation), of antimony determined in the reference solutions was in the range of 1.3-3.5%, while the accuracy, calculated as 100* Measured value/Certified value, was 108 % and 101% for EP-H-3 and EP-L-3 reference solutions, respectively (table 4.3).

Table 4.3 Concentration of Sb determined in the reference solutions.

Reference solution	Certified value		Measured value				Accuracy	Technique
	mg L^{-1}	SD	mg L^{-1}	SD	% RSD	[a]n	%	
EP-H-3	5.05	0.16	5.44	0.19	3.5	12	108	ICP-OES
EP-L-3	11.9	0.2	12.0	0.16	1.3	9	101	ICP-OES

[a]n = number of analyses

4.3.2.1 LDH-NO_3

Results show that MgAl-NO_3 remove $Sb(OH)_6^-$ from solution better than MgFe-NO_3; the removal capacity resulted 2MgAl-NO_3 >> 3MgAl-NO_3 ≥ 4MgAl-NO_3 >> 2MgFe-NO_3 ≥ 3MgFe-NO_3 > 4MgFe-NO_3 (fig. 4.11 and table 4.4).

Table 4.4 pH values and concentrations of Sb, NO_3, Mg, Fe and Al determined in solutions before the addiction of sorbents and at the end of experiments. Complete analyses are reported in Appendix II.

sample	time	pH	Sb	NO_3	Mg	[a]M^{3+}
	h		mmoles L^{-1}			
2MgAl-NO_3	0	5.5	10	0	0	0
	5	8.0	5.4	0.65	0.16	[b] < dl
3MgAl-NO_3	0	5.4	10	0	0	0
	5	9.8	7.6	0.39	0.20	< dl
4MgAl-NO_3	0	5.3	10	0	0	0
	5	9.7	7.8	0.39	0.22	< dl
2MgFe-NO_3	0	5.4	10	0	0	0
	5	9.8	8.5	0.27	0.49	< dl
3MgFe-NO_3	0	5.4	10	0	0	0
	5	9.6	8.6	0.39	0.36	< dl
4MgFe-NO_3	0	5.5	10	0	0	0
	5	9.9	9.3	0.40	0.28	< dl

[a]M^{3+} = Al or Fe; [b]dl = detection limit

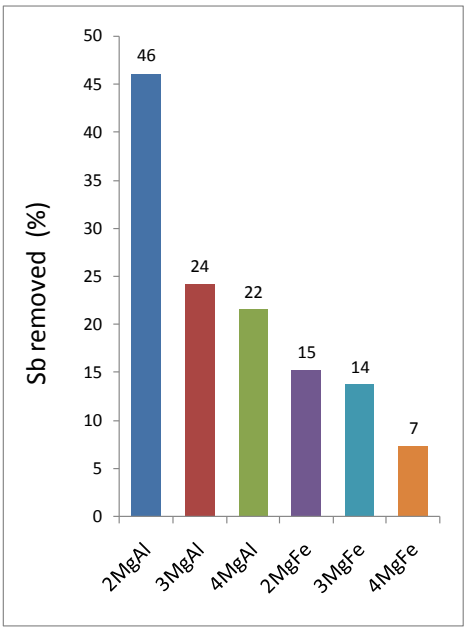

Figure 4.11 Percentage of antimony removed from solution at the end of speedy test.

Initial pH of $Sb(OH)_6^-$ solutions was slightly acid; as the sorbents were added to the solutions the pH values increased sharply and tended to stabilize at about 9-10, the only exception was represented by the experiment with 2MgAl-NO_3, whose pH values were in the range 8.0-8.5. The removal processes were very fast; the most important variations of $Sb(OH)_6^-$ concentration in solutions occurred during the first hour after the addition of sorbents, then the concentration remained almost constant (fig. 4.12).

Comparing the XRD patterns of sorbents before and after experiments, except the 4MgFe-NO_3 sample, it is possible to note a new peak at angular position ~19° 2θ in solids recovered after experiments (fig. 4.13).

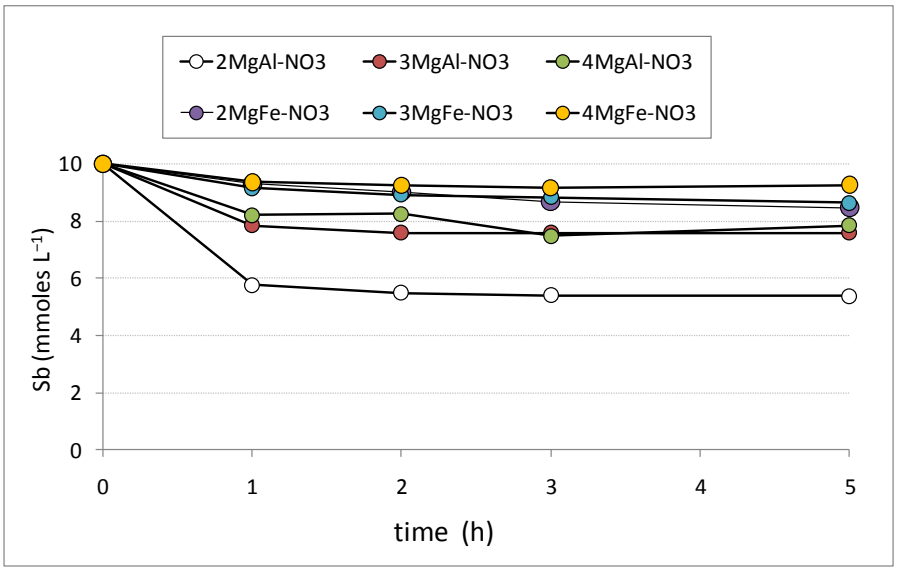

Figure 4.12 Concentrations of Sb determined in solution in function of the time during speedy sorption tests.

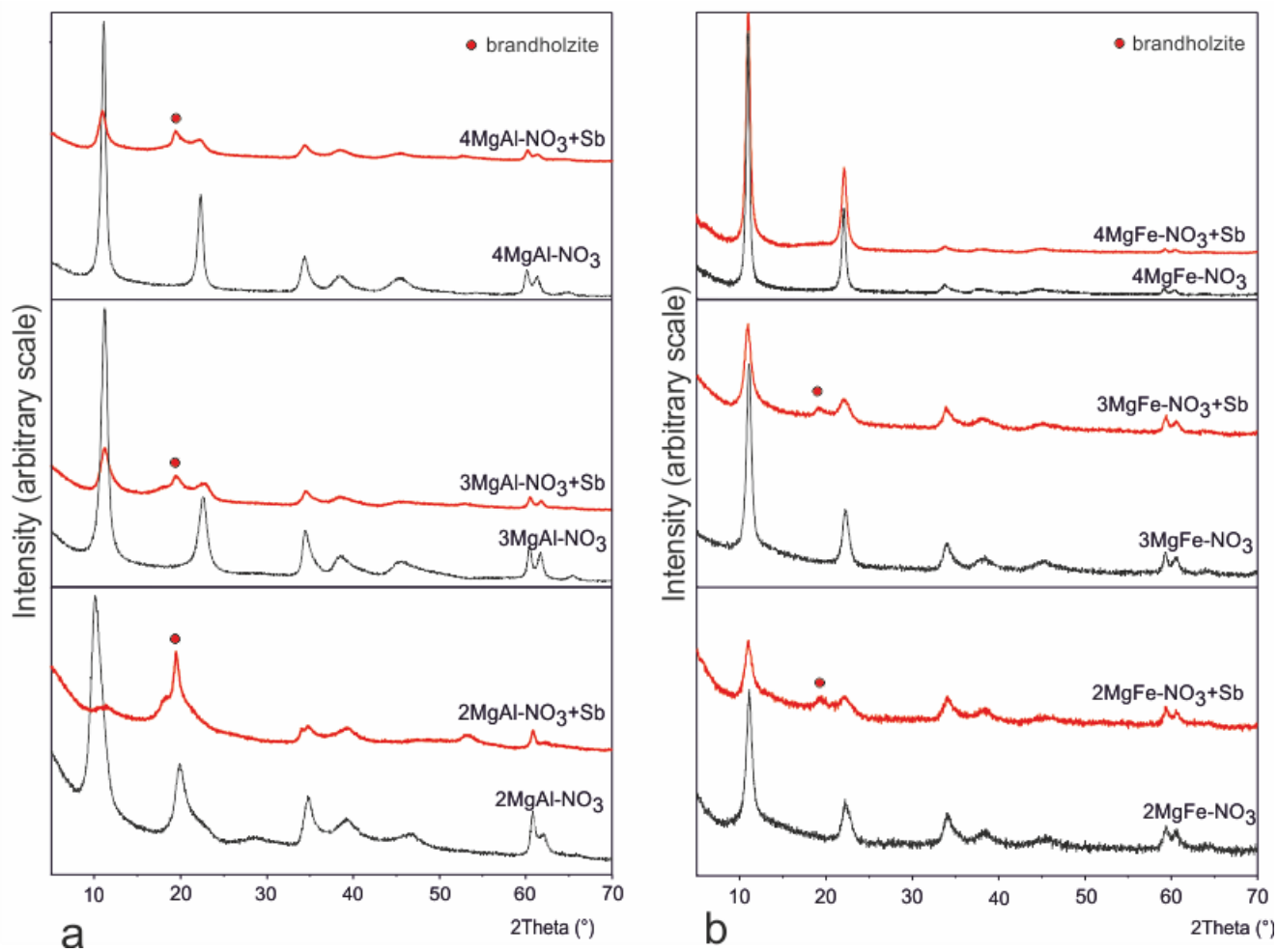

Figure 4.13 XRD patterns of (a) MgAl-NO_3 and (b) MgFe-NO_3 before and after speedy sorption tests.

The new peak can be attributable at a disordered Mg-Sb-phase called brandholzite $Mg[Sb(OH)_6]_2 \cdot 6H_2O$ (Kameda et al., 2011 and reference therein) and it is associated with the decrease of the intensity of peaks belonging to the original phases. The difference observed between the XRD patterns before and after experiments is related to the amount of $Sb(OH)_6^-$ removed from solutions. In fact the major variations were observed in sample 2MgAl-NO_3, where the basal reflections of the original 2MgAl-NO_3 phase were barely visible; on the contrary there were no appreciable differences between the 4MgFe-NO_3 XRD patterns before and after experiments.

These results suggest that $Sb(OH)_6^-$ was removed from solution primarily through the neoformation of a brandholzite-like compound, while there is no evidence of anion exchange processes. In fact, there is no relation between the concentrations of $Sb(OH)_6^-$ removed and nitrate released to solutions (see table 4.4), instead the presence of nitrate in solution was accompanied by small concentrations of magnesium, indicating that a partial dissolution of sorbents occurred. It could be attributable to the riequilibrium of sorbents in solutions (Ferreira et al., 2006), and could explain the increase of pH as a consequence of the release of hydroxyl groups in solution. Consequently, the lower intensity of peaks belonging to the LDH-NO_3 observed in the XRD patterns after experiments could be attributed either to the partial dissolution of solids or to the neoformation of a disordered brandholzite-like phase on the external surface of solids, as well as to both processes. Moreover, a limited exchange in the interlayer between NO_3^- and $Sb(OH)_6^-$ cannot be completely excluded.

Taking into account that most $Sb(OH)_6^-$ was removed very fastly in the first hour of all experiments, it is possible that the new phase was formed by means of the reorganization of $Sb(OH)_6^-$ adsorbed onto external surface of LDH, rather than by a dissolution-reprecipitation process. This could explain the greater efficacy of 2MgAl-NO_3 over the other sorbents. In fact, the 2MgAl-NO_3 showed the highest excess of positive charge in the brucite-like sheets, so it was particularly suitable for the interaction between the $Sb(OH)_6^-$ dissolved in solution and the surface of solid at the solid/liquid interface.

As previously observed (§ 4.2.2), probably in the samples 2MgFe-NO_3 and 3MgFe-NO_3 the amount of Fe^{3+} contained in the brucite-like sheets is less than expected, consequently the excess of positive charge is lower. This could explain the lower $Sb(OH)_6^-$ removal capacity of these samples, moreover it is possible that the Fe^{3+} confers more stability to the LDH structure than Al^{3+}, and therefore decreases the sorption capacity.

4.3.2.2 LDH-CO_3

4.3.2.2.a Preliminary sorption experiments

The concentration of $Sb(OH)_6^-$ in solution decreased sharply after the addition of the sorbents, with most $Sb(OH)_6^-$ removed in the first 6 hours and removal capacity measured at 48 h of 90-100 %. The only exception was represented by MgFe-c that removed most $Sb(OH)_6^-$ between 6 and 24 hours (fig. 4.14).

Moreover, 2MgAl-NO_3, which showed the high $Sb(OH)_6^-$ removal capacity during the speedy test, was significantly less effective with respect to the calcined LDH.

The initial slightly acid pH of $Sb(OH)_6^-$ 10 mM solutions (pH = 5.2-5.4) increased as soon the sorbents were added and tended to stabilize at high values (pH ~12) till the end of the experiments (table 4.5).

In the experiments performed with calcined LDH the pH of solutions reached very high values (~ 12), whereas was circumneutral when 2MgAl-NO_3 was used (fig.4.15).

Table 4.5 Antimony concentrations and pH values determined in solution before the addition of sorbents and at the end of experiments. Complete analyses are reported in appendix III.

	3MgAl-c		**3Mg(AlFe)-c**		**3MgFe-c**		**3ZnAl-c**		**2ZnAl-c**		**2MgAl-NO_3**	
time	pH	Sb	pH	Sb	pH	Sb	pH	Sb	pH	Sb	pH	Sb
h		mmoles L^{-1}		mmoles L^{-1}		mmoles L^{-1}		mmoles L^{-1}		mmoles L^{-1}		mmoles L^{-1}
0	5.4	10.2	5.4	11.1	5.4	10.4	5.2	10.3	5.3	10.2	5.2	9.7
48	11.9	1.2	12.1	0.7	12.2	1.0	12.0	0.8	11.9	0.6	7.7	5.1

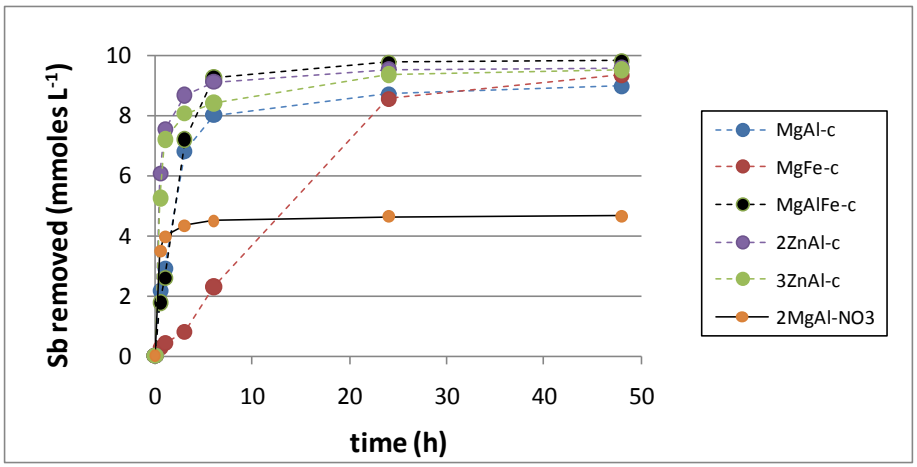

Figure 4.14 Concentrations of antimony removed from solution versus time in preliminary experiments.

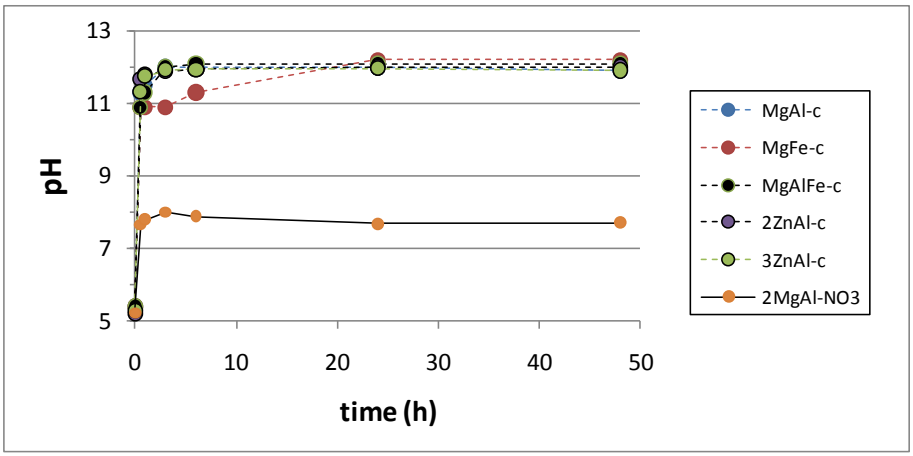

Figure 4.15 Variation of pH values determined in solution versus time in preliminary experiments.

This marked difference is due to the different behavior of calcined LDH with respect to the LDH-NO_3 when entering in contact with the solution: the moderate increase of pH measured in the experiment with 2MgAl-NO_3 can be due to the partial dissolution of the sorbent, while the marked increase of pH observed with calcined LDH was the consequence of reconstruction of the LDH structure that produces OH^-. The processes of calcination and rehydration of the hydrotalcite-like compounds are described by the equations [1] and [2], respectively (Kameda et al., 2011; Lazardis et al., 2003):

Calcination

$$[Mg_{1-x}Al_x(OH)_2](CO_3)_{(x/2)} \rightarrow Mg_{1-x}Al_xO_{1+x/2} + (x/2)CO_2 + H_2O \qquad [1]$$

Reconstruction

$$Mg_{1-x}Al_xO_{1+x/2} + x/nA^{n-} + (1+x/2)H_2O \rightarrow Mg_{1-x}Al_x(OH)_2A^{n-}_{x/n} + xOH^- \qquad [2]$$

XRD patterns of sorbents recovered after all experiments (Appendix III) show that calcined LDH with similar cationic compositions (i.e. hydrotalcite-like or zaccagnaite-like compounds), remove the $Sb(OH)_6^-$ from solution through similar removal processes.

For each cationic composition used, the samples showing the highest removal capacity, Mg(AlFe)-c and 2ZnAl-c, were selected to perform experiments with initial circumneutral pH and to perform experiments with different starting $Sb(OH)_6^-$ concentrations in solutions. The XRD patterns of these phases and the $Sb(OH)_6^-$ removal processes are discussed below.

4.3.2.2.b Experiments with different $Sb(OH)_6^-$ initial concentrations

The sorption capacity of sorbents was determined by the formula:

$$qt = [(C_i - C_f)*V)]/W$$

where:

qt = sorption capacity (mmoles g^{-1})

C_i = initial concentration of $Sb(OH)_6^-$ (mmoles L^{-1})

C_f = final concentration of $Sb(OH)_6^-$ (mmoles L^{-1})

V = volume of solution (L)

W = weight of sorbent (g)

Concentrations of $Sb(OH)_6^-$ removed from solution at the end of experiments increased as the initial

concentrations increased (fig.4.16). In every test it is evident the great removal capacity of both types of calcined LDH; the removal processes were fast: most $Sb(OH)_6^-$ was removed within six hours, irrespective of the initial $Sb(OH)_6^-$ concentrations (tab.4.6).

Both calcined LDH removed more than 99% of $Sb(OH)_6^-$ in experiments with lower initial $Sb(OH)_6^-$ concentrations (i.e. 1, 2.5 and 5 mM), while in experiments with 10 and 12.5 mM $Sb(OH)_6^-$ the percentage of $Sb(OH)_6^-$ removed was slightly lower, and for the highest initial $Sb(OH)_6^-$ concentration the Mg(AlFe)-c was slightly more effective than 2ZnAl-c.

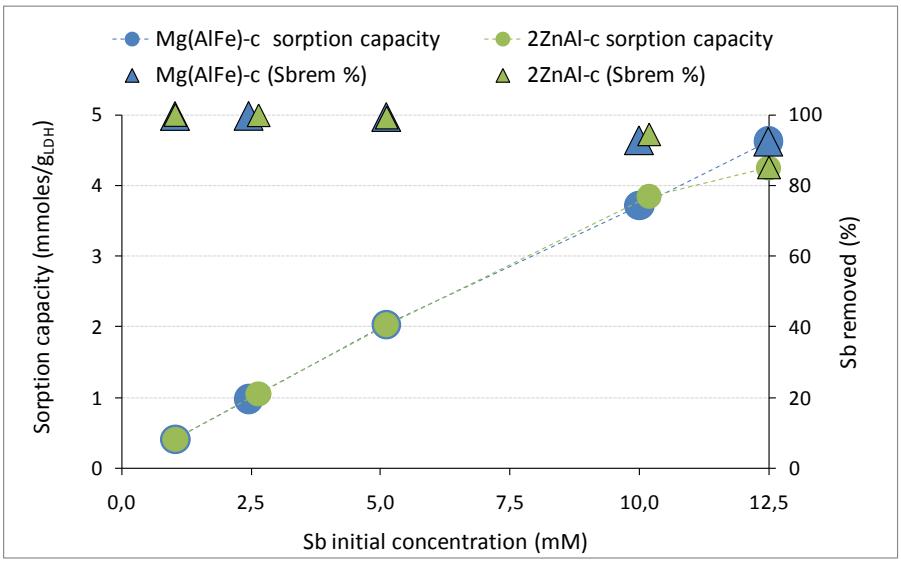

Figure 4.16 Antimony removed from solution in function of the different initial concentrations.

XRD patterns of Mg(AlFe)-CO_3, its calcined product and the solids recovered after batch experiments performed with different initial $Sb(OH)_6^-$ concentrations are reported in figure 4.17. XRD patterns of sorbents recovered after all experiments showed a new peak at the angular position ~19.2° 2θ attributable to a brandholzite-like compound (Kameda et al., 2011). The XRD patterns of solids recovered after experiments with 1, 2.5 and 5 mM $Sb(OH)_6^-$ initial concentrations, contained both hydrotalcite-like (basal reflections at the angular positions ~11.3° and ~22.6° 2θ) and brandholzite-like compounds (~19.2° 2θ). As the initial $Sb(OH)_6^-$ concentration increases, the intensity of the basal reflections of hydrotalcite-like solids decreases, while the new peaks ascribable to the brandholzite-like phase increase. In the XRD patterns relative to the experiments with 10 and 12.5 mM $Sb(OH)_6^-$ the basal reflections of hydrotalcite-like phase are not longer detectable, the peak at ~19.2° 2θ of the brandholzite-like phase became more pronounced and also other peaks are visible (~18° and ~33° 2θ).

The brandholzite is an antimony layered phase described by the general formula $\{Mg[Sb(OH)_6]_2 \cdot 6H_2O\}$.

Table 4.6 Concentrations of Sb, Mg, Al, Fe and Zn, and pH determined in solution during experiments with different initial Sb concentrations.

Sb 12.5 mM		2ZnAl-c		
time	pH	Sb	Zn	Al
h		mmoles L^{-1}		
0	5.6	12.3	[a]n.a.	n.a.
0.5	11.9	4.9	n.a.	n.a.
1	12.0	3.9	n.a.	n.a.
3	12.0	2.7	n.a.	n.a.
6	11.8	2.3	n.a.	n.a.
24	10.6	2.1	n.a.	n.a.
48	10.0	0.9	<0.01	0.2

Sb 12.5 mM		Mg(AlFe)-c			
time	pH	Sb	Mg	Al	Fe
h		mmoles L^{-1}			
0	5.6	12.4	n.a.	n.a.	n.a.
0.5	11.9	9.8	n.a.	n.a.	n.a.
1	12.0	7.7	n.a.	n.a.	n.a.
3	12.0	3.1	n.a.	n.a.	n.a.
6	11.8	1.5	n.a.	n.a.	n.a.
24	10.6	1.1	n.a.	n.a.	n.a.
48	10.0	0.9	0.13	<0.02	<0.01

Sb 10 mM		2ZnAl-c		
time	pH	Sb	Zn	Al
h		mmoles L^{-1}		
0	5.2	10.2	n.a.	n.a.
0.5	11.7	4.1	n.a.	n.a.
1	11.8	2.6	n.a.	n.a.
3	11.9	1.5	n.a.	n.a.
6	11.9	1.1	n.a.	n.a.
24	12.0	0.63	n.a.	n.a.
48	12.0	0.57	0.04	0.4

Sb 10 mM		Mg(AlFe)-c			
time	pH	Sb	Mg	Al	Fe
h		mmoles L^{-1}			
0	5.4	11.1	n.a.	n.a.	n.a.
0.5	10.9	9.2	n.a.	n.a.	n.a.
1	11.3	8.4	n.a.	n.a.	n.a.
3	12.0	3.3	n.a.	n.a.	n.a.
6	12.1	1.3	n.a.	n.a.	n.a.
24	12.1	0.8	n.a.	n.a.	n.a.
48	12.1	0.7	<0.02	<0.02	<0.01

Sb 5 mM		2ZnAl-c		
time	pH	Sb	Zn	Al
h		mmoles L^{-1}		
0	5.2	5.1	n.a.	n.a.
0.5	10.8	4.6	n.a.	n.a.
1	11.8	3.3	n.a.	n.a.
3	11.8	1.7	n.a.	n.a.
6	11.8	0.86	n.a.	n.a.
24	10.3	0.14	n.a.	n.a.
48	9.6	0.04	<0.01	<0.1

Sb 5 mM		Mg(AlFe)-c			
time	pH	Sb	Mg	Al	Fe
h		mmoles L^{-1}			
0	5.2	5.1	n.a.	n.a.	n.a.
0.5	11.1	4.6	n.a.	n.a.	n.a.
1	11.3	4.2	n.a.	n.a.	n.a.
3	11.8	2.0	n.a.	n.a.	n.a.
6	12.1	0.13	n.a.	n.a.	n.a.
24	11.8	0.05	n.a.	n.a.	n.a.
48	10.3	0.03	<0.02	<0.02	<0.01

Sb 2.5 mM		2ZnAl-c		
time	pH	Sb	Zn	Al
h		µmoles L^{-1}	mmoles L-1	
0	5.2	2641	n.a.	n.a.
0.5	11.4	313	n.a.	n.a.
1	11.4	41	n.a.	n.a.
3	11.5	17	n.a.	n.a.
6	11.5	13	n.a.	n.a.
24	11.5	70	n.a.	n.a.
48	11.0	5	<0.01	0.3

Sb 2.5 mM		Mg(AlFe)-c			
time	pH	Sb	Mg	Al	Fe
h		µmoles L^{-1}	mmoles L^{-1}		
0	5.1	2454	n.a.	n.a.	n.a.
0.5	11.4	491	n.a.	n.a.	n.a.
1	11.5	0.6	n.a.	n.a.	n.a.
3	11.6	0.2	n.a.	n.a.	n.a.
6	11.6	0.6	n.a.	n.a.	n.a.
24	11.6	0.5	n.a.	n.a.	n.a.
48	11.6	5.6	<0.02	<0.02	<0.01

Sb 1 mM		2ZnAl-c		
time	pH	Sb	Zn	Al
h		µmoles L^{-1}	mmoles L-1	
0	5.3	1031	n.a.	n.a.
0.5	11.3	12.0	n.a.	n.a.
1	11.3	9.3	n.a.	n.a.
3	11.3	5.4	n.a.	n.a.
6	11.4	7.0	n.a.	n.a.
24	11.4	8.2	n.a.	n.a.
48	10.5	1.2	<0.01	<0.1

Sb 1 mM		Mg(AlFe)-c			
time	pH	Sb	Mg	Al	Fe
h		µmoles L^{-1}	mmoles L^{-1}		
0	5.2	1031	n.a.	n.a.	n.a.
0.5	10.7	5.1	n.a.	n.a.	n.a.
1	10.7	4.3	n.a.	n.a.	n.a.
3	10.7	5.9	n.a.	n.a.	n.a.
6	11.0	3.7	n.a.	n.a.	n.a.
24	11.0	6.8	n.a.	n.a.	n.a.
48	11.4	2.7	0.12	<0.02	0.02

[a]n.a. = not analized

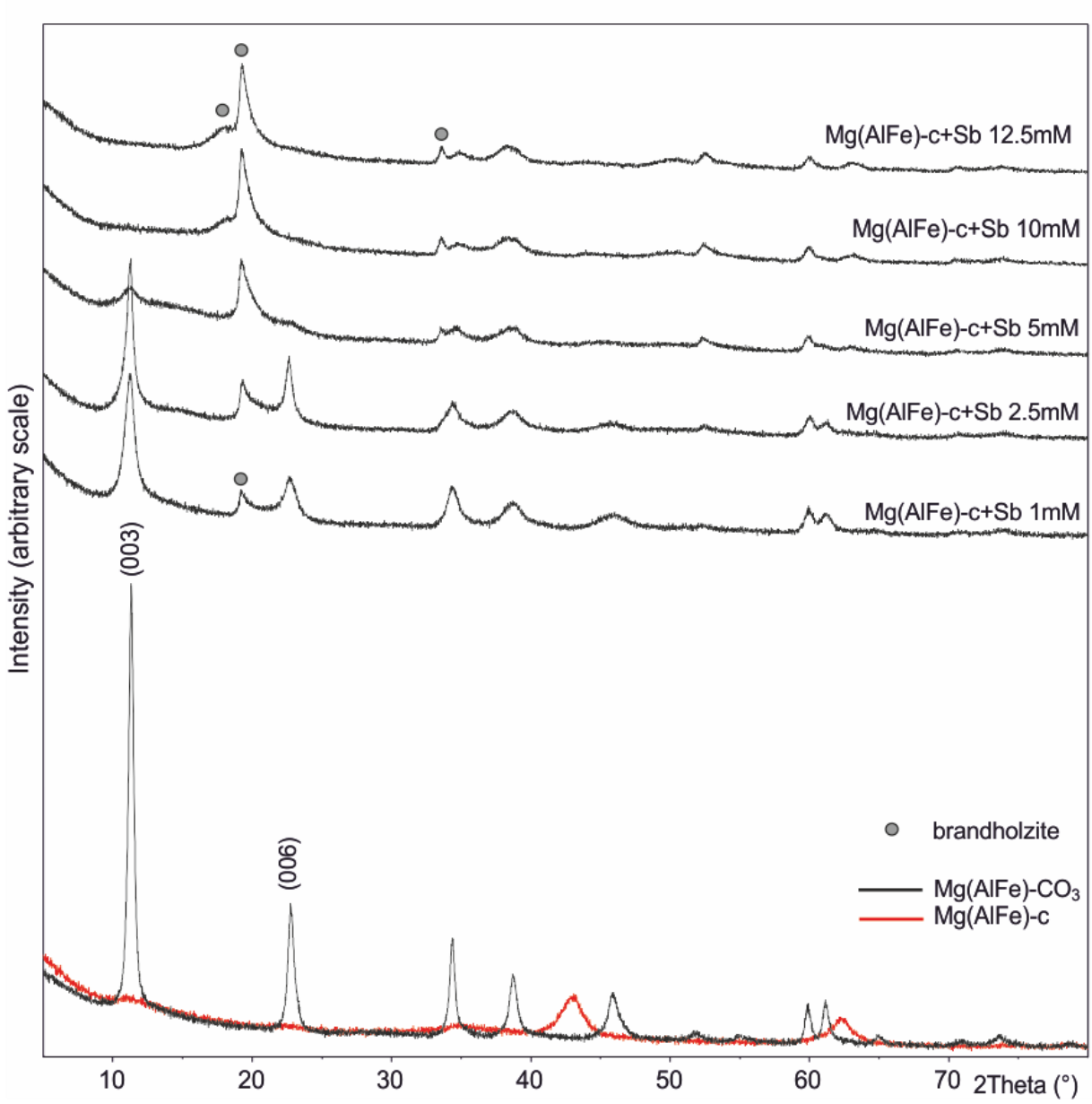

Figure 4.17 XRD patterns of Mg(AlFe)-CO_3 and its relative calcined phases before and after the sorption experiments with different initial $Sb(OH)_6^-$ concentrations in solution.

The structure of brandholzite consists of two different types of layers: $\{Sb(OH)_6]_9\}^{9-}$ and $\{[Sb(OH)_6]_3[Mg(H_2O)_6]_6\}^{9+}$, alternatively stacked along the *c* axis; the layers are composed by $Sb(OH)_6$ and $Mg(H_2O)_6$ octahedra interconnected by hydrogen bonds only (Friedrich et al., 2000). The brandholzite has a layered structure, but differs from the LDH structure, therefore $Sb(OH)_6^-$ was removed from solution through a process other than the simple reconstruction of the hydrotalcite-like structure.

After the addition of the sorbents the pH values of solutions increased rapidly, and reached the range in which CO_3^{2-} is the dominant carbonatic species, thus the reconstruction of the Mg(AlFe)-CO_3 was favored because the CO_3^{2-} has high affinity for the interlayer; however at high pH values also the OH^- can compete for the entry in the interlayer. Results suggest that in experiments with 1, 2.5 and 5 mM

$Sb(OH)_6^-$, the Mg(AlFe)-c that did not react with the $Sb(OH)_6^-$ to form a brandholzite-like compounds, reconstructed the LDH structure. Further studies are needed in order to verify if the reconstruction of the LDH structure is contemporary with the formation of the brandholzite-like phase, or begins after that most of the $Sb(OH)_6^-$ is removed and the CO_3^{2-} and/or the OH^- become the main anionic specie in solution. The thickness of the interlayer may be useful to assess what anionic specie (the CO_3^{2-} or the OH^-) prevails in the interlayer region; the interlayer distance of LDH intercalated with OH^- should be lower than that of a LDH with CO_3^{2-} (Cavani et al., 1991; Koritnig et al., 1975). The angular positions of (003) basal reflection determined in the original Mg(AlFe)-CO_3 and in the samples recovered after experiments performed with 1, 2.5 and 5 mM $Sb(OH)_6^-$ concentrations, show a low increase in the interlayer distance as the initial $Sb(OH)_6^-$ concentration increases (table 4.7). The increase suggests that low amount of $Sb(OH)_6^-$ could be present in the interlayer, while does not permit to exclude the presence of OH^-. It is possible that the interlayer is inhomogeneous and contain both OH^- and CO_3^{2-}, as well as a low amount of $Sb(OH)_6^-$; this could also explain the enlargement of the (003) basal reflection of samples recovered after experiments with respect to the original Mg(AlFe)-CO_3, that indicates a loss of the structural order. Moreover this could explain the slight fluctuation of $Sb(OH)_6^-$ concentration in solution in the experiments with 1 and 2.5 mM $Sb(OH)_6^-$, as a result of the exchange between the $Sb(OH)_6^-$ intercalated and the CO_3^{2-} and/or OH^- in solution, due to the lower specific charge of $Sb(OH)_6^-$ with respect both CO_3^{2-} and OH^-.

Table 4.7 Angular position of the (003) basal reflection of Mg(AlFe)-CO_3 and samples recovered after sorption experiments with 1, 2.5 and 5 mM $Sb(OH)_6^-$ starting concentration in solution.

sample	**(003)**	**$d_{(003)}$**
	°2 θ	Å
Mg(AlFe)-CO_3	11.317	7.813
Mg(AlFe)-c +Sb 1 mM	11.313	7.815
Mg(AlFe)-c +Sb 2.5 mM	11.275	7.842
Mg(AlFe)-c +Sb 5 mM	11.248	7.860

There is a good correspondence in the angular positions of the new peak observed in the XRD patterns of 2MgAl-NO_3, 2MgFe-NO_3 and Mg(AlFe)-c recovered after the experiments. This peak belongs to the brandholzite-like phase, so it is possible to say that the main removal process of $Sb(OH)_6^-$ is the same for the above-cited experiments and is conditioned by the presence of Mg^{2+} at the surface of calcined and uncalcined LDH (fig.4.18).

The calcined LDH showed the major sorption capacity thanks to the higher reactivity surface, while for the LDH-NO_3 the type of M^{3+} cation seems to influence the structural properties of the sorbents and

consequently the sorption capacity.

It is possible that trivalent cations are present in the structure of brandholzite as impurities and contribute to the low crystallinity; moreover, because a moderate dissolution of sorbents occurred, is not excluded that trivalent cations could precipitate as amorphous hydroxides contributing to the $Sb(OH)_6^-$ removal from solution.

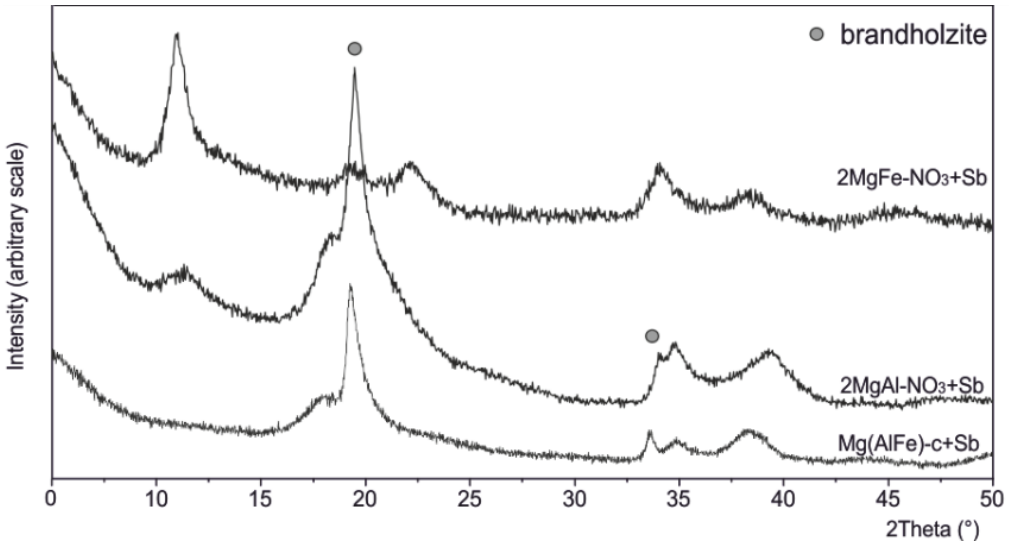

Figure 4.18 XRD patterns of 2MgAl-NO_3 and 2MgFe-NO_3 after speedy sorption test and XRD pattern of Mg(AlFe)-c recovered after preliminary experiment.

XRD atterns of 2ZnAl-CO_3, its calcined product and the solids recovered after batch experiments performed with different initial $Sb(OH)_6^-$ concentrations are reported in figure 4.19. Results indicate that the 2ZnAl-c removed $Sb(OH)_6^-$ from solution through the reconstruction mechanism (memory effect). In fact, XRD patterns of the solids recovered after the experiments showed new peaks ascribable to a LDH mineral named zincalstibite. The zincalstibite belongs to the cualstibite group (Mills et al., 2012) and is described by the formula $Zn_2Al(OH)_6[Sb(OH)_6]$. Structure of zincalstibite consists of brucite-like sheets, containin Zn^{2+} and Al^{3+} in the Zn/Al = 2 molar ratio, regularly alternating along the *c* axis with interlayer composed by isolated $Sb(OH)_6^-$ octahedra without additional water (Bonaccorsi et al., 2007; Mills et al., 2012).

The removal process is very fast, most $Sb(OH)_6^-$ was removed within three hours and the solution pH values sharply increased as soon as the sorbents were added (table 4.6). The XRD patterns of sorbents relative to the experiments with low initial $Sb(OH)_6^-$ concentrations (i.e. 1, 2.5 and 5 mM) showed peaks belonging to two different LDH: the peaks at ~9°, ~18.1°, ~19.6 and 21.3° 2θ are attributable to the zincalstibite-like phase, while the peaks at ~11.7 and ~23.5° 2θ are compatible with the original carbonate LDH (table 4.8). As the initial $Sb(OH)_6^-$ concentrations increased the intensity of 2ZnAl-CO_3 peaks decreased, and in turn the intensity of zincalstibite peaks increased.

Table 4.8 Angular position of the (003) basal reflection of 2ZnAl-CO_3 and samples recovered after sorption experiments with 1, 2.5 and 5 mM $Sb(OH)_6^-$ starting concentration in solution.

sample	(003)	$d_{(003)}$
	°2θ	Å
2ZnAl-CO_3	11.669	7.578
2ZnAl -c +Sb 1 mM	11.697	7.559
2ZnAl -c +Sb 2.5 mM	11.689	7.564
2ZnAl -c +Sb 5 mM	11.707	7.559

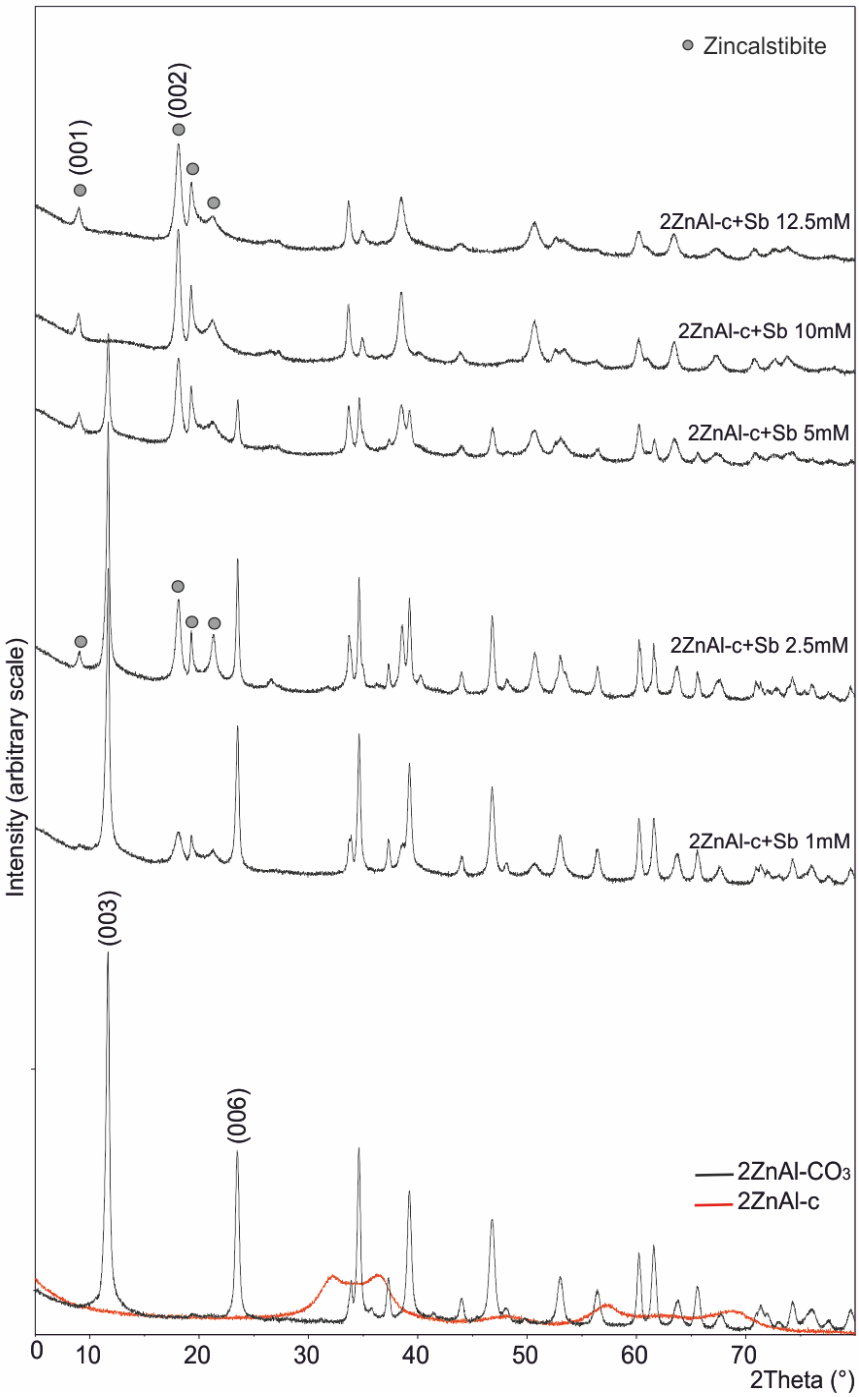

Figure 4.19 XRD patterns of 2ZnAl-CO_3 and its relative calcined phases before and after the sorption experiments with different initial $Sb(OH)_6^-$ concentrations in solution.

The sorbents of experiments performed with 10 and 12.5 mM initial $Sb(OH)_6^-$ concentrations no longer showed the XRD peaks of the carbonate phase, and the concentrations of $Sb(OH)_6^-$ in solution decreased till the end of experiments, so it is excluded the release of $Sb(OH)_6^-$ in favor of the entrance of CO_3^{2-} or OH^- in the interlayer. However at the pH values ~10-12, the CO_3^{2-} and the OH^- can compete for the entry in the interlayer, therefore is possible the presence of these anions intercalated as impurities.

Little fluctuations of $Sb(OH)_6^-$ in solution were observed during the experiments with 1 and 2.5 mM initial $Sb(OH)_6^-$ concentrations: in these cases, due to the relatively low initial $Sb(OH)_6^-$ concentrations, it is possible that, after the removal of most $Sb(OH)_6^-$, the CO_3^{2-} and/or OH^- become the dominant dissolved anionic species in solution and, thus, could compete for the entrance in the interlayer. At the same way, the presence of OH^- and /or CO_3^{2-}in the interlayer of the zaccagnaite-like compounds is not excluded.

Further studies are needed to assess whether the reconstruction of carbonate and antimonate LDH are contemporary, and under what conditions the reconstruction of one phase prevails over the other.

Results of batch experiments performed with initial circumneutral pH are reported in Appendix IV. There were no significative differences with respect to the results obtained in the preliminary sorption experiments, indicating that the initial slightly acid pH of $Sb(OH)_6^-$ solution did not affect the removal processes.

4.3.3 Effects of coexistent anions in solution

Sorption experiments were performed with coexistent anions in solutions in order to assess their competitive effect on the $Sb(OH)_6^-$ removal capacity of LDH. For this study, the possible competitors were chosen considering the chemical composition of the waters draining the Su Suergiu abandoned mine (§ 3), consequently experiments were carried out with equal molar concentrations in solution of $Sb(OH)_6^-$ and SO_4^{2-}, $Sb(OH)_6^-$ and HCO_3^- or $Sb(OH)_6^-$ and $HAsO_4^{2-}$. The SO_4^{2-} and HCO_3^- anions were chosen because they are the main anionic species in the contaminated mine water of Su Suergiu. The $HAsO_4^{2-}$ anion was selected because of its high toxicological relevance and its high concentration, up to 2-3 mg L^{-1}, in waters flowing at Su Suergiu. Moreover, As(V) represents an excellent competitor; in fact, several studies reported the high affinity for As with both calcined and uncalcined LDH with various cationic and anionic compositions (Goh et al., 2008 and reference therein; Ardau et al. 2013; Wang et al., 2009).

4.3.3.1 Materials and methods

Solutions for competition experiments were prepared dissolving an appropriate amount of Na_2SO_4, $NaHCO_3$ or $Na_2HAsO_4 \cdot 7H_2O$ and $KSb(OH)_6$ in Milli-Q water. To avoid the precipitation of the slightly soluble $Na[Sb(OH)_6]$ (Diemar et al., 2009 and reference therein) and its impact on the removal processes, the initial $Sb(OH)_6^-$ concentration in solution and the liquid/$solid_{LDH}$ ratio were changed compared to the previous sorption experiments.

For the batch tests, 0.1 g of Mg(AlFe)-c or 2ZnAl-c was suspended, under stirring, in 400 ml of solution containing equal concentrations (1 mM) of dissolved $Sb(OH)_6^-$ and competitors; experiments without competitors were also performed as a reference. At defined times (0, 0.5, 1, 3, 6, 24 and 48 hours) pH of solutions was measured and small volumes of solutions were sampled, filtered through 0.45 µm (filter OlimPeak, polycarbonate) and acidified with 1% v/v HNO_3 suprapure for chemical analyses by ICP-OES. At the end of experiments solid sorbents were recovered and washed with distilled water using a filtration system. Sorbents were dried at room temperature and successively characterized by powder XRD diffraction.

4.3.3.2 Results and discussion

Both 2ZnAl-c and Mg(AlFe)-c showed high $Sb(OH)_6^-$ removal capacity with coexistent SO_4^{2-} and HCO_3^-, while the presence of $HAsO_4^{2-}$ reduced dramatically the $Sb(OH)_6^-$ removal capacity of both sorbents (fig.4.20).

Therefore, the competition effect on the $Sb(OH)_6^-$ removal results $HAsO_4^{2-}$ >> HCO_3^- > SO_4^{2-}. In all experiments the concentration of Na in solution did not vary significantly with time, so it is excluded that the precipitation of $Na[Sb(OH)_6]$ affected the removal processes (table 4.9 and 4.10).

Table 4.9. Concentrations of $Sb(OH)_6^-$ and coexistent oxyanions in solution and pH values of solution determined during competition experiments performed with Mg(AlFe)-c.

Mg(AlFe)-c	Sb		Sb+SO_4^{2-}				Sb+$HAsO_4^{2-}$				Sb+ HCO_3^-		
time	pH	Sb	pH	Sb	SO_4^{2-}	Na	pH	Sb	$HAsO_4^{2-}$	Na	pH	Sb	Na
h		mmoles L^{-1}		mmoles L^{-1}				mmoles L^{-1}				mmoles L^{-1}	
0	5.2	1.03	5.1	1.03	1.08	2.06	8.6	1.03	1.02	2.04	8.3	1.02	1.11
0.5	10.5	0.87	10.6	0.89	1.01	2.12	10.5	1.01	0.94	2.03	10.4	0.90	1.03
1	10.6	0.73	10.7	0.75	1.00	2.18	10.5	1.01	0.90	2.08	10.5	0.79	1.06
3	10.8	0.43	10.9	0.44	0.92	2.12	10.6	1.00	0.77	2.06	10.6	0.64	1.06
6	10.8	0.34	10.9	0.33	0.93	2.16	10.6	0.99	0.68	2.09	10.5	0.60	1.05
24	9.6	0.31	9.6	0.30	1.03	2.37	10.3	1.03	0.48	2.22	9.6	0.57	1.10
48	9.3	0.29	9.1	0.28	1.06	2.11	9.8	0.99	0.43	2.02	9.5	0.51	0.99

Table 4.10. Concentrations of $Sb(OH)_6^-$ and coexistent oxyanions in solution and pH values of solution determined during competition experiments performed with 2ZnAl-c.

2ZnAl-c	Sb		Sb+SO_4^{2-}				Sb+$HAsO_4^{2-}$				Sb+HCO_3^-		
time	pH	Sb	pH	Sb	SO_4^{2-}	Na	pH	Sb	$HAsO_4^{2-}$	Na	pH	Sb	Na
h		mmoles L^{-1}		mmoles L^{-1}				mmoles L^{-1}				mmoles L^{-1}	
0	5.1	1.02	5.2	1.01	1.08	2.13	8.6	1.02	1.03	2.06	8.2	1.03	1.04
0.5	10.4	0.61	10.6	0.68	0.97	2.13	9.2	0.99	0.98	2.05	10.0	0.60	1.02
1	10.5	0.54	10.6	0.60	0.98	2.12	9.2	0.98	0.96	2.07	10.1	0.54	1.02
3	10.5	0.42	10.7	0.53	0.97	2.12	9.2	0.97	0.94	2.04	10.1	0.50	1.05
6	10.6	0.33	10.5	0.42	0.97	2.10	9.2	0.96	0.91	2.07	10.1	0.47	1.03
24	9.6	0.21	9.9	0.29	1.01	2.21	8.2	0.95	0.87	2.10	10.0	0.37	1.04
48	8.5	0.15	9.5	0.22	1.04	1.96	8.1	0.93	0.87	1.97	8.7	0.24	0.96

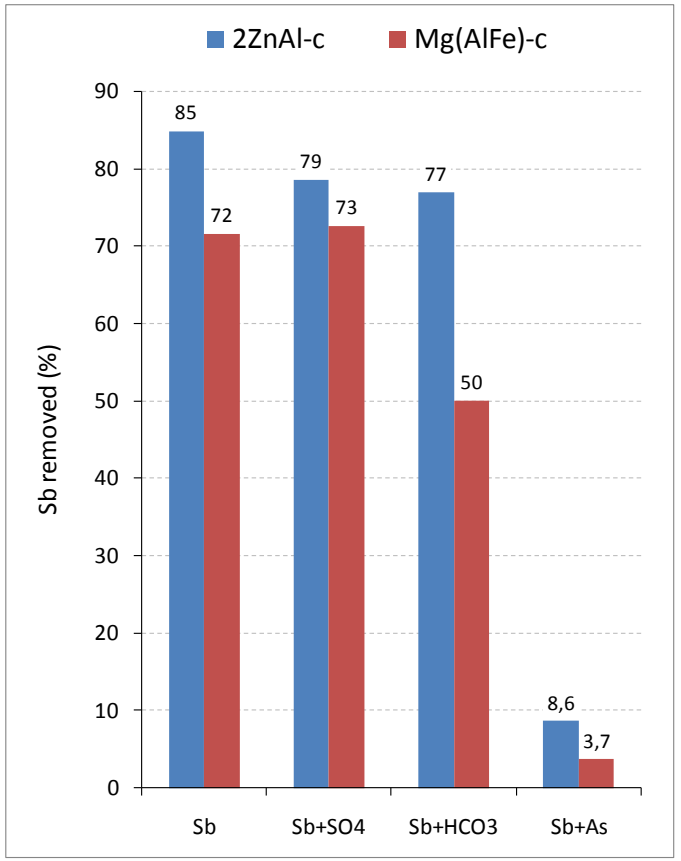

Figure 4.20. Percentage of $Sb(OH)_6^-$ removed from solution at the end of competition experiments. The experiments are marked as follow: **Sb =** experiments with $Sb(OH)_6^-$ 1mM; **Sb+SO4 =** experiments with equal molar concentrations of $Sb(OH)_6^-$ and SO_4^{2-}; **Sb+HCO3 =** experiments with equal molar concentrations of $Sb(OH)_6^-$ and HCO_3^-; **Sb+As** = experiments with equal molar concentrations of $Sb(OH)_6^-$ and $HAsO_4^{2-}$.

In experiments performed with Mg(AlFe)-c without competitors in solution and with coexistent SO_4^{2-} most $Sb(OH)_6^-$ was removed within six hours (fig. 4.21). The presence of SO_4^{2-} did not affect the $Sb(OH)_6^-$ removal process: the trend of $Sb(OH)_6^-$ concentrations in solution is the same in both experiments. In presence of coexistent HCO_3^-, the removal $Sb(OH)_6^-$ capacity of Mg(AlFe)-c decrease significantly. The most competitive effect was obtained with $HAsO_4^{2-}$: at the end of the experiment less than 4% of $Sb(OH)_6^-$ and about 60% of $HAsO_4^{2-}$ were removed from solution. The removal process appear slower with respect to the other experiments, in fact most of $HAsO_4^{2-}$ was removed within 24 hours. It seems that at the end of experiment the equilibrium between the sorbent and $HAsO_4^{2-}$ was still incomplete (fig.4.21)

XRD patterns of solids recovered after experiments are in agreement with results of chemical analyses (fig. 4.22). Patterns of Mg(AlFe)-c after experiment without competitors and with coexistent SO_4^{2-} or HCO_3^- show well defined reflections at ~19° 2θ, attributable to brandholzite-like compound. The XRD pattern of sorbent relative to the experiment with HCO_3^- show also a broad peak at angular position ~12° 2θ and an enlargement on the right shoulder of the peak at ~19° 2θ, ascribable respectively to the (003) and (006) reflections of the LDH structure. This could explain the decrease of the $Sb(OH)_6^-$ removal capacity; in fact, both formation of brandholzite-like compound and reconstruction of hydrotalcite-like compound occurred. Even the presence of CO_3^{2-} in solution (pH = 9.5 - 10.6) might have favored the reconstruction of the Mg(AlFe)-CO_3, although the formation of brandholzite-like compound prevailed.

On the contrary, the peak of brandholzite-like compound is just a slight hump in the XRD pattern of solid recovered after experiment with coexistent $HAsO_4^{2-}$, while the basal reflections attributable to a LDH layered structure are well recognizable; therefore it is possible to assume that $HAsO_4^{2-}$ was incorporated in the interlayer of a less ordered LDH. At the experimental pH conditions (9.8-10.5) the $HAsO_4^{2-}$ species dominates the aqueous As(V) speciation, previous authors discussed about the speciation of As(V) in the LDH interlayer (Ardau et al., 2013 and reference therein), but at the present the knowledge is still incomplete. At the pH values of experiment, it is possible that also a minor amount of CO_3^{2-} and/or OH^- entry in the interlayer, this could explain the enlargement of peak at ~12° 2θ due to a less ordered structure.

The results obtained, in agreement with previous studies (Kameda et al., 2011), showed that the coexistence of SO_4^{2-} does not affect the $Sb(OH)_6^-$ removal capacity of Mg(AlFe)-c, whereas in presence of carbonate species the $Sb(OH)_6^-$ removal capacity decrease significantly due to the contemporary reconstruction of the hydrotalcite-like phase and the formation of the brandholzite-like compound. It was also observed that the coexistence of As(V) affects seriously the $Sb(OH)_6^-$ removal capacity of Mg(AlFe)-c, due to the high affinity of As(V) for the LDH (Türk et al., 2009; Wang et al., 2009).

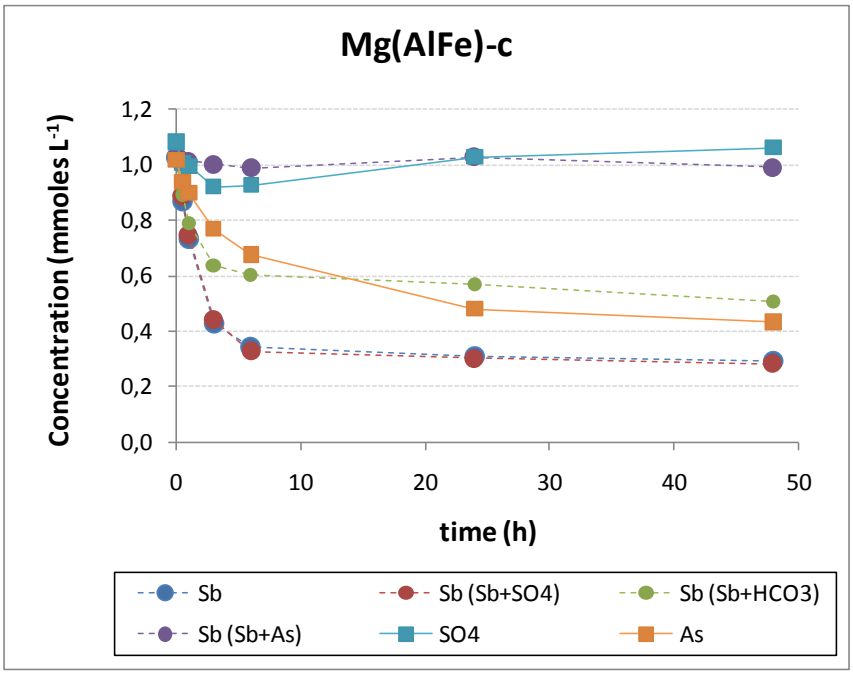

Figure 4.21 Concentrations of $Sb(OH)_6^-$, SO_4^{2-} and As in solutions during competition experiments performed with Mg(AlFe)-c. The experiments are marked as follow: **Sb** = experiment with $Sb(OH)_6^-$ 1mM; **Sb+SO4** = experiment with equal molar concentrations of $Sb(OH)_6^-$ and SO_4^{2-} ; **Sb+HCO3** = experiment with equal molar concentrations of $Sb(OH)_6^-$ and HCO_3^- ; **Sb+As** = experiment with equal molar concentrations of $Sb(OH)_6^-$ and $HAsO_4^{2-}$.

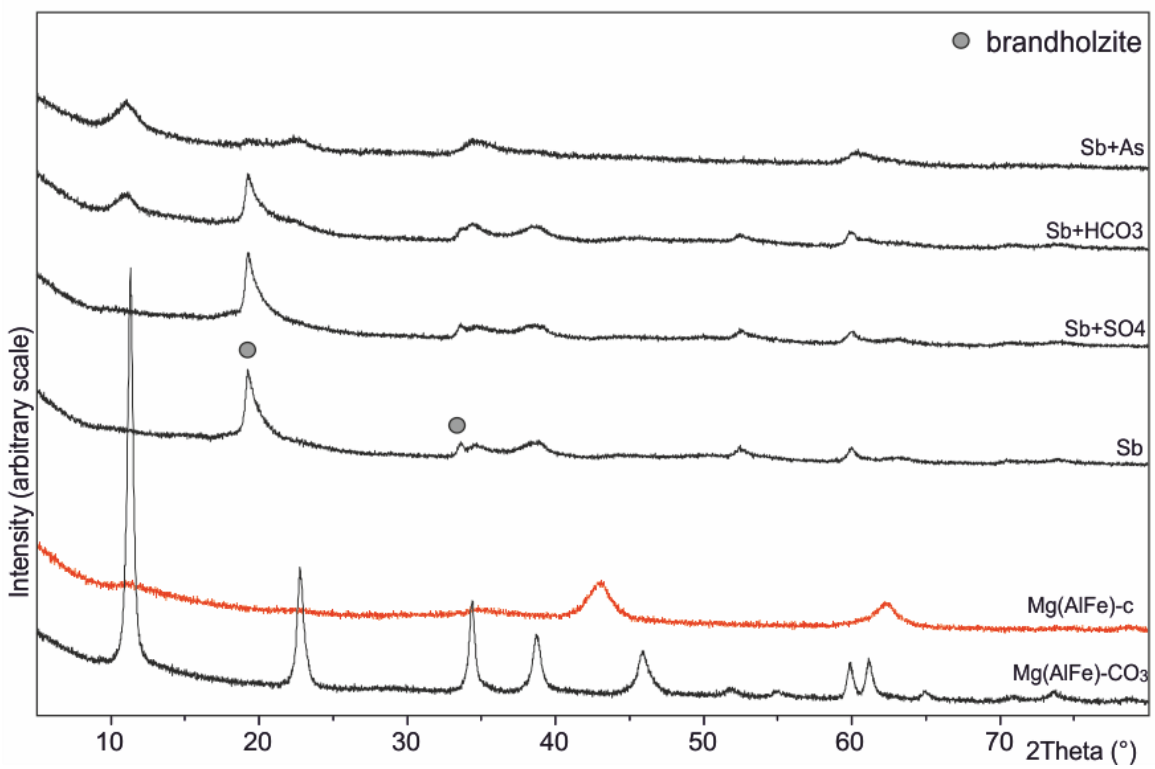

Figure 4.22 XRD patterns of Mg(AlFe)-CO_3 and its calcinate products before and after experiment without coexistent anions in solution (Sb), and with the coexistent $Sb(OH)_6^-$ and SO_4^{2-} (**Sb+SO4**), $Sb(OH)_6^-$ and HCO_3^- (**Sb+HCO3**), $Sb(OH)_6^-$ and $HAsO_4^{2-}$ (**Sb+As**).

The sorption capacity of 2ZnAl-c slightly decreased in presence of coexistent SO_4^{2-} and HCO_3^-, total amount of $Sb(OH)_6^-$ removed from solution at the end of experiments was close to that determined in the experiment without competitors (fig.4.20). The greatest variations of $Sb(OH)_6^-$ in solution were observed within the six hours, even if at the end of the experiments the equilibrium between the sorbents and the solutions was not complete (fig.4.23). In presence of $HAsO_4^{2-}$ the concentrations of $Sb(OH)_6^-$ removed dramatically decreased, but contrary to that observed when Mg(AlFe)-c was used, in this case at the end of experiment a high concentration of $HAsO_4^{2-}$ in solution was measured: at the end of the time of reaction, less than 10% and 12% of $Sb(OH)_6^-$ and $HAsO_4^{2-}$, respectively, were removed from solution.

The XRD pattern of solid recovered after experiment performed without competitors in solution shows peaks indicating the presence of two different phases: the peaks at angular positions about 11.6° and 23.5° 2θ° are compatible with the basal reflection (003) and (006), respectively, of the original 2ZnAl-CO_3, whereas the peaks at ~9°, 18° and 19° 2θ are ascribable to the zincalstibite-like compound (fig.4.24). Peaks at the same angular positions can be observed in the XRD pattern of solid recovered after experiment with coexistent SO_4^{2-}. These results suggest that at the solution pH values, determined during these experiments, the CO_3^{2-} and/or the OH^- anions occurring naturally in the water were taken to reconstruct the original LDH structure. As observed in previous studies (Ardau et al., 2013), the SO_4^{2-} resulted low affine with ZnAl-LDH; in presence of coexistent HCO_3^-, in agreement with the chemical results that showed a slight decrease of $Sb(OH)_6^-$ sorption capacity, the peaks belonging the zincalstibite-like phase lose intensity, on the contrary the intensity of peaks of carbonate phase increase.

In the XRD pattern of solid recovered after the experiment with $HAsO_4^{2-}$, the presence of two broad undefined humps in the angular ranges 30-33° and 35-37° 2θ indicates that at the end of experiment part of the 2ZnAl-c did not react and explain the lower pH value with respect to those of the other experiments, and the lower removal capacity. The peaks belonging the zincalstibite-like phase are less intense than those of sorbents relative to the other experiments, whereas the peaks compatible with the original carbonate phase are well defined, therefore it is possible that the low amount of $HAsO_4^{2-}$ is intercalated in the interlayer.

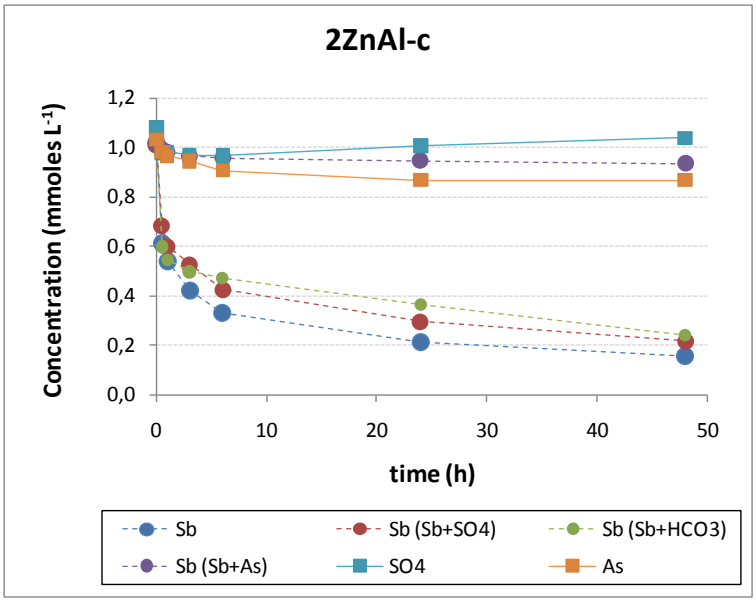

Figure 4.23 Concentrations of $Sb(OH)_6^-$, SO_4^{2-} and As in solutions during competition experiments performed with 2ZnAl-c. The experiments are marked as follow: **Sb =** experiments with $Sb(OH)_6^-$ 1mM; **Sb+SO4 =** experiments with equal molar concentrations of $Sb(OH)_6^-$ and SO_4^{2-} ; **Sb+HCO3 =** experiments with equal molar concentrations of $Sb(OH)_6^-$ and HCO_3^- ; **Sb+As** = experiments with equal molar concentrations of $Sb(OH)_6^-$ and $HAsO_4^{2-}$.

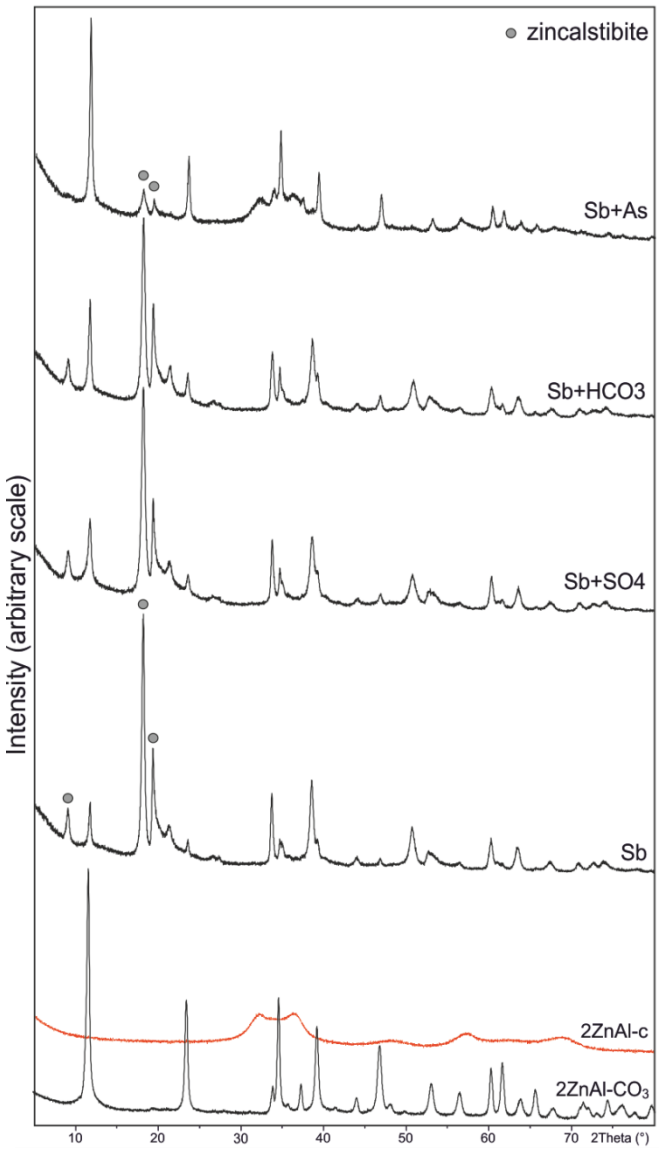

Figure 4.24 XRD patterns of 2ZnAl-CO_3 and its calcined products before and after experiment without coexistent anions in solution (**Sb**), and with the coexistent $Sb(OH)_6^-$ and SO_4^{2-} (**Sb+SO4**), $Sb(OH)_6^-$ and HCO_3^- (**Sb+HCO3**), $Sb(OH)_6^-$ and $HAsO_4^{2-}$ (**Sb+As**).

4.3.4 Summary

Synthetic MgAl/MgFe-NO_3 and calcined LDH, obtained from hydrotalcite-like [Mg_3^{2+} M^{3+}-c, with M^{3+}= Al^{3+} and/or Fe^{3+}] and zaccagnaite-like [ZnAl-c] compounds, were tested for the $Sb(OH)_6^-$ removal from aqueous solution. Results showed that both calcined and nitrate LDH are able to remove $Sb(OH)_6^-$, and calcined LDH are most effective than LDH-NO_3.

Results of speedy sorption experiments suggest that both MgAl-NO_3 and MgFe-NO_3 LDH remove $Sb(OH)_6^-$ from solution through the formation of a brandholzite-like compounds, while the anion exchange process was not observed but is not excluded; moreover, Al/Fe hydroxides precipitated after partial dissolution of the sorbents, could contribute to the removal of $Sb(OH)_6^-$. The $Sb(OH)_6^-$ removal from solution through the interaction at the liquid/solid interface, between the $Sb(OH)_6^-$ dissolved and the positive surface of the brucite-like sheets of LDH-NO_3, could explain the higher efficacy showed by the 2MgAl-NO_3 LDH that presents the highest excess of positive charge in the brucite-like sheet.

The calcined LDH tested, removed $Sb(OH)_6^-$ through different processes, both fast and effective. As observed in the experiments performed with LDH-NO_3, the calcined hydrotalcite-like phases uptake $Sb(OH)_6^-$ through the neoformation of a brandholzite-like compound; however the calcined phase results more effective than the LDH-NO_3 thanks to the higher reactive surface. The 2ZnAl-c removed the $Sb(OH)_6^-$ by means of the reconstruction of the zincalstibite-like phase, a ZnAl LDH containing the $Sb(OH)_6^-$ intercalated.

The presence of LDH-CO_3 has been detected at the end of experiment with relative low initial $Sb(OH)_6^-$ concentration in solution, performed with both Mg(AlFe)-c and 2ZnAl-c. Further investigation are needed in order to assess the evolution of the removal processes during the first hours of reactions, in particular when both carbonate and antimonate phases are present.

The competition experiments show that coexistent sulfate did not affect the $Sb(OH)_6^-$ removal capacity of both calcined sorbents, whereas in presence of carbonate specie the 2ZnAl-c resulted the most effective. In presence of equal concentrations of $HAsO_4^{2-}$ and $Sb(OH)_6^-$ dissolved, the $Sb(OH)_6^-$ removal capacity of both 2ZnAl-c and Mg(AlFe)-c decrease dramatically. However, the Mg(AlFe)-c removed high amount of $HAsO_4^{2-}$, whereas when the 2ZnAl-c were used, less than 15% of both As and Sb were removed from solution and the at the end of experiment part of the sorbent did not react.

4.4 ATR-IR study of $Sb(OH)_6^-$ removal from aqueous solutions by calcined LDH

4.4.1 State of art

The Total Attenuated Reflection IR spectroscopy (ATR-FTIR) is an analytical method useful to improve the comprehension of sorption processes. ATR-FTIR spectra can provide information about the behavior of inorganic ions onto oxide surfaces, such as differentiation between inner-sphere or outer-sphere complex (Lefèvre, 2004). Moreover, ATR-FTIR allows to record spectra of aqueous solutions and gives some important data on the geometry of the hydrolysis species (Davantès and Lefèvre, 2013; Muller et al., 2008). ATR-FTIR permits the study in situ of sorption processes, a suitable method for sorbents with high reactive surface like metal oxides and LDH. Previous authors used the ATR-FTIR to study the interlayer anion orientation of MgAl-NO_3 LDH (Wang et al., 2007) and the anion exchange processes between SO_4^{2-} and (poly)molybdate using ZnAl-SO_4 LDH (Davantès and Lefèvre, 2013). The adsorption of Sb(V) ion was investigated onto iron oxides by McComb et. al (2007). Previous studies reported that the $Sb(OH)_6^-$ ion contains an octahedral SbO_6 core that exhibits six normal mode vibrations, but only the ν_3 corresponding to the ν(Sb-O) mode asymmetric stretch motion (500-680 cm^{-1}) and the ν_4 relative to the δ(Sb-O) bending motions (230-320 cm^{-1}) are detectable by IR. Studies performed on solid hexahydroxyantimonate salts have identified other bands attributable to $Sb(OH)_6^-$: the ν(O-H) stretch bands at 3220 cm^{-1}, the δ(O-H) and γ(O-H) in plane deformation bands at 1105 and 735 cm^{-1}, respectively (McComb et al., 2007 and reference therein).

In this study the ATR-FTIR spectroscopy was used to better understand the removal processes of $Sb(OH)_6^-$ from solution by calcined LDH. The ATR-FTIR was used to characterize the hydrotalcite-like and zaccagnaite-like compounds and their calcined products; the $Sb(OH)_6^-$ spectrum in aqueous solution was recorded in order to be able to compare it with the spectrum of $Sb(OH)_6^-$ sorbed into LDH. The removal processes were studied between batch and in situ ATR-FTIR experiments.

4.4.2 Materials and methods

4.4.2.1 Instrument

ATR-IR spectra were measured by a dry-air-purged Thermo Scientific Nicolet 6700 spectrometer equipped with a Mercury Cadmium Telluride (MCT) detector. Spectral resolution was 4 cm^{-1} and spectra were averaged over 512 scans. The used ATR accessory is an horizontal diamond/ZnSe crystal (A = 3.14 mm^2) with one internal reflection on the upper surface and an angle of incidence of 45° (Smart MIRacle from PIKE). Data were reprocessed with the OMNIC software.

4.4.2.2 ATR-IR spectra of $Sb(OH)_6^-$ in solution

The $Sb(OH)_6^-$ solutions were prepared by dissolving $KSb(OH)_6$ in Milli-Q water (Millipore, 18.2 MΩ cm^{-1}). Due to the low solubility of antimony salt, the spectra of $Sb(OH)_6^-$ in solutions were determined on 0.05 and 0.025 M solutions. At 0.05 M concentration Sb(V) could form polymers, simulation with MEDUSA database showed that the polymerization occurs at pH <6.5. In order to recover the spectra of Sb polymers, the ATR-IR spectra of $Sb(OH)_6^-$ 0.05 M were determined at different pH values. The pH of solution was adjusted using NaOH or HCl 0.1 N, the ATR-IR spectra were measured with water on diamond/ZnSe crystal as reference spectrum.

4.4.2.3 Characterization of LDH by ATR-FTIR

The ATR-IR spectra of hydrotalcite-like (Mg(AlFe)-CO_3) and zaccagnaite-like (2ZnAl-CO_3) compounds, their calcined products and samples recovered after sorption experiments with 1, 5 and 10 mM $Sb(OH)_6^-$ solutions (§ 4.3) were recorded. The ATR-IR spectra were determined on a film of LDH prepared directly on the surface of the ATR crystal with air as reference spectrum. To obtain a uniform film of sample on the crystal, the sorbents were suspended in Milli-Q water, 1 µL of suspension was pipetted onto the crystal and dried with a slight flow of N_2.

4.4.2.4 Batch experiments

Batch experiments were carried out suspending 0.1g of Mg(AlFe)-c or 2ZnAl-c, under stirring, in 100 ml of $Sb(OH)_6^-$ 10 mM solution. Time of reaction was 24h, experiments were performed at room temperature and free atmosphere. Before the addition of the sorbents and at fixed time, the pH was monitored and small volumes of suspension were sampled for the ATR-FTIR and ICP-OES analyses. The suspensions were filtered through 0.02 µm (filter Sartorius, polycarbonate) and solutions for ICP-OES analyses were acidified with 1% v/v HNO_3 suprapure. The solids for ATR-FTIR analyses were washed with Milli-Q water, put on the crystal and dried with a gentle flow of N_2; the spectra were recorded with air as reference spectrum. At the end of experiments solid sorbents were filtered (0.02 µm), washed with Milli-Q water and dried at room temperature for XRD analyses. XRD patterns were recovered with an automated Panalytical X'pert Pro diffractometer, with Ni-filter and Cu-Kα_1 radiation (λ=1.54060 Å), operating at 40kV and 40mA, with the X'Celerator detector. To compare the results, analogus experiments were performed using Milli-Q water only.

4.4.2.5 In situ ATR-FTIR experiments

Tests in situ were performed with 2ZnAl-c; the ATR-IR spectra were recorded on a film of sorbent in contact with a flux of $Sb(OH)_6^-$ solution, using a flow cell connected to a peristaltic pump (0.6 mL min^{-1}). The film of 2ZnAl-c was deposited on the crystal following the protocol illustrated by Davantès and

Lefèvre (2013): 1 µL of 2ZnAl-c suspension was pipetted onto the crystal and dried with a light flow of N_2, the procedure was repeated three times. Subsequently a drop of water was put on the film to record the background. One experiment was performed with a 5 mM $Sb(OH)_6^-$ solution for 14 hours; another experiment was carried out using a 10 mM $Sb(OH)_6^-$ solution varying the pH in the range of 10-5.2, the pH was modified adding NaOH or HCl 0.1 M. The experiments were performed under controlled atmosphere (N_2 flux) to avoid the contamination of CO_2.

4.4.3 Results and discussion

4.4.3.1 ATR-IR spectra of $Sb(OH)_6^-$ in solution

The ATR-IR spectra of 0.05 and 0.025 M $Sb(OH)_6^-$ solutions do not show high intensity as a consequence of the low concentration of solutions, however it is possible to recognize defined absorption peaks at about 3100, ~1640,~1030, ~990 and ~740 cm^{-1} (fig. 4.25a).

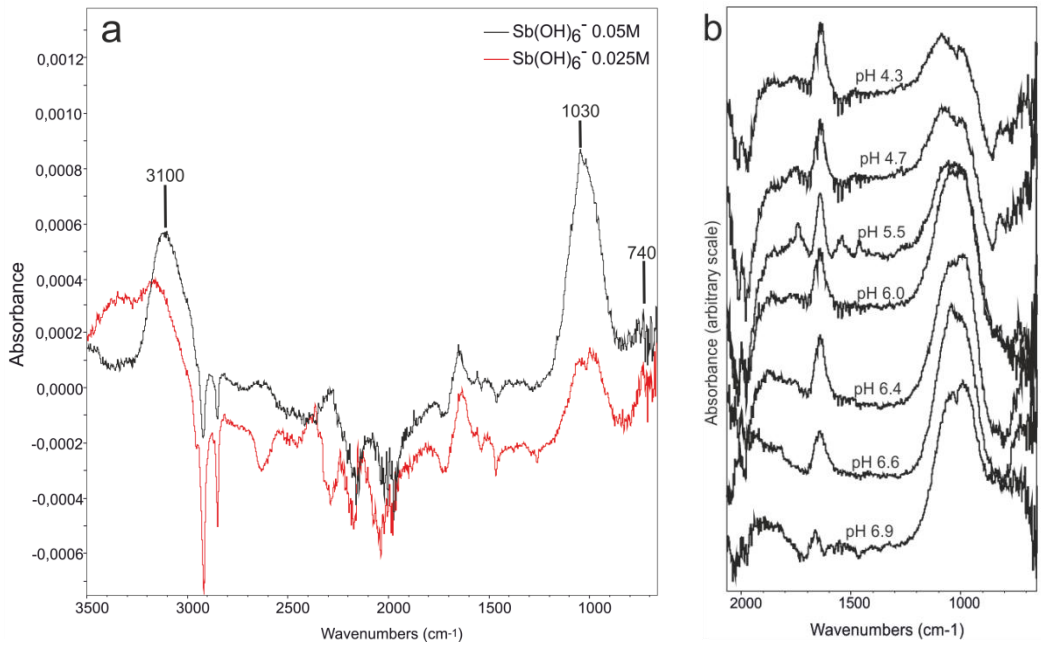

Figure 4.25 (a) ATR-IR spectra of $Sb(OH)_6^-$ in 0.05 and 0.025 M aqueous solutions. (**b**) ATR-IR spectra of $Sb(OH)_6^-$ in 0.05 M aqueous solutions recovered at different pH. Water on the ZnSe crystal was used as reference spectrum.

According to previous studies, the peaks observed in the spectrum can be assigned to the $Sb(OH)_6^-$. The peak at 3100 cm^{-1} is attributed to the O-H stretch [ν(O-H)] mode, the peak at 1030 cm^{-1} observed in the spectrum of $Sb(OH)_6^-$ 0.05M solution is composed by two peak at ~1044 and 980 cm^{-1} (recognized in the $Sb(OH)_6^-$ 0.025M spectrum) assigned to the in-plane deformation [δ(O-H)] mode, and the peak at about 740 cm^{-1} is relative to the out-of-plane O-H deformation [γ(O-H)] mode.

The peak at 1650 cm^{-1} is relative to water, a further water band is visible at 3300 cm^{-1} in the spectrum of $Sb(OH)_6^-$ 0.025M as a broad hunch on the left shoulder of the peak at 3100 cm^{-1}.

The ATR-IR spectra of $Sb(OH)_6^-$ (fig.4.25b) collected at different pH (4.3 < pH < 6.9) do not change significantly, indicating the absence of polymerization or evolution in the geometry of $Sb(OH)_6^-$ in solution. Depending on the change of the intensity of the signal, it is possible recognize two peaks at ~1044 and 980 cm^{-1} also in 0.05 M $Sb(OH)_6^-$ solutions.

4.4.3.2 Characterization of LDH by ATR-FTIR

The ATR-IR spectrum of Mg(AlFe)-CO_3 shows bands ascribable to the LDH structure (fig. 4.26a). The broad band at 3500 cm^{-1} is due to the O-H stretching mode [ν(O-H)] of water molecules in the interlayer and the broad band at about 3000 cm^{-1} is relative to the hydrogen bonds that connected both water molecules and carbonate dispersed in the interlayer (Ferreira et al., 2004 and reference therein). The peak at 1650 cm^{-1} corresponds to the HOH deformation [δ(H-O-H)] of water molecules in the interlayer, while the peak at 1362 cm^{-1} is attributable to the ν_3 asymmetric stretching mode of carbonate in the interlayer. In the ATR-FTIR spectrum of 2ZnAl-CO_3 (fig.4.26b) the peak at 1364 cm^{-1} and the broad band in the region 1500-1670 cm^{-1} are attributable respectively to the presence of carbonate and water in the interlayer (Lozano et al., 2012; He et al., 2010). The region 2800-3600 cm^{-1} is relative to the presence of water molecules and anions in the interlayer. In both Mg(AlFe)-CO_3 and 2ZnAl-CO_3 spectra, the bands in the region below the 1000 cm^{-1} are relative to the vibration metal-oxygen-metal in the brucite-like sheets.

The spectra of calcined solids, Mg(AlFe)-c and 2ZnAl-c, indicate the loss of the layered structure, even if low residual water and carbonates can be still present.

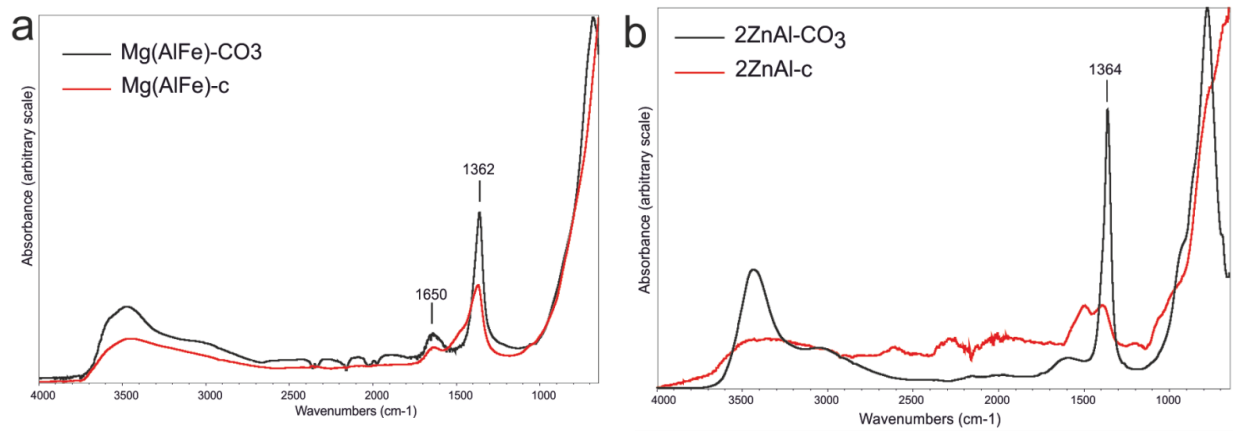

Figure 4.26 ATR-IR spectra of (**a**) Mg(AlFe)-CO_3 and its calcined product, and (**b**) 2ZnAl-CO_3 and its calcined product; with air as reference spectrum.

The sorbents recovered after sorption experiments with different initial $Sb(OH)_6^-$ concentrations in solution (§ 4.3) are marked with the label of the calcined LDH followed by the initial concentration of $Sb(OH)_6^-$.

4.4.3.2.a Mg(AlFe)-c

The ATR-FTIR and XRD results are in agreement. The XRD patterns of samples Mg(AlFe)-c+Sb 1mM and Mg(AlFe)-c+Sb 5 mM show the presence of both brandholzite-like compound and carbonate LDH (fig.4.27a), the intensity of the reflections of the carbonate phase decreases as the initial concentration of $Sb(OH)_6^-$ increases, becoming not detectable in the XRD pattern of sample Mg(AlFe)-c+Sb 10mM. The ATR-IR spectrum of Mg(AlFe)-c+Sb 1mM shows a well defined peak at 1362 cm^{-1} indicating the presence of carbonate in the interlayer accompanied by the water bands at 1650 cm^{-1} and in the region of 3000-3500 cm^{-1} (4.27b). These peaks are visible also in the ATR-IR spectra of the other Mg(AlFe)-c+Sb samples indicating the presence of carbonate in both of them; this means that the carbonate phase is also present in the Mg(AlFe)-c+Sb 10mM samples, but probably is not enough and/or is less ordered to be detectable by XRD.

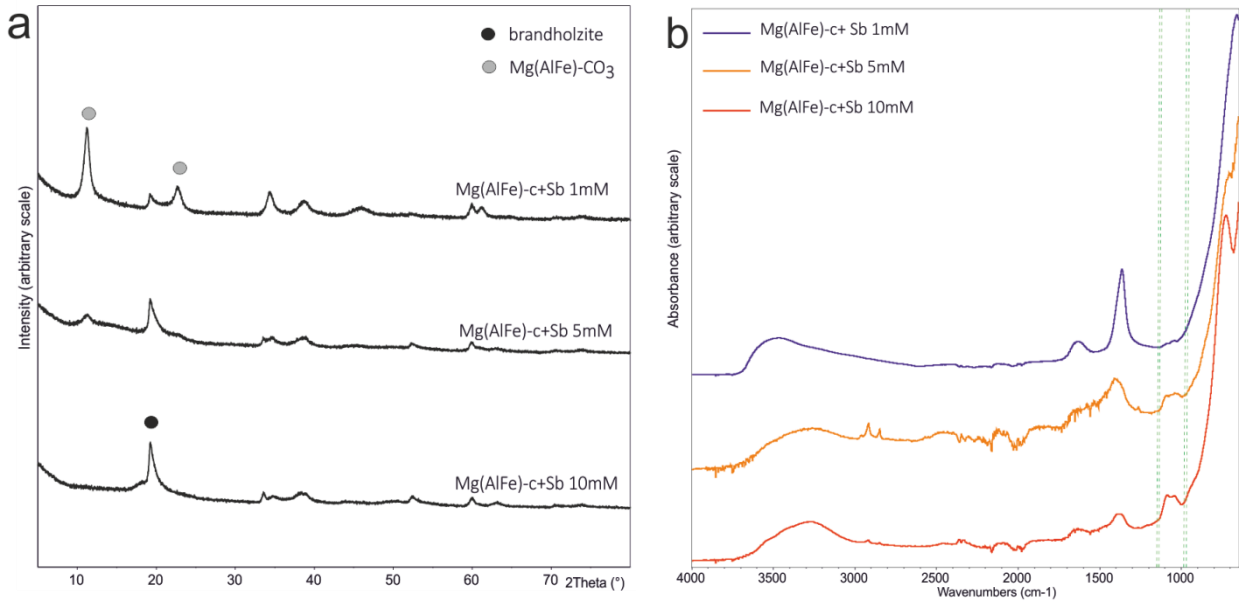

Figure 4.27 (**a**) XRD patterns and (**b**) ATR-IR spectra of Mg(AlFe)-c after sorption experiments performed with different $Sb(OH)_6^-$ concentrations. Air on the crystal was reference spectrum. The green dashed lines delimit the new peaks in the region 1000-1100 cm^{-1} of ATR-IR spectra.

Two peaks at ~1090 and ~1040 cm^{-1}, that not appear in the spectra of the original carbonate LDH or in the calcined samples, are barely visible in the spectrum of Mg(AlFe)-c+Sb 1mM and became clearly visible as the initial concentration of $Sb(OH)_6^-$ increase.

4.4.3.2.b 2ZnAl-c

XRD patterns of 2ZnAl-c recovered after experiments with $Sb(OH)_6^-$ 1 and 5 mM solutions show the presence of both 2ZnAl-CO_3 and zincalstibite-like compounds (fig. 4.28a), while only the antimonate phase is detectable after experiment with 10 mM $Sb(OH)_6^-$ initial concentration. In the same way, in the

ATR-IR spectra of 2ZnAl-c+Sb 1mM the bands of the 2ZnAl-CO_3 (the peak of carbonate at 1362 cm^{-1}, and the water and hydrogen bonds bands in the region 1650 cm^{-1} and 3000-3550 cm^{-1}, respectively) are well defined (fig.4.28b). The peak of carbonate loses intensity in 2ZnAl-c+Sb 5mM and is not visible in the 2ZnAl-c+Sb 10 mM sample, indicating the absence of carbonate.

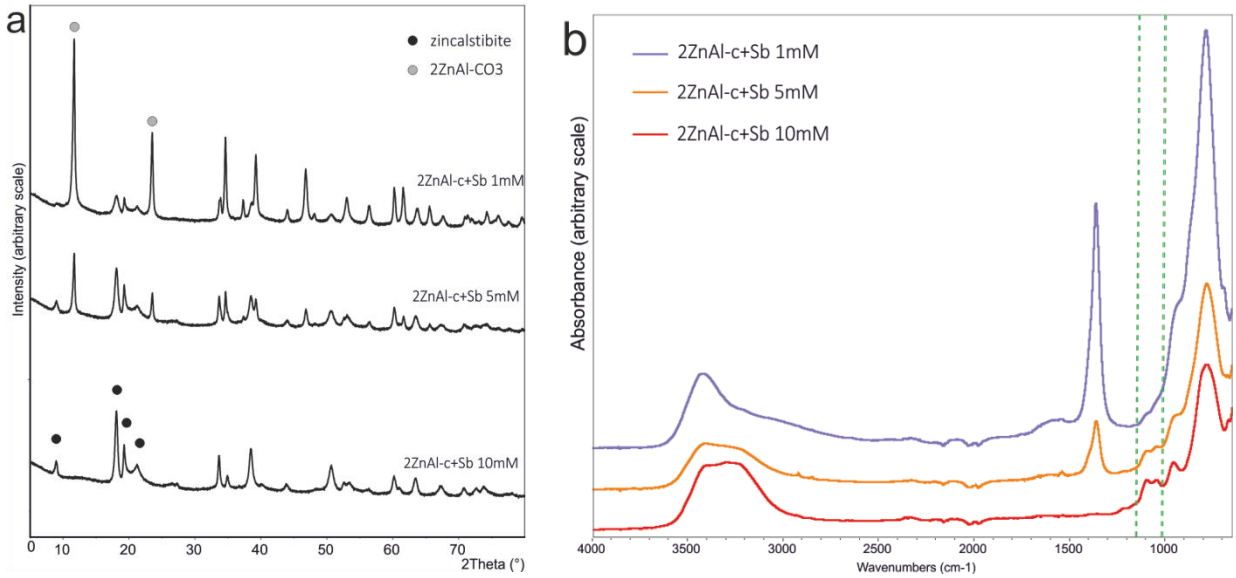

Figure 4.28 (**a**) XRD patterns and (**b**) ATR-IR spectra of 2ZnAl-c after sorption experiments performed with different $Sb(OH)_6^-$ concentrations, air on the crystal was reference spectrum. The green dashed lines delimit the new peaks in the region 1000-1100 cm^{-1} of ATR-IR spectra.

Two new peaks are present in the same position to those observed in the Mg(AlFe)-c +Sb samples (at 1090 cm^{-1} and 1040 cm^{-1}), and become marked as the initial $Sb(OH)_6^-$ concentration of sorption experiments increase.

In figure 4.29 the spectra of sorbents recovered after experiments with $Sb(OH)_6^-$ 10 mM initial concentration, are compared with the spectrum of $Sb(OH)_6^-$ 0.05 M solution. It is possible to note that the new peaks of solids observed in the region 1000 -1100 cm^{-1}, not ascribable to the carbonate phases or their calcined products, are compatible with the peaks assigned to the in-plane deformation [δ(O-H)] mode of $Sb(OH)_6^-$ in solution. The bands of $Sb(OH)_6^-$ at 760 cm^{-1} and 3100 cm^{-1} (not showed in the figure) are not recognizable due to the overlap in the solid by the bands relative to the metal-oxygen-metal and hydrogen bonds vibrations, respectively.

In case of adsorption through outer-sphere complex, the spectrum of the adsorbed specie should be similar to that of the species in solution because there is not significant deformation of the geometry of the molecule, while a little shift between the peaks of the sorbed and of the solution species can occur as a consequence of the change of the liquid-solid environment. Therefore ATR-IR results suggest that the new peaks observed in sorbents recovered after sorption experiments are relative to the presence

of antimony in the solids. The geometry of the $Sb(OH)_6^-$ does not change from the liquid to the solid form, this means that antimony is present in the solids structure as $Sb(OH)_6^-$ specie and is adsorbed through outer-sphere complexes.

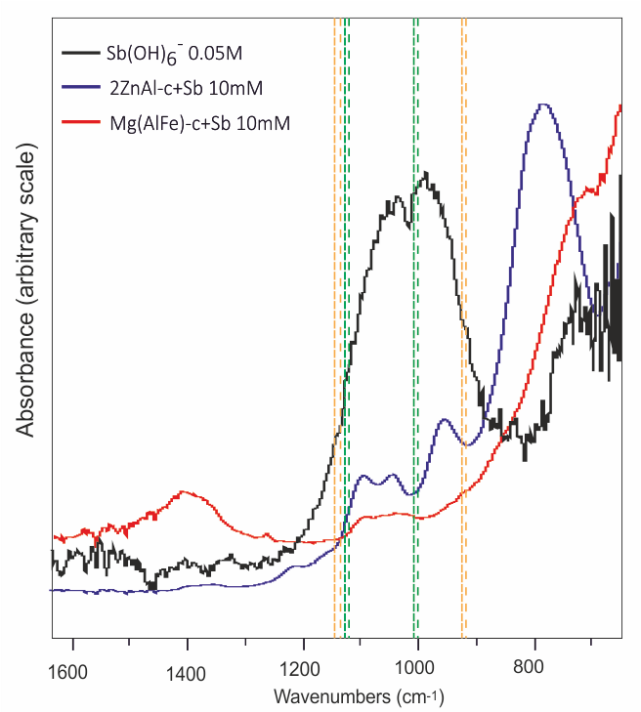

Figure 4.29 ATR-IR spectra of 2ZnAl-c+Sb 10mM and Mg(AlFe)-c+Sb 10mM compared with the spectrum of $Sb(OH)_6^-$ 0.05 M in solution.

The green dashed lines delimit the new peak in the region 1000-1100 cm^{-1}. The orange dashed lines delimit the peaks ascribable to $Sb(OH)_6^-$ 0.05M in solution.

These results are coherent with the formation of brandholzite-like and zaccagnaite-like compounds as $Sb(OH)_6^-$ removal processes by Mg(AlFe)-c and 2ZnAl-c, respectively (§ 4.3). In fact antimony is present in the structure of both brandholzite-like and zaccagnaite-like compounds as $Sb(OH)_6^-$, and is connected with the other units of the structures by means of Coulombic interaction or hydrogen bonds.

It should be considered that it is not possible to recognize or exclude the presence of hydroxyl groups in the interlayer of LDH phases, because the peaks of hydroxyl group in the interlayer (3500-3700 cm^{-1}) fall in the range of the water molecules (Linares et al., 2014).

4.4.3.3 Batch experiments

Samples recovered after the batch experiments are marked with the label of the calcined LDH followed by "+Sb" to indicate experiments performed with $Sb(OH)_6^-$ in solution, or "-blk" for experiments with only Milli-Q water.

4.4.3.3.a Mg(AlFe)-c

In both experiments the sharp increase of pH values indicates the rehydration of the sorbents (table 4.11). Concentration of $Sb(OH)_6^-$ in solution decreased during the time and, at the end of experiments,

the $Sb(OH)_6^-$ removed was about 32%. The sorption capacity was equal to 3.2 mmoles g_{LDH}^{-1} (close to that observed in the sorption experiments performed with different solid/solution ratio (§ 4.3.))

Table 4.11 pH values and $Sb(OH)_6^-$ determined in solution during batch experiments performed with Mg(AlFe)-c.

Mg(AlFe)-c blk			Mg(AlFe)-c +Sb		
time	pH	Sb	time	pH	Sb
h		mmoles L^{-1}	h		mmoles L^{-1}
0	5.6	0	0	5.6	9.8
0.12	10.0	0	0.12	10.0	8.8
1	10.3	0	1	10.2	7.9
2	10.3	0	2	10.2	7.1
4	10.3	0	4	10.1	7.4
24	10.3	0	24	10.8	6.7

The ATR-IR spectra of Mg(AlFe)-c blk show the progressive increase of broad peaks in the region 3600-3000 cm^{-1} and below 1000 cm^{-1} attributable to a gradual reconstruction of the LDH structure, while the peaks at 1362 cm^{-1} and 1645 cm^{-1} indicate the presence of carbonate and water in the interlayer, respectively (fig.30a). Also ATR-IR spectra of Mg(AlFe)-c +Sb show the reconstruction of the layered structure and the entrance of carbonate in the interlayer, while the $Sb(OH)_6^-$ band appears well defined only at the end of experiment (fig.30b). The comparison of spectra recorded at 1 hour (fig.31) suggests that the adsorption of $Sb(OH)_6^-$ onto the Mg(AlFe)-c starts as soon as the solid comes into contact with the $Sb(OH)_6^-$ solution, however further investigations are needed to better understand the evolution of the sorbent surface during the first hours.

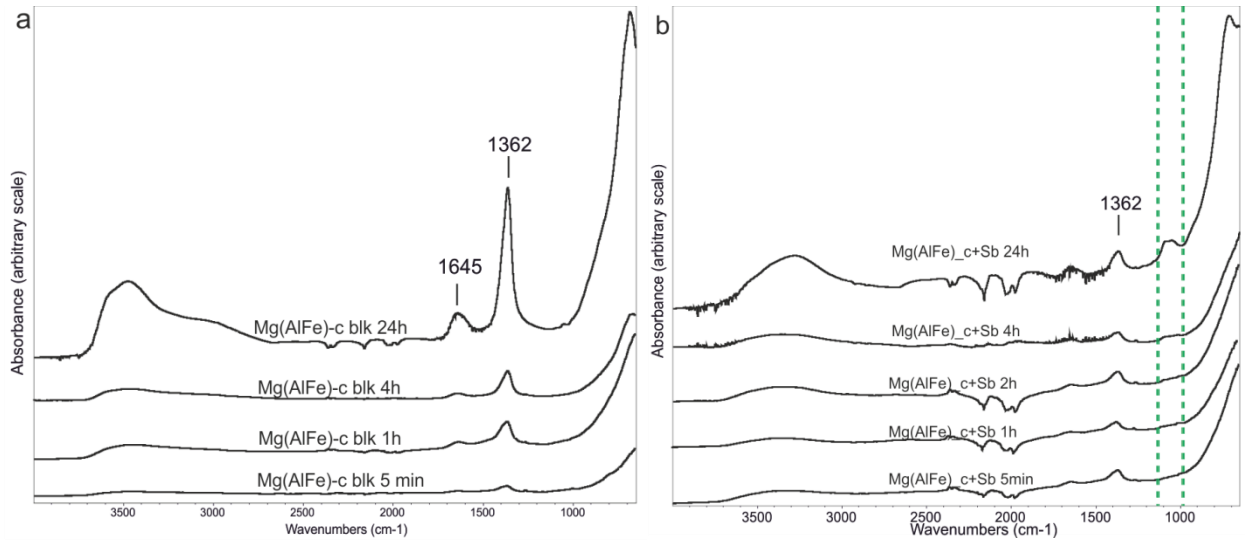

Figure 4.30 ATR-IR spectra of (**a**) Mg(AlFe)-c blk and (**b**) Mg(AlFe)-c +Sb determined at fixed time during batch experiments, with air as reference spectrum.

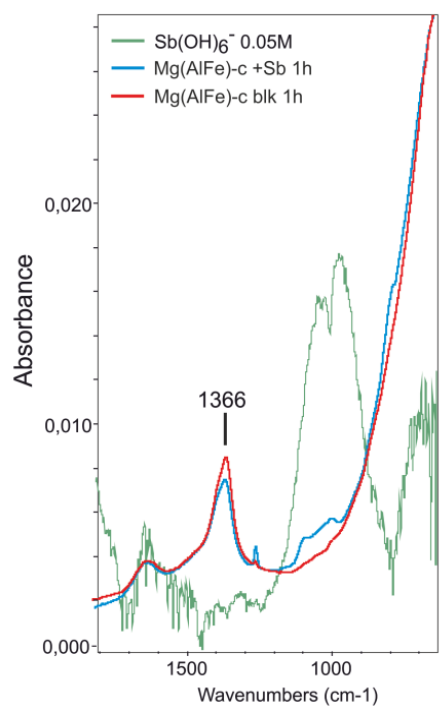

Figure 4.31 ATR-IR spectra of (**a**) Mg(AlFe)-c blk and (**b**) Mg(AlFe)-c +Sb determined 1 hour after the addition of sorbents in solution.

ATR-IR spectrum of $Sb(OH)_6^-$ 0.05M is out of scale.

XRD pattern of Mg(AlFe)-c blk recovered at the end of experiments confirms the presence of LDH-CO_3 through the peaks at low angles ascribable to the basal reflection of hydrotalcite-like compound. The XRD pattern of Mg(AlFe)-c +Sb shows marked peaks at ~18° and 19° 2θ attributable to the brandholzite-like compound, and a broad peak at about 12° 2θ ascribable to LDH-CO_3 (fig.4.32).

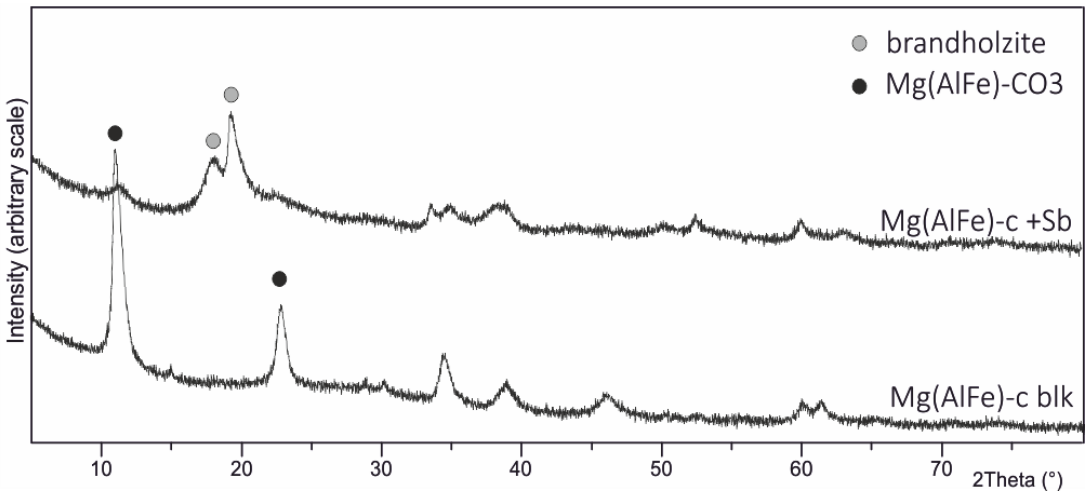

Figure 4.32 XRD patterns of Mg(AlFe)-c blk and Mg(AlFe)-c +Sb samples recovered after batch experiments.

4.4.3.3.b 2ZnAl-c

Also in experiments performed with 2ZnAl-c the sharp increase of pH values indicate the rehydration of the sorbents (table 4.12). Concentration of $Sb(OH)_6^-$ 10 mM solution decreases as 2ZnAl-c was added to solution, and at the end of experiment the $Sb(OH)_6^-$ removed was about 36% and sorption capacity resulted to be 3.6 mmoles g_{LDH}^{-1}.

Table 4.12 pH values and $Sb(OH)_6^-$ determined in solution during batch experiments performed with 2ZnAl-c.

2ZnAl-c blk			2ZnAl-c +Sb		
time	pH	Sb	time	pH	Sb
h		mmoles L^{-1}	h		mmoles L^{-1}
0	5.6	0	0	5.6	9.8
0.4	8.8	0	0.4	9.8	9.1
1	9.3	0	1	10.8	7.1
2	9.2	0	2	10.8	7.3
4	9.0	0	4	10.8	6.7
24	8.0	0	24	9.9	6.3

ATR-IR spectra of both 2ZnAl-c+Sb and 2ZnAl-c blk show a rapid and progressive increase of bands in the region 3600-3000 cm^{-1} and below 1000 cm^{-1} (fig. 4.33), indicating the reconstruction of the layered structure as soon as the sorbents were added to the solutions. In the spectra of 2ZnAl-c blk the progressive increment of carbonate peak, at ~1360 cm^{-1}, is relative to the reconstruction of LDH-CO_3 phase.

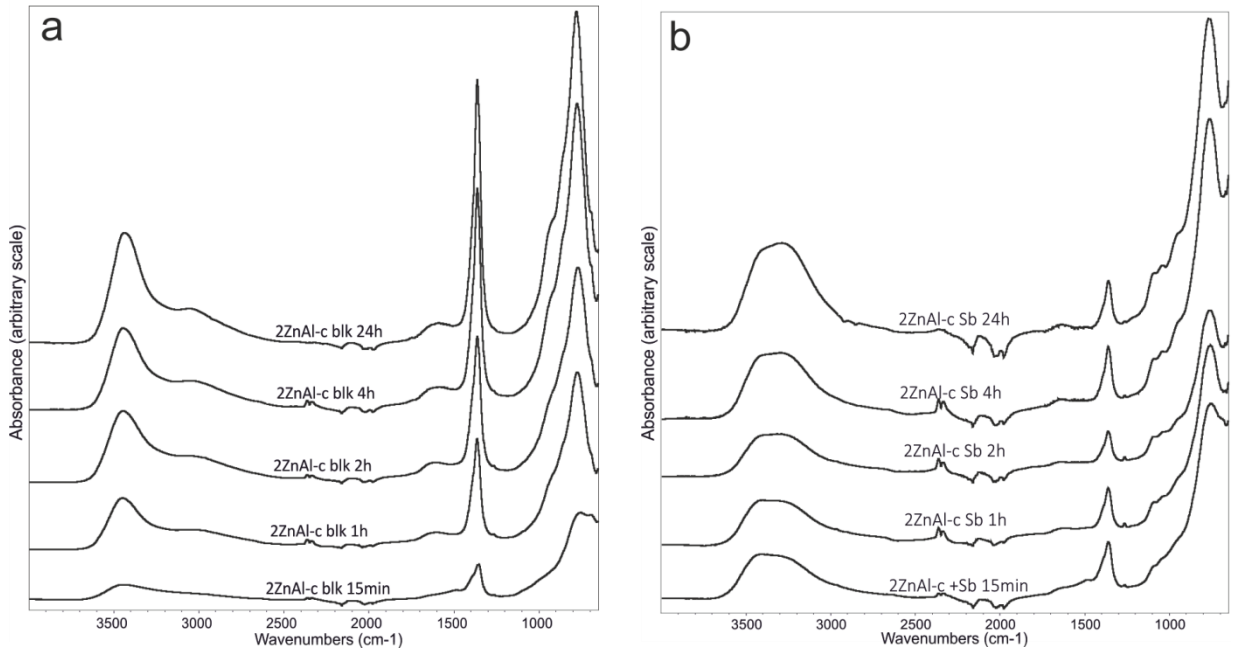

Figure 4.33 ATR-IR spectra of (**a**) 2ZnAl-c blk and (**b**) 2ZnAl-c +Sb determined at fixed time during batch experiments, with air as reference spectrum.

In agreement with the ATR-IR spectra, XRD pattern of 2ZnAl-c blk sample recovered at the end of the experiment shows peaks referable to zaccagnaite-like compound.

The peaks of both $Sb(OH)_6^-$ (region 1100-1000 cm^{-1}) and carbonate (~1360 cm^{-1}) are present in the spectra of 2ZnAl-c +Sb since the beginning of the experiments, suggesting the contemporary adsorption

of these anionic species with the preferential adsorption of antimony during the experiment; however, due to the complexity of the spectra in the region below 1000 cm^{-1}, it is not possible to state with certainty how the structures evolve during experiment. The XRD pattern of 2ZnAl-c+Sb confirms the presence of both zaccagnaite and zincalstibite-like compound, with the predominance of the last one (fig.4.34).

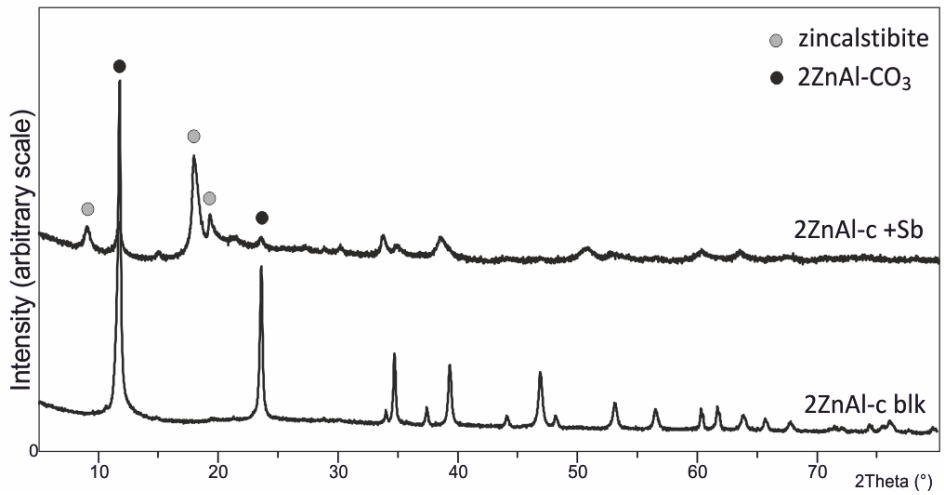

Figure 4.34 XRD patterns of 2ZnAl-c blk and 2ZnAl-c +Sb samples recovered after batch experiments.

4.4.3.4 In situ ATR-FTIR experiments

Spectra of in situ experiment performed with a flux of $Sb(OH)_6^-$ 5 mM solution onto a film of 2ZnAl-c (fig. 4.35) show the sharp decrease of the calcined solid peaks with the contemporary increment of the peaks related to LDH structure as soon as the solution interacts with the sorbent. The evolution of the structure is visible during the first 3 hours, while spectra recorded between 4 and 14 hours (not shown) do not show further evolution of the structure. Although the experiment was performed under controlled N_2 atmosphere, the presence of carbonate was detected at ~1360 cm^{-1}.

In the experiment performed changing pH of solution, the initial pH of $Sb(OH)_6^-$ 10 mM solution was ~6 (fig.4.36). The film of 2ZnAl-c was equilibrated with solution for three hours; successively the pH was increased till 10 and the spectrum was recorded after 20 minutes of riequilibrium between sorbent and solution. This operation was repeated decreasing slowly the pH till 5.2. ATR-IR spectra show the rapid decrease of 2ZnAl-c peaks and the adsorption of $Sb(OH)_6^-$, while the spectra acquired at different pH values do not show significant variations, suggesting that, at these experimental conditions (low amount of sorbent, high concentration of $Sb(OH)_6^-$, atmosphere controlled with a flux of N_2) the pH does not influence the adsorption and does not determine the desorption of $Sb(OH)_6^-$ or the dissolution of the sorbent.

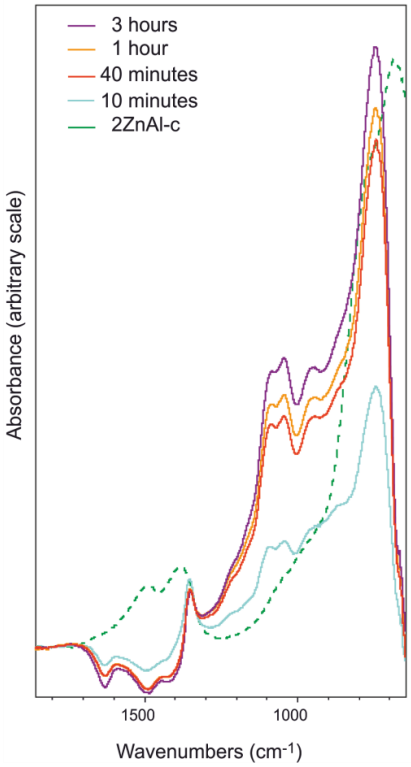

Figure 4.35 In situ ATR-IR spectra recovered as function of time with a flux of $Sb(OH)_6^-$ 5 mM solution onto a film of 2ZnAl-c. A drop of water on the film of sorbent was used as reference spectrum.

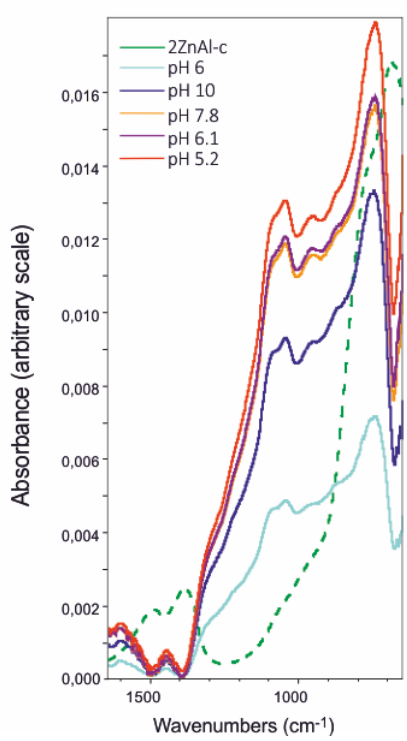

Figure 4.36 In situ ATR-IR spectra recovered at different pH of a flux of $Sb(OH)_6^-$ 10 mM solution onto a film of 2ZnAl-c. A drop of water on the film of sorbent was used as reference spectrum.

4.4.4 Summary

ATR-FTIR was used to characterize the hydrotalcite-like (Mg(AlFe)-CO_3) and zaccagnaite-like (2ZnAl-CO_3) compounds, and their calcined products. Moreover the removal processes of $Sb(OH)_6^-$ from solution by calcined LDH were investigated.

ATR-IR spectra show that both Mg(AlFe)-c and 2ZnAl-c adsorbed $Sb(OH)_6^-$ through the formation of outer-sphere complex; these results, in agreement with the XRD data, are compatible with the formation of either brandholzite-like or zaccagnaite-like compounds as $Sb(OH)_6^-$ removal processes from solution by Mg(AlFe)-c and 2ZnAl-c, respectively. Moreover there is no evidence of other types of sorption processes. The adsorption of $Sb(OH)_6^-$ is very fast and in experiments performed in free atmosphere, ATR-IR spectra indicated that the $Sb(OH)_6^-$ and the carbonate are adsorbed contemporary by both Mg(AlFe)-c and 2ZnAl-c. Some questions are still open and need further investigations: the region of the ATR-IR spectra below 1000 cm^{-1} is composed by the overlap of several signals related to the oxygen-metal-oxygen vibration and it is not possible to distinguish if the development of the carbonate and the antimonate phases is contemporary during the first hours of experiments, or if one of them prevails during the reconstruction of the structures. Moreover the overlap of the signals does not permit to individuate (or exclude) the presence of hydroxyl group in the interlayer of LDH.

4.5 Removal of antimony by LDH: sorption test with antimony polluted water collected at Su Suergiu abandoned mine

4.5.1 Mine water

The antimony removal capacity of calcined LDH, Mg(AlFe)-c and 2ZnAl-c, was tested on the antimony polluted water sampled in the abandoned mine of Su Suergiu (§ 3). The mine area of Su Suergiu is in the south east of Sardinia; the mineralization is hosted in Paleozoic black schists and metalimestones, and consists of stibnite, scheelite, pyrite and arsenopyrite with quartz and calcite in the gangue (Funedda et al., 2005). The ore were mined underground since the 1858, while the foundry activity started in 1892. After the definitive closure of all activities in 1987, mining wastes and foundry slags have been left on the ground, without actions addressed to mitigate the environmental impact; the volume of slag heaps is estimated at about 66,000 m^3 (RAS, 2003).

The waters draining the mine area are characterized by slightly alkaline pH and oxidizing conditions, with high concentrations of antimony (up to 10^4 µg L^{-1}) and arsenic (up to 10^3 µg L^{-1}) (Cidu et al., 2012). The highest concentrations of antimony are usually detected in the waters flowing downstream of the foundry slag. These waters also contain high concentration of arsenic, sulfate and bicarbonate that may compete with antimony in the sorption processes. For these reasons the slag drainage was chosen to perform the sorption test with LDH; in the present case the water was collected at the sampling point SU1 (fig.4.37), under low flow conditions (date of sampling 30.6.2014).

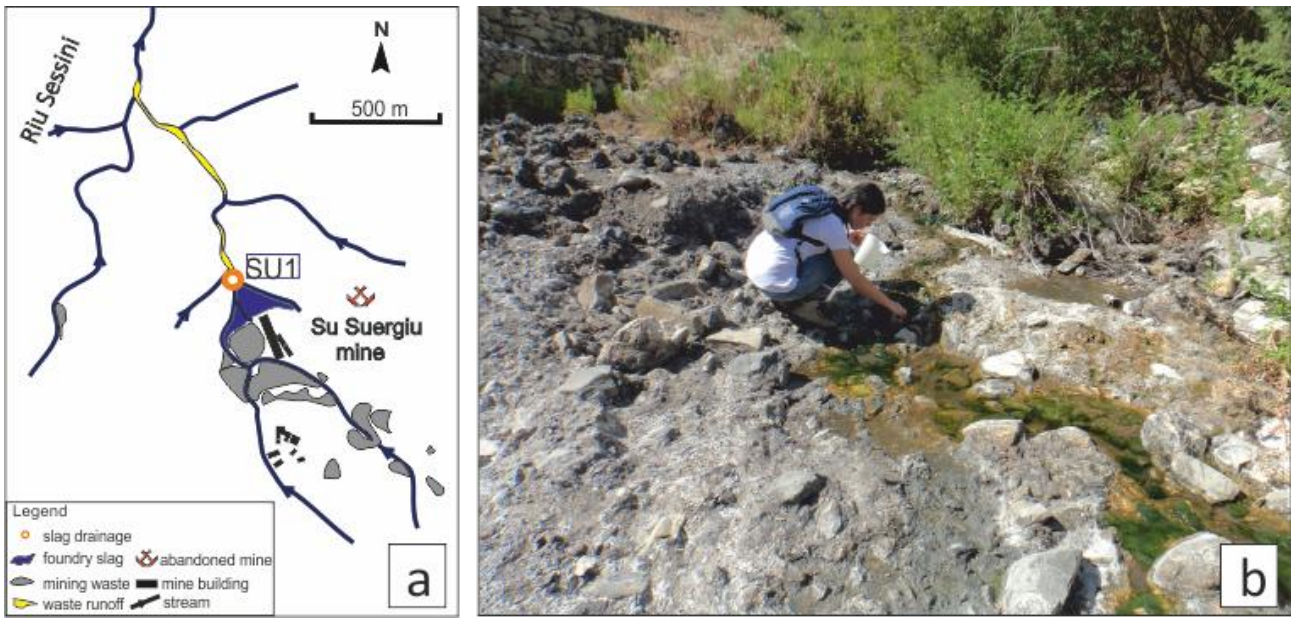

Figure 4.37 (**a**) Location of the sampling point SU1 and (**b**) sampling operation.

The physical and chemical parameters (T°C, pH, EC and Eh) were measured at the sampling site; 4 L of unfiltered water were sampled for sorption experiments in HDPE bottles, whereas other aliquots were filtered through 0.45 µm (OlimPeak, polypropylene) and acidified with 1% v/v HNO_3 suprapure for analyses by ICP-MS and ICP-OES, or with 1% v/v HNO_3 suprapure plus 0.2 w/v tartaric acid for Sb(III) analyses by ASV; the aliquot for analysis of major ions by IC was only filtered.

4.5.2 Sorption experiments

Water for sorption experiments was filtered (0.45 µm) in laboratory few hours after the sampling and stored in HDPE bottles at 4°C for one night; batch experiments started less than 24 hours after the sampling. Different solid/solution ratios were used: 0.1, 0.25, 0.5 and 1 g of 2ZnAl-c or Mg(AlFe)-c were suspended in 400 ml of SU1 water. Experiments performed with Mg(AlFe)-c are labeled as A (1 g of sorbent), B (0.5 g), C (0.25 g) and D (0.1 g), whereas experiments carried out with 2ZnAl-c are: E (1 g), F (0.5 g), G (0.25 g) and H (0.1 g). Experiments were performed at room temperature; time of reaction was 24 hours under vigorous stirring. Before the addiction of the sorbents and at fixed time (0, 0.3, 1, 3, 5 and 24 hours) pH of solutions was measured. At the end of the experiments, the solutions were recovered for chemical analyses using a filtration system (0.45 µm, filters Nuclepore polycarbonate) connected to a vacuum pump. For each solution an unacified aliquot was used for analyses of major ions by IC and another was acidified with 1% v/v HNO_3 for ICP-OES and ICP-MS analyses. After the filtration, solid sorbents were washed with distilled water and dried at room temperature. Mineralogical analyses of sorbents, before and after experiments, were carried out by powder X-ray diffraction (XRD).

4.5.3 Results and discussion

4.5.3.1 Mine water (SU1)

Water sampled showed slightly alkaline and oxidizing conditions, the high value of EC is related to the high content of calcium and sulfate. Chemical composition was Ca-sulfate dominant, with sulfate deriving from the oxidation of sulfides; the presence of carbonate species avoided the decrease of pH (§ 3.5). As a consequence of the interaction with the foundry slag, the solution showed high concentration of Sb(tot) (9900 µg L^{-1}) and As (3386 µg L^{-1}) (table 4.13). Concentration of Sb(III) was determined to be 147 µg L^{-1}. Results of speciation calculation indicated that Sb(V) and Sb(III), respectively occur as $Sb(OH)_6^-$ (100%) and $Sb(OH)_3$ (99.9%) aqueous species (§ 3.4).

Table 4.13 The pH, EC values and concentrations of major ions, Zn, Al, Fe, Sb(tot) and As determined in SU1 water before and after sorption experiments.

	sample	amount of sorbent	label	EC	pH	SO_4^{2-}	HCO_3^-	Cl	F	Ca	Mg	Na	K	Zn	Al	Fe	Sb(tot)	As	Sb rem	As rem
		g		uS/cm		mg L^{-1}				mg L^{-1}				µg L^{-1}			µg L^{-1}		%	
	SU1			2400	8.2	1006	485	59	1.7	362	63	166	7	30	< 29	< 20	9900	3386		
SU1 +	MgAlFe-c	1	A	1745	9.7	771	18	63	0.1	129	59	162	4.6	< 18	< 29	< 20	1008	< 0.5	90	100
SU1 +	MgAlFe-c	0.5	B	1990	9.4	956	29	63	0.1	80	109	166	4.8	< 18	< 29	< 20	432	6.5	96	100
SU1 +	MgAlFe-c	0.25	C	2120	9.2	1048	48	64	0.4	68	140	166	4.6	< 18	18	140	169	25	98	100
SU1 +	MgAlFe-c	0.1	D	2240	8.4	1066	127	64	0.8	131	120	166	4.7	< 18	700	< 20	9830	150	4	96
SU1 +	2ZnAl-c	1	E	2040	7.9	958	80	63	0.3	244	25	163	4.3	242	28	< 20	20	4.5	100	100
SU1 +	2ZnAl-c	0.5	F	2140	8.0	1008	125	63	0.5	234	45	167	4.8	260	67	< 20	34	8.3	100	100
SU1 +	2ZnAl-c	0.25	G	2240	8.1	1054	169	65	1.1	264	56	161	4.4	174	105	< 20	78	35	99	99
SU1 +	2ZnAl-c	0.1	H	2330	8.1	1077	252	64	1.6	278	62	168	4.4	1485	78	< 20	6190	92	41	97

4.5.3.2 SU1 + Mg(AlFe)-c

Solutions recovered at the end of experiments performed with Mg(AlFe)-c showed significant decrease of EC values especially for A and B experiments, combined with the decrease of Ca and/or HCO_3^- concentrations (table 4.13). A significant decrease of dissolved SO_4^{2-} was also observed in experiment A. Moreover in experiments B, C and D the increase of Mg concentrations in solutions indicated the partial dissolution of the sorbents (fig. 4.38).

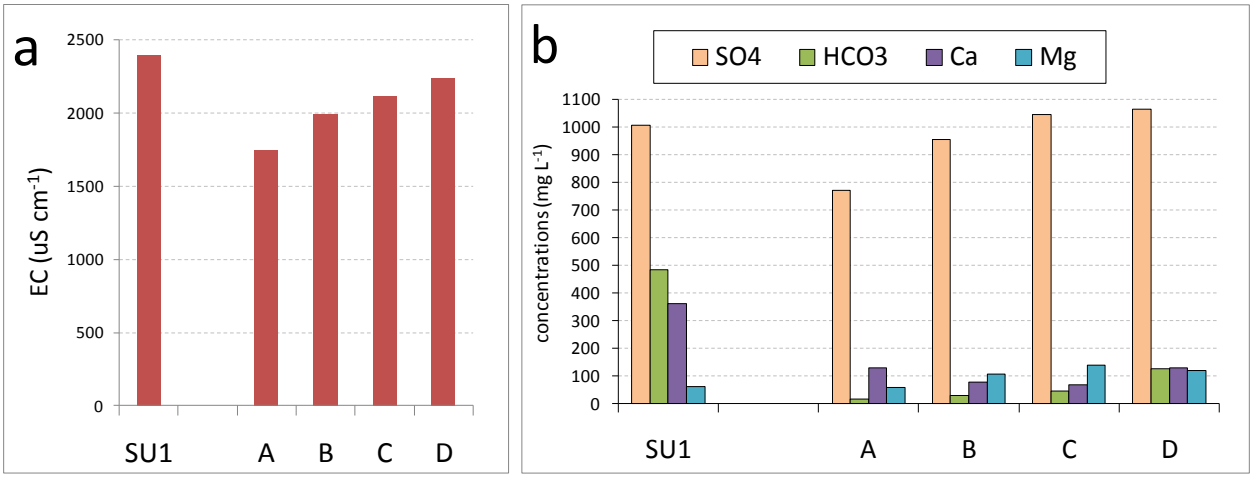

Figure 4.38 (**a**) EC values and (**b**) concentrations of SO_4^{2-}, HCO_3^-, Ca and Mg determined in SU1 sample and in solutions recovered after experiments performed with 1 g (**A**), 0.5 g (**B**), 0.25 g (**C**) and 0.1 g (**D**) of Mg(AlFe)-c.

After the addition of Mg(AlFe)-c in solution, the increment of pH observed was related to the amount of sorbent used. The pH increased sharply in solution of experiments A and B, the increment was less sharp in solution of experiment C while the variation of pH was very limited in the experiment with the lowest amount of sorbent (fig.4.39).

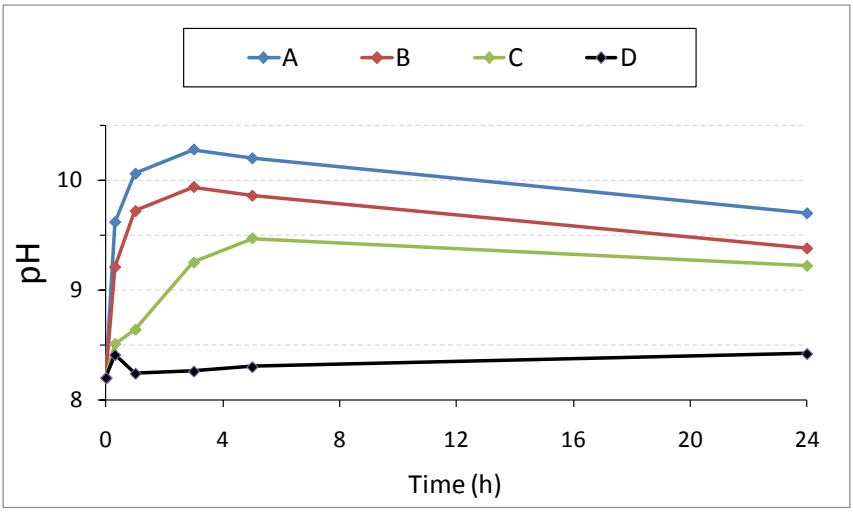

Figure 4.39 Variation of pH values determined in solution in function of the time in sorption experiments performed with 1 g (**A**), 0.5 g (**B**), 0.25 g (**C**) and 0.1 g (**D**) of Mg(AlFe)-c.

At the end of experiments B and C more than 95% of Sb(tot) was removed from the solutions, in experiment A was about 90% while less than 5% Sb(tot) was removed in experiment D. In all experiments more than 96 % of As was removed (fig.4.40).

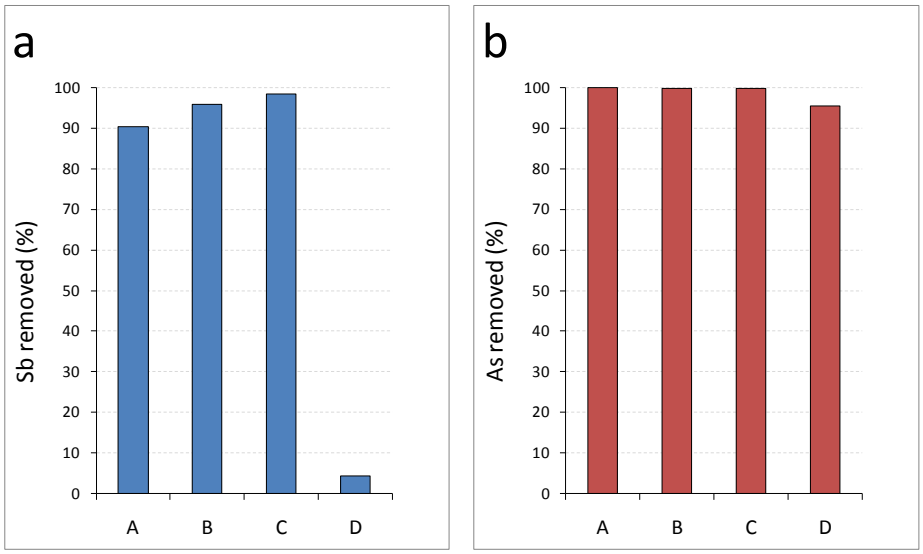

Figure 4.40 Percentage of Sb(tot) (**a**) and As (**b**) removed from solutions at the end of experiments performed with 1 g (**A**), 0.5 g (**B**), 0.25 g (**C**) and 0.1 g (**D**) of Mg(AlFe)-c.

XRD patterns of sorbents recovered after experiments A, B and C show the peaks at low angular positions attributable to the layered structure of LDH, whereas only the peak at ~10° 2θ is barely visible in the XRD pattern relative to the experiment D (fig.4.41). The XRD patterns of all samples contain also well defined peaks ascribable to calcite, whereas the peaks belonging to the brandholzite-like compounds were never detected.

These results suggest that the increase of pH values, related to the rehydration of the Mg(AlFe)-c, favored the precipitation of calcite thanks to the prevalence of CO_3^{2-} as carbonate species and the high concentration of Ca in the SU1 water.

The highest values of pH (up to 10.3), were measured during experiment A. However, the concentration of Ca in solution at the end of experiment was higher than in solutions of experiments B and C suggesting a minor calcite precipitation. It is possible that, due to the high amount of sorbent, the precipitation of calcite was partially inhibited by the uptake of CO_3^{2-} during the reconstruction of the LDH structure. On the contrary, in experiments B and C, even if the pH values were lower, the minor quantities of sorbents needed less CO_3^{2-} for the reconstruction of the LDH structure thus permitting the precipitation of a greater amount of calcite.

At the pH values determined in all experiments, the As prevails in solution as $HAsO_4^{2-}$; this species has high affinity with the LDH (Türk et al., 2009), therefore As should be removed from solution through the entry in the interlayer region.

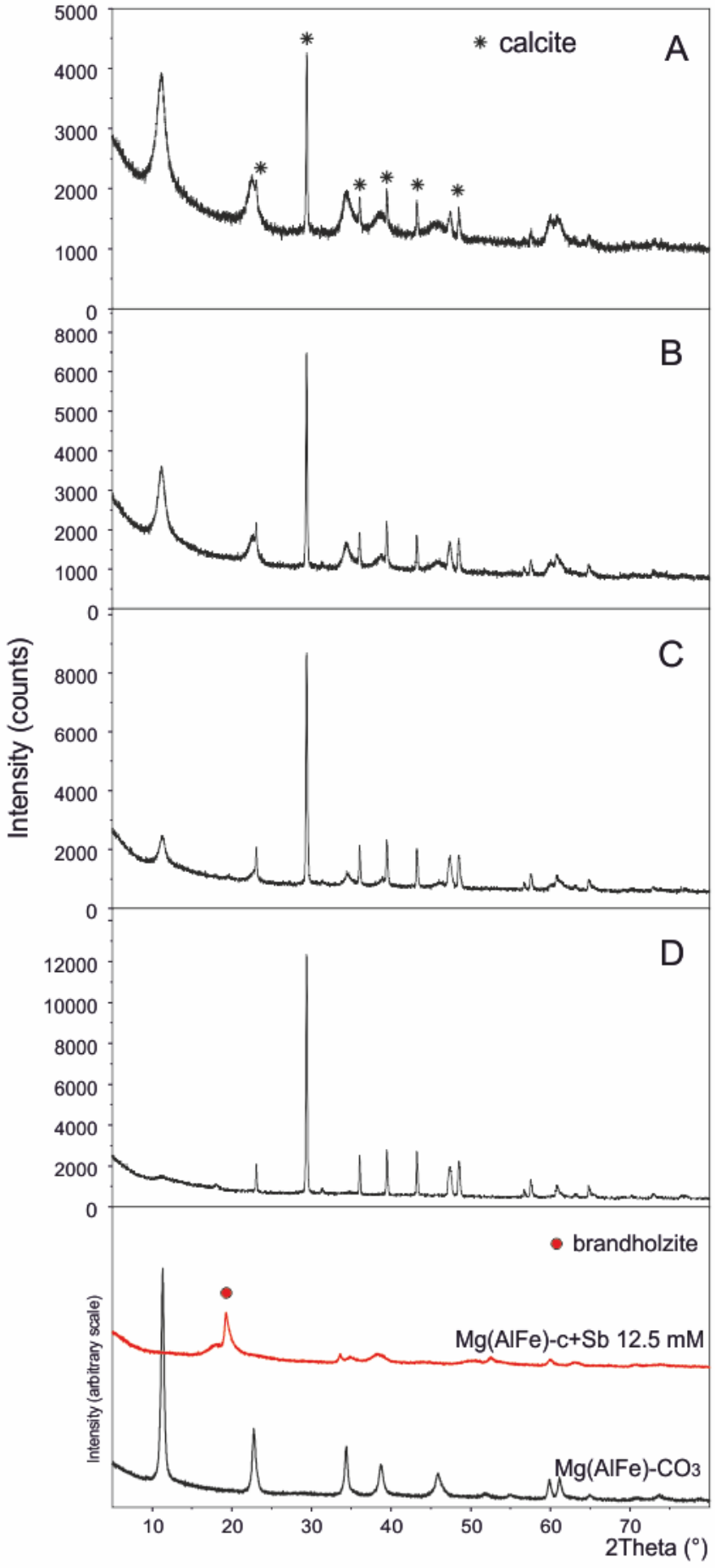

Figure 4.41 XRD patterns of sorbents recovered after experiments performed with 1 g (**A**), 0.5 g (**B**), 0.25 g (**C**) and 0.1 g (**D**) of Mg(AlFe)-c.

XRD pattern of Mg(AlFe)-CO_3 and the sorbent recovered after the sorption experiment performed with initial concentration 12.5 mM of $Sb(OH)_6^-$ in solution are reported to compare the results.

Being the initial concentration of Sb(tot) in the SU1 water too low to reach the saturation of brandholzite, it is probable that also Sb(tot) was removed from solution by means of the incorporation in the interlayer during the reconstruction of the LDH.

The concentrations of Mg determined in solution at the end of experiments B and C indicate the dissolution of the sorbents, but not resulted in the experiment A. In experiments B and C the Sb(tot) removed from solution (96% and 98%, respectively) was higher than in experiment A (90%) even if the amounts of sorbents were lower. This different efficacy in the Sb(tot) removal can be attributable to the different pH values of solutions. In fact, even if in experiment A was used the greatest amount of sorbent and there is no evidence of its dissolution, the high pH values implies that also the OH^- can compete for the entry in the interlayer. Moreover, as a consequence of the dissolution of the sorbents in experiments B and C, both Sb(tot) and As could be sorbed also by amorphous Al and/or Fe hydroxides.

In general, the thickness of the interlayer can give important information about the nature and the orientation of the anionic species intercalated (Palmer et al., 2009; Wang et .al 2009 and reference therein). In the present case could be useful to distinguish the prevalent species in the interlayer to better understand the removal processes. The thickness of LDH intercalated with OH^- should be lower than CO_3^{2-} (Cavani et al., 1991; Koritnig et al., 1975), however, also $HAsO_4^{2-}$ and Sb(tot) (and SO_4^{2-} in experiments A and B) can influence the thickness of the interlayer. Therefore, more detailed analyses of solids recovered after experiments are needed in order to better characterize the interlayer composition.

In experiment D the low amount of Sb(tot) removed from solution may be attributable on several factors.

The concentration of Mg in solution indicates the dissolution of at least 69 wt% of Mg(AlFe)-c used, therefore the amount of anions that can be intercalated during the reconstruction of the LDH structure decreases significantly. Moreover, the amount of Mg(AlFe)-c is not enough to increase considerably the pH of solution during the rehydration, thus the competition effect operated by CO_3^{2-} or OH^- decreases. Results indicate that in these conditions, even if the concentration of Sb(tot) was higher than that As, the $HAsO_4^{2-}$ is removed from solution better than Sb(tot), maybe due to its major affinity with the LDH. In addition also amorphous Al end Fe hydroxides may have contributed to the removal processes.

4.5.3.3 SU1 + 2ZnAl-c

Solutions recovered at the end of experiments performed with ZnAl-c showed, with respect to the SU1 water, lower EC values mainly due to the decrease of HCO_3^- and Ca concentrations that is more pronounced with increasing the amount of sorbent used (fig.4.42). Moreover the concentrations of Zn and Al in solution indicate a low dissolution of sorbents (table 4.10).

During the first hours after the addition of the sorbent, low increase of pH values, attributed to the rehydration of 2ZnAl-c, was determined only in solutions of experiments E and F (fig.4.43).

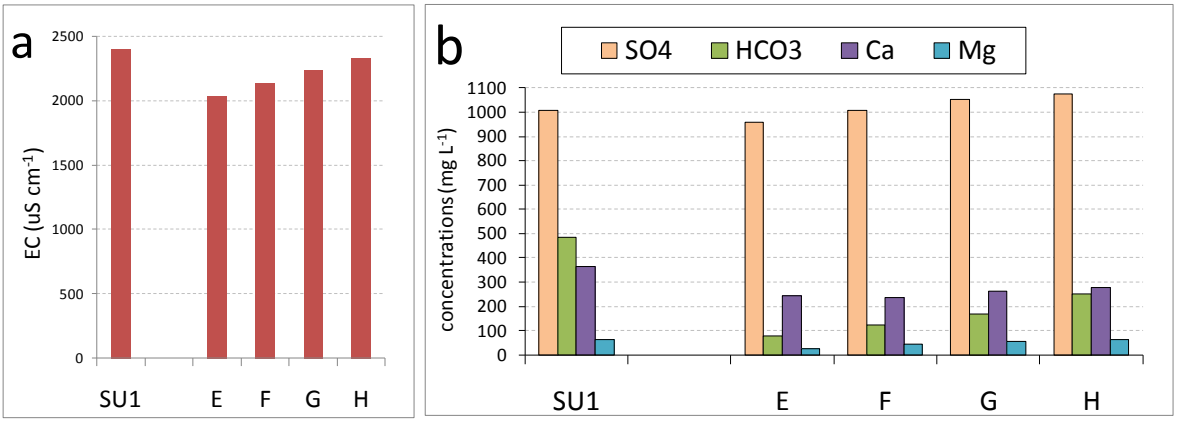

Figure 4.42 (**a**) EC values and (**b**) concentrations of SO_4^{2-}, HCO_3^-, Ca and Mg determined in SU1 sample and in solutions recovered after experiments performed with 1 g (**E**), 0.5 g (**F**), 0.25 g (**G**) and 0.1 g (**H**) of 2ZnAl-c.

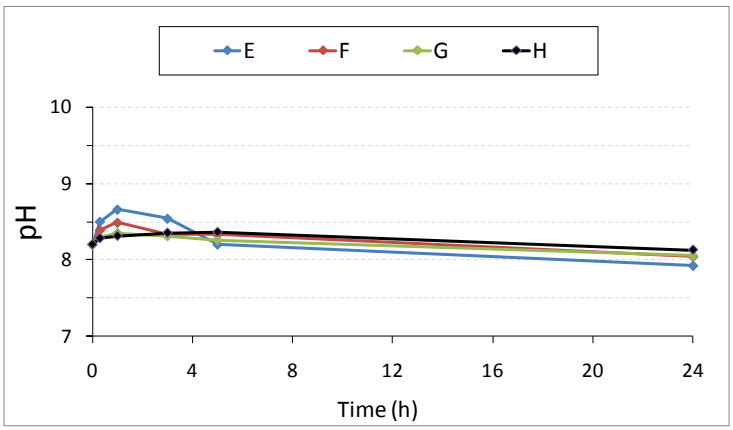

Figure 4.43 Variation of pH values determined in solution in function of the time in sorption experiments performed with 1 g (**E**), 0.5 g (**F**), 0.25 g (**G**) and 0.1 g (**H**) of 2ZnAl-c.

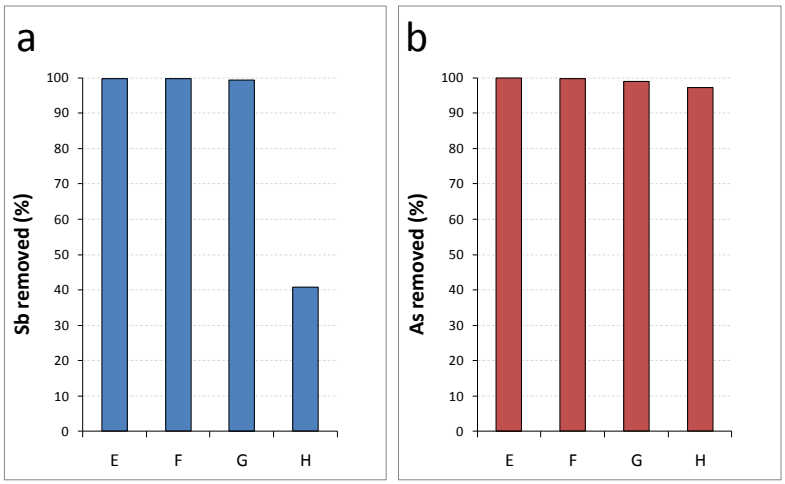

Figure 4.44 Concentration of Sb (**a**) and As(**b**) determined in SU1 sample and in solutions recovered after experiments performed with 1 g (**E**), 0.5 g (**F**), 0.25 g (**G**) and 0.1 g (**H**) of 2ZnAl-c.

At the end of experiments E, F, and G both Sb(tot) and As in solution are totally removed from solution or nearly so; only at the end of experiment H the Sb(tot) removed from solution was about 40% whereas As removed was 97 % (fig.4.44).

XRD patterns of all sorbents recovered after experiments show peaks at the same angular position of the basal reflection belonging to the original phase 2ZnAl-CO_3, also the peaks ascribable to calcite are present in experiments E, F and G (fig.4.45).

The decrease of both Ca and Mg concentrations determined in solution at the end of experiments E, F and G, is attributable to the precipitation of calcite. In general in experiments performed with 2ZnAl-c is observed a minor decrease of Ca concentrations with respect the analogous experiments performed with the Mg(AlFe)-c, indicating the precipitation of minor amount of calcite, maybe due to the different ranges of pH values determined in the experiments performed with the two different sorbents.

Considering that in the SU1 water the concentration of HCO_3^- was very high with respect to Sb(tot), and that the 2ZnAl-CO_3 LDH phase prevails in the final solids of experiments E, F, and G, it is plausible that the Sb(tot) is removed from solution by means of the incorporation in the interlayer region during the rehydration of the 2ZnAl-c phase. Nevertheless, it is not possible to exclude the formation of the antimonate LDH (zincalstibite) in amount not detectable with the XRD analyses.

In the range of pH measured during the experiments, the As prevails in solution as $HAsO_4^{2-}$. Considering the high affinity of $HAsO_4^{2-}$ for LDH having ZnAl cationic composition (Ardau et al., 2013), probably also $HAsO_4^{2-}$ enters as minor component in the interlayer of the reconstructing 2ZnAl-CO_3 LDH. Moreover, both $HAsO_4^{2-}$ and Sb(tot) could be adsorbed onto amorphous Al-hydroxides precipitated after the dissolution of low amount of sorbents.

The solid recovered after the experiment H shows the peaks at low angular range relative to the basal reflection of the 2ZnAl-CO_3 LDH and a peak at about 18° 2θ attributable to the zincalstibite-like compound. The defined peaks at ~16.8°, 20° and 29° 2θ are ascribable to the monohydrocalcite; furthermore a broad hump in the range 30-40° 2θ indicates that part of 2ZnAl-c did not react at the end of the experiment (fig.4.45). A possible explanation may be that the amount of sorbent used was too low, therefore the CO_3^{2-}, derived from the dissociation of HCO_3^- to buffer the increment of pH subsequent to the rehydration of the 2ZnAl-c, was not enough and the reconstruction of the carbonate LDH and the precipitation of calcite were hindered. In these conditions the competition of CO_3^{2-} with respect to Sb(tot) decreases and it is possible the reconstruction of both 2ZnAl-CO_3 and zincalstibite-like structure. Furthermore, due to its higher affinity for LDH interlayer and its initial lower concentration with respect to Sb(tot), As was almost completely removed, while the less affine SO_4^{2-} remained in solution. Also in this case the precipitation of Al as amorphous Al-hydroxides could contribute to the Sb(tot) and As removal from solution.

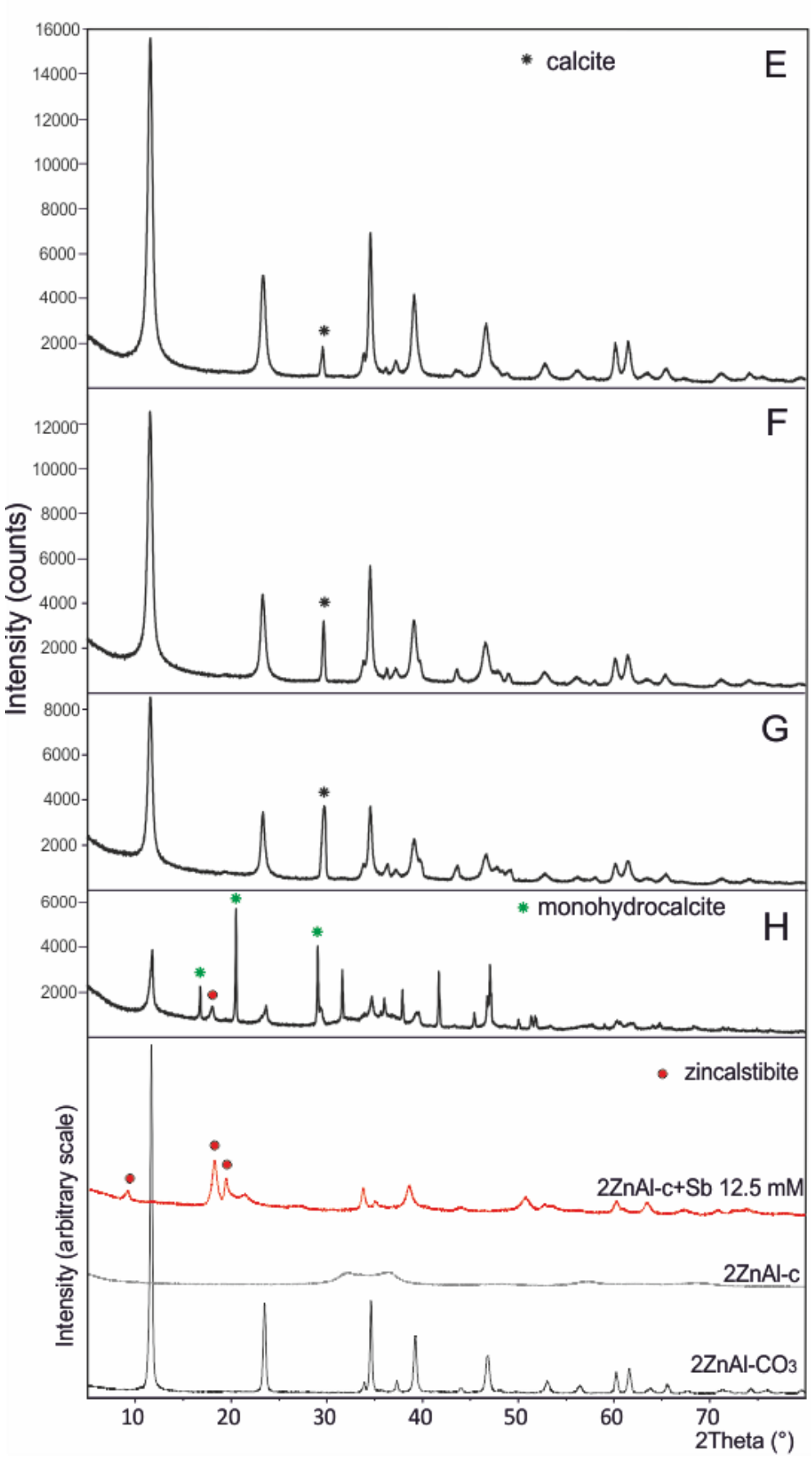

Figure 4.45 XRD patterns of sorbents recovered after experiments performed with 1 g (**E**), 0.5 g (**F**), 0.25 g (**G**) and 0.1 g (**H**) of 2ZnAl-c.

XRD patter of 2ZnAl-CO_3, its calcined product and the sorbent recovered after the sorption experiment performed with initial concentration of $Sb(OH)_6^-$ 12.5 mM in solution are reported to compare the results.

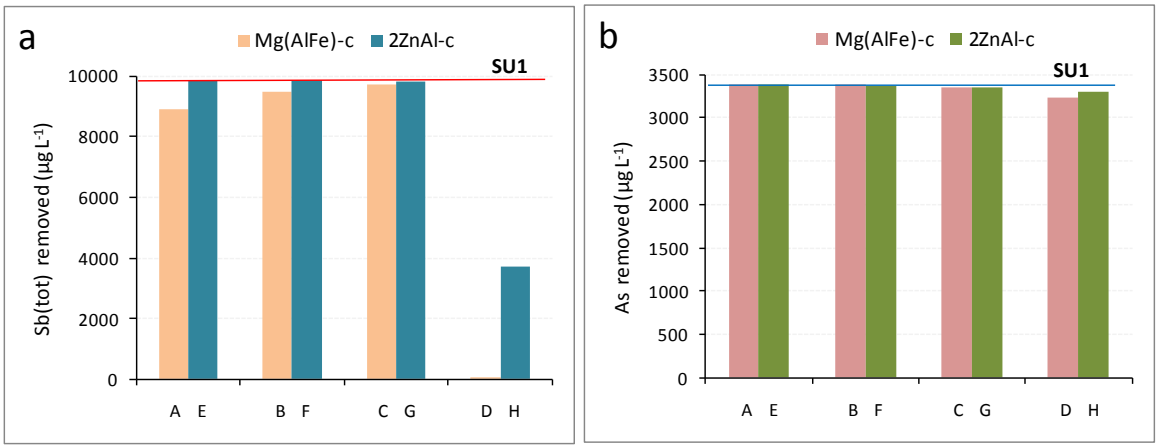

Figure 4.46 Concentrations of (a) Sb(tot) and As (b) removed from SU1 water at the end of sorption experiments. The red line (a) and the blue line (b) indicate the initial Sb(tot) and As concentrations, respectively.

Comparing the concentration of Sb(tot) and As removed from solution at the end of experiments by Mg(AlFe)-c and 2ZnAl-c, it is possible to note that 2ZnAl-c removed Sb(tot) better than Mg(AlFe)-c, whereas the sorbents show similar As removal capacity (fig.4.46). Supposing that both Mg(AlFe)-c and 2ZnAl-c removed Sb(tot) by its intercalation in the interlayer region of reconstructed LDH, the difference in the amount of Sb(tot) removed could be attributable to the higher pH reached in solution during the experiments with Mg(AlFe)-c, that implies the major competition for the entry in the interlayer operated by CO_3^{2-} and OH^- against Sb(tot). Another reason could be the major dissolution of the sorbents detected in the Mg(AlFe)-c experiments. In this case part of the contaminants in solution could be adsorbed by the amorphous Al-Fe hydroxides precipitated in solution that have high sorption capacity at low pH. Most detailed analyses of solids recovered after sorption experiments are needed in order to better understand the presence of secondary phases (i.e. amorphous Fe and/or Al hydroxides) and their role (in presence of LDH) in the removal of Sb(tot) and As from solution.

4.5.4 Summary

Sorption experiments were performed with the slag drainage collected at Su Suergiu, characterized by slightly alkaline pH and high concentrations of both antimony and competitor anions in solution. The results confirm the good antimony removal capacity of both Mg(AlFe)-c and 2ZnAl-C, and encourage further investigations; moreover in all experiments also good arsenic removal capacity was observed.

It was noted that due to the relative low concentration of antimony in the SU1 water, compared to antimony concentration utilized in the sorption experiments performed with synthetic solutions, the formation of brandholzite was never detected as antimony removal process in experiment performed with Mg(AlFe)-c, while the presence of the zincalstibite-like compound was observed only in one experiment in which the 2ZnAl-c was used.

Results showed that the key factor is the solid/liquid ratio that, in particular in experiment performed with Mg(AlFe)-c, determined the variation of pH and thus the evolution of the entire processes in

solutions. The dissolution of both Mg(AlFe)-c and 2ZnAl-c were detected in some experiments. The M^{3+} (Al^{3+} and/or Fe^{3+}) ion can be precipitated as amorphous hydroxides and contributed to the removal processes, whereas both Mg and Zn could remain in solution. One important open question is directed on the occurrence of the dissolution of the sorbents and the impact of the introduction of the metals contained in these materials in the aquatic system. Therefore future studies should be developed in order to assess the most appropriate solid/liquid ratio in order to obtain the greatest advantage from the use of these materials in the removal of antimony, and arsenic as well.

CHAPTER 5. Conclusions

In the last years, the topic of antimony has been arising great interest, due to the environmental impact linked to its extraction and use in several industrial applications. Many authors have investigated the different respects of antimony pollution; nevertheless, many points need to be better clarified in order to plan future remediation strategies.

For this reason, in this work, a multidisciplinary approach to the antimony issue was followed, aimed at improving our knowledge. On the one hand, geochemical characterization of antimony polluted water draining the abandoned mine of Su Suergiu (SE Sardinia) was performed in order to understand antimony speciation and dispersion mechanisms, on the other hand a removal technique by means of synthetic LDH minerals was tested. The study provided interesting results in each investigated field.

Being the determination of total antimony insufficient to assess the fate and the impact of this contaminant on the environment, in this study the water analyses included the determination of both Sb(III) and Sb(V). Speciation of antimony in aqueous solutions can be obtained through the determination of Sb(tot), either by ICP-MS or ICP-OES, and Sb(III) using ASV. The Sb(V) concentration is calculated by subtracting Sb(III) from Sb(tot). Due to its thermodynamic instability the concentration of Sb(III) decreases during the time, therefore a sample stabilization is needed to avoid that the Sb(III) oxidation affects the results. For this reason, during this work, a stabilization technique has been investigated. Several reagents (i.e. 1% v/v HCl; 0.1% w/v L(+) ascorbic acid; 0.2% v/w L(+) tartaric acid plus 0.1% v/v HNO_3) were tested with both synthetic solutions and natural waters. The most effective Sb(III) stabilization of antimony polluted water (containing high Sb(V) concentration) resulted the L(+) tartaric acid plus nitric acid, however the instability of Sb(III) even in stabilized sample, leads to suggest to carry out analyses as soon as possible, within 7 days upon the water collection (Cidu et al., 2015). Further investigations are needed to validate and/or improve this method.

The analysis of the waters draining the Su Suergiu abandoned mine allows to state that antimony pollution is extended for several kilometers downstream the mine area. In agreement with previous surveys (Cidu et al., 2008a, b), it was observed that the antimony contamination of water system is mainly due to the interaction of water with the foundry slag; in fact the slag drainage showed the highest antimony concentration (up to 10^4 µg L^{-1}) whereas waters flowing out the adits appear as a minor source of contamination. Waters draining Su Suergiu are characterized by slightly alkaline pH and the oxidizing conditions that favor the prevalence of Sb(V) in solution, less toxic but more mobile than the Sb(III) form [Sb(III) ≤ 6 % Sb(tot)]. There are no evidences of natural attenuation processes like precipitation of Sb-bearing phases or sorption on particulate phases, consequently, the only natural abatement of antimony concentration in solution is represented by the dilution process.

The mine drainages are collected by the Riu Ciurixeda catchment; the Riu Ciurixeda about 3 kilometers down the mine area flows into the Flumendosa River, the most important water body of south Sardinia

which provides water for both agricultural and domestics uses. The Riu Ciurixeda shows a strong antimony contamination (10^3 µg L^{-1}) given by the contribution of the mine drainages and also by the interaction between water and foundry slag widely dispersed along the river banks till the confluence of Riu Ciurixeda into the Flumendosa River.

After the confluence of Riu Ciurixeda into the Flumendosa River the antimony concentration decreases significantly, however, dissolved antimony still exceeds the recommended limit for drinking water of both WHO (20 µg L^{-1}) and EC (5 µg L^{-1}), especially under high flow condition (up to 51 µg L^{-1}). These results suggest that possible actions aimed to mitigate the antimony contamination in the water system, should be addressed directly on the slag heaps, which represent the primary source of contamination at Su Suergiu. An appropriate intervention should be aimed to limit the interaction between slag heaps and water, and to stop the dispersion of the slag waste downstream the mine area. Eventually, actions addressed on the mitigation of antimony, through the treatment of the contaminated waters, should be carried out by means of sorbents having high affinity for Sb(V) and able to remove anions under slightly alkaline pH and oxidizing conditions.

For these reasons the second part of this work was focused on testing the efficacy of synthetic LDH minerals in Sb(V) removal from aqueous solution. In a first stage, LDH with different compositions were synthesized and used in sorption tests with synthetic Sb(V)-bearing solutions in order to identify the most effective phases and their Sb(V) removal processes. Successively these sorbents were used in sorption tests carried out with slag drainages collected at Su Suergiu.

The following phases were tested: nitrate LDH with composition MgAl/MgFe-NO_3; carbonate calcined LDH obtained from hydrotalcite-like [$Mg_3^{2+}M_1^{3+}$-c, with M^{3+}= Al^{3+} and/or Fe^{3+}] and zaccagnaite-like [ZnAl-c] compounds. Results showed that both calcined and nitrate LDH are able to remove $Sb(OH)_6^-$ from solution, and that calcined LDH are most effective than LDH-NO_3.

Among the calcined LDH tested, the more effective Mg(AlFe)-c and 2ZnAl-c were selected. These phases remove $Sb(OH)_6^-$ from solution through different processes, both fast and efficient: the Mg(AlFe)-c uptake $Sb(OH)_6^-$ through the formation of a brandholzite-like compound {$Mg[Sb(OH)_6]_2 \cdot 6H_2O$}, a Sb-bearing layered phase; whereas the 2ZnAl-c removed the $Sb(OH)_6^-$ by its intercalation in the interlayer during the reconstruction of a zincalstibite-like LDH [$Zn_2Al(OH)_6(Sb(OH)_6]$. Experiments performed with coexistent anions in solution indicated that the competition effect on the $Sb(OH)_6^-$ removal results $HAsO_4^{2-} >> HCO_3^- > SO_4^{2-}$.

Also ATR-FTIR analyses were performed in order to characterize these materials and their $Sb(OH)_6^-$ removal processes. ATR-IR, in agreement with the XRD data, showed that both Mg(AlFe)-c and 2ZnAl-c adsorbed $Sb(OH)_6^-$ through the formation of outer-sphere complex; these results, are compatible with the formation of either brandholzite-like or zaccagnaite-like compounds as result of $Sb(OH)_6^-$ removal processes from solution by Mg(AlFe)-c and 2ZnAl-c, respectively. The ART-IR spectra of experiments

performed in free atmosphere, shows a very fast adsorption of $Sb(OH)_6^-$, and the contemporary carbonate adsorption by both Mg(AlFe)-c and 2ZnAl-c. However further studies are needed in order to better understand the evolution of the removal processes during the first hours of reactions.

The last stage of this work consisted in sorption experiments performed with the slag drainage collected at Su Suergiu, which are characterized by slightly alkaline pH and high concentration of both antimony and competitor anions in solution. Also these tests confirm the good antimony removal capacity and encourage further investigations. Both Mg(AlFe)-c and 2ZnAl-C removed Sb under slightly alkaline pH and oxidizing condition, and showed good Sb removal capacity in presence of higher concentrations of coexistent anions. Moreover also good arsenic removal capacity was observed.

The relative low concentration of antimony in the mine drainage water (sample SU1), with respect to the synthetic solutions used in the first sorption experiments, did not allow the formation of brandholzite in experiment performed with Mg(AlFe)-c; instead, in batch tests performed with 2ZnAl-c the presence of the zincalstibite-like compound was observed, even if in only one experiment. In fact, in these experiments results suggest that both Sb and As are removed from solution by the intercalation in the interlayer during the reconstruction of LDH-CO_3(OH).

Results showed that the key factor is the solid/liquid ratio that, especially in experiment performed with Mg(AlFe)-c, determined the variation of the pH and thus the evolution of the whole processes in solutions. The dissolution of both Mg(AlFe)-c and 2ZnAl-c was detected in several experiments. The M^{3+} (Al^{3+} and/or Fe^{3+}) can precipitate as amorphous hydroxides, contributing to the removal processes, whereas both Mg and Zn tend to remain in solution. The possible dissolution of the sorbents and the environmental impact produced by the introduction in the aquatic system of the metals contained in these materials is an important open question. Therefore, future studies should be addressed to assess the most appropriate solid/liquid ratio in order to optimize the antimony removal.

Bibliography

Accornero M., Marini L., Lelli M., 2008. The dissociation constant of antimonic acid at 10-40°C. Journal of Solution Chemistry; 37(6), 785-800.

Ambe S., 1987. Adsorption kinetics of antimony (V) ions onto α-Fe_2O_3 surfaces from an aqueous solution. Langmuir; 3, 489-493.

Ardau C., Frau F., Lattanzi P., 2013. New data on arsenic sorption properties of Zn-Al sulphate layered double hydroxides: influence of competition with other anions. Applied Clay Science; 80-81, 1-9.

Asaoka S., Takahashi Y., Araki Y., Tanimizu M., 2012. Comparison of antimony and arsenic behavior in an Ichinokawa River water–sediment system. Chemical Geology; 334, 1–8.

Ashley P.M., Craw D., Graham B.P., Chappell D.A., 2003. Environmental mobility of antimony around mesothermal stibnite deposits, New South Wales, Australia and southern New Zealand. Journal of Geochemical Exploration; 77(1), 1-14.

Ball J.W. and Nordstrom D.K., 1991. User's manual for WATEQ4F, with revised thermodynamic data base and test cases for calculating speciation of major, trace, and redox elements in natural waters: U.S. Geological Survey Open-File Report 91-183, 189p.

Belzile N., Chen Y.W., Wang Z.J., 2001. Oxidation of antimony(III) by amorphous iron and manganese oxyhydroxides. Chemical Geology; 174(4), 379-387.

Biddau R., 2012. Approccio geochimico statistico per la valutazione del background geochimico nelle acque sotterranee. Applicazioni agli acquiferi della Sardegna. FSE 2007-2013, L.R.7/2007, Regione Autonoma della Sardegna, Cagliari; 2012. 123 [in Italian].

Bonaccorsi E., Merlino S., Orlandi P., 2007. Zincalstibite, a new mineral, and cualstibite: crystal chemical and structural relationships. American Mineralogist; 92(1), 198-203.

Braterman P.S., Xu Z.P., Yarberry F., 2004. CHAPTER 8 Layered Double Hydroxides (LDHs). In: Auerbach S.M., Carrado K.A. and Dutta P.K. (Eds.), Handbook of layered materials.

Cabon J.Y. and Madec C.L., 2004. Determination of major antimony species in seawater by continuous flow injection hydride generation atomic absorption spectrometry. Analytica Chimica Acta; 504(2), 209–215.

Carmignani L., Cocozza T., Ghezzo C., Pertusati P.C., Ricci C.A., 1986. Outlines of the Hercynian basement of Sardinia. In: Carmignani L., Cocozza T., Ghezzo C., Pertusati P.C., Ricci C.A., editors. Guide book to the excursion on the Paleozoic basement of Sardinia I.G.C.P., Newsletter Pisa: Pacini Editore, 11-21. [Special Issue].

Carriazo D., del Arco M., Martín C., Rives V., 2007. A comparative study between chloride and calcined

carbonate hydrotalcites as adsorbent for Cr(VI). Applied Clay Science; 37(3-4), 231-239.

Casiot C., Ujevic M., Munoz M., Seidel J.L., Elbaz-Poulichet F., 2007. Antimony and arsenic mobility in a creek draining an antimony mine abandoned 85 years ago (Upper Orb Basin, France). Applied Geochemistry; 22(4), 788–798.

Cavani F., Trifirò F., Vaccari A., 1991. Hydrotalcite-type anionic clays: preparation, properties and applications. Catalysis Today; 11(2), 173-301.

Cidu R., 2000. Trace elements: Li, Be, B, Al, V, Cr, Co, Ni, Se, Sr, Ag, Sn, Ba, and Tl. in: L. Nollet (Ed.), Handbook of Water Analysis, Marcel Dekker, New York; Chapter 23, 459–482.

Cidu R., Caboi R., Biddau R., Petrini R., Slejko F., Flora O., Aiuppa A., Parello F., Valenza M., 2008a. Caratterizzazione idrogeochimica ed isotopica e valutazione della qualità delle acque superficiali e sotterranee campionate nel Foglio 549 Muravera. In: Ottonello G. (Ed.) GEOBASI. Pacini Editore, Pisa, 149-183 [in Italian] ISBN 978-88-7781-926-0.

Cidu R., Fanfani L., Frau F., Biddau R., Cabras R., Da Pelo S., 2008b. The abandoned antimony-mine of SE Sardinia: impact on surface waters. Proceedings IMWA 2008, 127-130, Karlovy Vary, Czech Republic, 1-5 June 2008 ISBN 978-80-248-1767-5.

Cidu R., Frau F., 2009. Distributions of trace elements in filtered and non filtered aqueous fractions: insights from rivers and streams of Sardinia (Italy). Applied Geochemistry; 24(4), 611-623. http://dx.doi.org/10.1007/s12665-010-0874-y.

Cidu R., Biddau R., Dore E., 2012. Antimony contamination of surface water at abandoned Sardinian mine sites. Proc. IMWA 2012, Bunburry Australia (McCullough C.D., Lund MA, Wyse L., Eds.), 301-307. ISBN 978-0-7298-0707-4.

Cidu R., Biddau R., Dore E., Vacca A., Marini L., 2014. Antimony in the soil-water-plant system at the Su Suergiu abandoned mine (Sardinia, Italy): strategies to mitigate contamination. Science of the Total Environment; 497-498, 319-331.

Cidu R., Biddau R., Dore E., 2015. Determination of trace of Sb(III) using ASV in Sb-rich water samples affected by mining. Analytica Chimica Acta; 854, 34-39.

Davantès A. and Lefèvre G., 2013. In situ real time infrared spectroscopy of sorption of (poly)molybdate ions into layered double hydroxides. The journal Physical Chemistry A; 117(48), 12922-12929.

Rojas Delgado R., De Pauli C.P., Barriga Carrasco C., Avena M.J., 2008. Influence of M^{II}/M^{III} ratio in surface-charging behavior of Zn-Al layered double hydroxides. Applied Clay Science. 40(1-4), 27-37.

Diemar G.A., Filella M., Leverett P., Williams P.A., 2009. Dispersion of antimony from oxidizing ore deposits. Pure and Applied Chemistry; 81(9), 1547-1553.

Ferreira O.P., Alves O.L., Gouveia D.X., Souza Filho A.G., de Paiva J.A.C., Mendes Filho J., 2004. Thermal decomposition and structural reconstruction effect on Mg-Fe- based hydrotalcite compounds. Journal of Solid State chemistry; 177(9), 3058-3069.

Ferreira O.P., de Moraes S.G., Duran N., Cornejo L., Alves O.L., 2006. Evaluation of boron removal from water by hydrotalcite-like compounds. Chemosphere; 62(1), 80-88.

Filella M., Belzile N., Chen Y.-W., 2002a. Antimony in the environment: a review focused on natural waters: I. Occurrence. Earth Science Reviews; 57(1-2), 125-176.

Filella M., Belzile N., Chen Y.-W., Quentel F., 2002b. Antimony in the environment: a review focused on natural waters: II. Relevant solution chemistry. Earth Science Reviews(1-4); 59, 265-285.

Filella M., Philippo S., Belzile N., Chen Y., Quentel F., 2009. Natural attenuation processes applying to antimony: a study in the abandoned mine of Goesdorf, Luxembourg. Science of the Total Environment; 407(24), 6205-6216.

Friedrich A., Wildner M., Tillmanns E., Merz P.L., 2000. Crystal chemistry of the new mineral brandholzite, $Mg(H_2O)_6[Sb(OH)_6]_2$, and of the synthetic analogues $M^{2+}(H_2O)_6[Sb(OH)_6]_2$ (M^{2+} = Mg, Co). American Mineralogist; Volume 85(3-4), 593-599.

Funedda A., Naitza S., Tocco S., 2005. Caratteri giacimentologici e controlli strutturali nelle mineralizzazioni idrotermali tardo-erciniche ad As-Sb-W-Au del basamento metamorfico paleozoico della Sardegna sud-orientale. Resoconti Associazione Mineraria Sarda CX, 25-46 [in Italian].

Gadhari N.S., Sanghavi B.J., Srivastava A.K., 2011. Potentiometric stripping analysis of antimony based on carbon paste electrode modified with hexathia crown ether and rice husk. Analytica Chimica Acta; 703(1), 31–40.

Gebel T., 1997. Arsenic and antimony: comparative approach on mechanistic toxicology. Chemico-Biological Interactions; 107(3), 131-144.

Goh K-H., Lim T-T., Dong Z., 2008. Application of layered double hydroxides for removal of oxyanions: a review. Water Research; 42(6), 1343-1368.

Guo X., Wu Z., He M., Meng X., Jin X., Qiu N., Zhang J., 2014. Adsorption of antimony onto iron oxyhydroxides: adsorption behavior and surface structure. Journal of Hazardous Materials; 276, 339-345.

Hiller E., Laninská B., Chovan M., Jurkovič L., Klimko T., Jankulár M., Hovorič R., Šottnik P., Flaková R., Zenišova Z., Ondrejková I., 2012. Arsenic and antimony contamination of waters, stream sediments and soils in the vicinity of abandoned antimony mines in the Western Carpathians, Slovakia. Applied Geochemistry; 27, 598–614.

He H., Kang H., Ma S., Bai Y., Yang X., 2010. High adsorption selectivity of ZnAl layered double

hydroxides and the calcined materials toward phosphate. Journal of Colloid and Interface Science; 343(1), 225-231.

IGEA, 2009. Piano di investigazione iniziale dell'area mineraria di "Su Suergiu". Campo Pisano: IGEA S.p.A. [in Italian].

Italia. Decreto Legislativo 2 Febbraio 2001, n.31. Attuazione della Direttiva 98/83/CE relativa alla qualità delle acque destinate al consumo umano. Gazzetta Ufficiale - Serie Generale n. 52, 3 Marzo 2001.

Kameda T., Honda M., Yoshioka T., 2011. Removal of antimonate ions and simultaneous formation of a brandholzite-like compound from magnesium-aluminum oxide. Separation and Purification Technology; 80(2), 235-239.

Kentjono L., Liu J.C., Chang W.C., Irawan C., 2010. Removal of boron and iodine from optoelectronic wastewater using Mg-Al (NO_3) layered double hydroxides. Desalination; 262(1), 280-283.

Koritnig S. and Süsse P., 1975. Meixnerite, $Mg_6Al_2(OH)_{18}{\cdot}4H_2O$, ein neues magnesium-aluminium-hydroxid-mineral. Tschermaks Mineralogische und Petrographische Mitteilungen; 22(1), 79–87.

Krachler M., Emons H., Zheng J., 2001. Speciation of antimony for the 21th century: promises and pitfalls. Trends in Analytical Chemistry; 20(2), 79-90.

Lazardis N.K., and Asouhidou D.D., 2003. Kinetics sorptive removal of chromium(VI) from aqueous solutions by calcined Mg-Al-CO_3 hydrotalcite. Water Research; 37(12), 2875-2882.

Lefèvre G., 2004. In situ Fourier-transform infrared spectroscopy studies of inorganic ions adsorption on metal oxides and hydroxides. Advances in Colloid and Interface Science; 107(2), 109-123.

Leuz A.K., Mönch H., Johnson C.A., 2006. Sorption of Sb(III) and Sb(V) to goethite: influence on Sb(III) oxidation and mobilization. Environmental Science & Technology; 40(23), 7277-7282.

Leverett P., Reynolds J.K., Roper A.J., Williams P.A., 2012. Tripuhyite and schafarzikite: two of the ultimatesinks for antimony in the natural environment. Mineralogical Magazine; 76(4), 891–902.

Li Z., 2005. Novel solid base catalysts for Michael additions. Synthesis, characterization and application. Doctoral dissertation, Humboldt-Universitat zu Berlin, Germany.
http://edoc.hu-berlin.de/dissertationen/li-zhijian-2005-08-18/HTML/front.html

Linares C.F., Bretto P., Álvarez R., Ocanto F., Corao C., Betancourt P., Brito J.L., 2014. Evaluation of calcined hydrocalumite-type materials as supports of CoMo and NiMo for thiophene hydrodesulfuration reaction. Matherial Research; 17(4), 823-828.
http://dx.doi.org/10.1590/S1516-14392014005000085

Lozano R.P., Rossi C., La Iglesia Á., Matesanz E., 2012. Zaccagnaite-3R, a new Zn-Al polytype from El Soplao cave (Cantabria, Spain). American Mineralogist; Volume 97(4), 513-523.

Manohara G.V., Prasanna S.V., Kamath P.V., 2011. Structure and composition of the layered double hydroxides of Mg and Fe: implications for anion-exchange reactions. European Journal of Inorganic Chemistry; 2011(16), 2624-2630.

Marcellino S., Attar H., Lièvremont D., Lett M.-C., Barbier F., Lagarde F., 2008. Heat-treated Saccharomyces cerevisiae for antimony speciation and antimony(III) preconcentration in water samples. Analytica Chimica Acta; 629(1), 73–83.

Marguí E., Sagué M., Queralt I., Hidalgo M., 2013. Liquid phase microextraction strategies combined with total reflection X-ray spectrometry for the determination of low amounts of inorganic antimony species in waters. Analytica Chimica Acta; 786, 8–15.

McComb K.A., Craw D., McQuillan A.J., 2007. ATR-IR spectroscopy study of antimonate adsorption to iron oxide. Langmuir; 23(24), 12125-12130.

Mills S.J., Christy A.G., Génin J-M. R., Kameda T., Colombo F., 2012. Nomenclature of the hydrotalcite supergroup: natural layered double hydroxides. Mineralogical Magazine; 76(5), 1289-1336.

Mitsunobu S., Takahashi Y., Sakai Y., Inumaru K., 2009. Interaction of synthetic sulfate green rust with antimony(V). Environmental Science & Technology; 43(2), 318-323.

Mitsunobu S., Takahashi Y., Terada Y., Sakata M., 2010. Antimony(V) incorporation into synthetic ferrihydrite, goethite, and natural iron oxyhydroxides. Environmental Science & Technology; 44(10), 3712-3718.

Müller K., Brendler V., Foerstendorf H., 2008. Aqueous Uranium-(VI) Hydrolysis Species Characterized by Attenuated Total Reflection Fourier-Transform Infrared Spectroscopy. Inorganic Chemistry; 47(21), 10127−10134.

Nedim A., Zümreoglu-Karan B., Temel A., 2007. Boron removal by hydrotalcite-like, carbonate-free Mg-Al-NO_3-LDH and a rationale on the mechanism. Microporous and Mesoporous Materials; 98(1-3), 1-5.

Nishad P.A., Bhaskarapillai A., Velmurugan S., 2014. Nano-titania-crosslinked chitosan composite as superior sorbent for antimony(III) and (V). Carbohydrate Polymers; 108, 169-175.

Nordstrom D.K., 1977. Thermochemical redox equilibria of Zoßell's solution. Geochimica et Cosmochimica Acta; 41, 1835-1841.

Palmer S.J., Frost R.L., 2010. Use of hydrotalcites for the removal of toxic anions from aqueous solutions. Industrial & Engineering Chemistry Research; 49(19), 8969-8976.

Palmer S.J., Soisonard A., Frost R.L., 2009. Determination of the mechanism(s) for the inclusion of arsenate, vanadate, or molybdate anions into hydrotalcites with variable cationic ratio. Journal of Colloid and Interface Science; 329(2), 404-409.

Quentel F., Filella M., 2002. Determination of inorganic antimony species in sea water by differential pulse anodic stripping voltammetry: stability of the trivalent state. Analytica Chimica Acta; 452(2), 237-244.

Quentel F., Filella M., Elleouet C., Madec C.-L., 2004. Kinetics studies on Sb(III) oxidation by hydrogen peroxide in aqueous solutions. Environmental Science & Technology; 38(10), 2843-2848.

Quentel F., Filella M., Elleouet C., Madec C.-L., 2006. Sb(III) oxidation by iodate in seawater: A cautionary tale. Science of the Total Environment; 355(1), 259-263.

RAS Regione Autonoma della Sardegna, 1998. Nuovo studio dell'idrologia superficiale della Sardegna. Cagliari: Assessorato della programmazione, bilancio ed assetto del territorio, Ente Autonomo del Flumendosa. [in Italian]

RAS Regione Autonoma della Sardegna, 2003. Piano Regionale di Gestione dei Rifiuti — Piano di Bonifica dei Siti Inquinati. 255 pp. Allegato 5 — Schede dei siti minerari dimessi; [Cagliari, in Italian].

RAS Regione Autonoma della Sardegna, 2013. Carta geologica di base della Sardegna in scala 1:25000. http://www.sardegnageoportale.it/argomenti/cartageologica.html.

Rakshit S., Sarkar D., Punamiya P., Datta R., 2011. Antimony sorption at gibbsite-water interface. Chemosphere; 84(4), 480-483.

Renedo O.D. and Martínez M.J.A., 2007. Anodic stripping voltammetry of antimony using gold nanoparticle-modified carbon screen-printed electrodes. Analytica Chimica Acta; 589(2), 255–260.

Ritchie V.J., Ilgen A.G., Mueller S.H., Trainor T.P., Goldfarb R.J., 2013. Mobility and chemical fate of antimony and arsenic in historic mining environments of the Kantishna Hills district, Denali National Park and Preserve, Alaska. Chemical Geology; 335, 172–188.

Rojas Delgado R., De Pauli C.P., Barriga Carrasco C., Avena M.J., 2008. Influence of M^{II}/M^{III} ratio in surface-charging behavior of Zn–Al layered double hydroxides. Applied Clay Science; 40(1), 27–37.

Roper A.J., Williams P.A., Filella M., 2012. Secondary antimony minerals: phases that control the dispersion of antimony in the supergene zone. Chemie der Erde-Geochemistry; 72, 9–14.

Séby F., Gleyzes C., Grosso O., Plau B., Donard O.F.X., 2012. Speciation of antimony in injectable drugs used for leishmaniasis treatment (Glucantime®) by HPLC-ICP-MS and DPP. Analytical and Bioanalytical Chemistry; 404(10), 2939–2948. doi:http://dx.doi.org/10.1007/s00216-012-6427-3.

Secchi F. and Lorrai M., 2001. Some geological and environmental aspects of the Sarrabus-Gerrei Region (SE Sardinia, Italy). vol. LXXI Rendiconti del Seminario di Facoltà di Scienze dell'Università di Cagliari; 71(2), 187-208.

Thanabalasingam P. and Pickering W.F., 1990. Specific sorption of antimony (III) by the hydrous oxides of Mn, Fe and Al. Water, Air, & Soil Pollution; 49(1-2), 175-185.

Toghill K.E., Lu M., Compton R.G., 2011. Electroanalytical determination of antimony. International Journal of Electrochemical Science; 6(8), 3057–3076.

Türk T., Alp I., Deveci H., 2009. Adsorption of As(V) from water using Mg–Fe-based hydrotalcite (FeHT). Journal of Hazardous Materials; 171(1), 665–670.

United States Environmental Protection Agency, 1979. Water Related Fate of the 129 Priority Pollutants, Doc. 745-R-00-007; USEPA 1979 Washington, DC; Vol. 1.

Vaccari A., 1998. Preparation and catalytic properties of cationic and anionic clays. Catalysis Today; 41 (1-3), 53-71.

Wang S.L. and Wang P.C., 2007. In-situ XRD and ATR-FTIR study on the molecular orientation of the interlayer nitrate in Mg/Al-layered double hydroxides in water. Colloids and Surfaces A; 292(2), 131-138.

Wang S.-L., Liu C.H., Wang M.K., Chuang Y.H., Chiang P.N., 2009. Arsenate adsorption by Mg/Al-NO_3 layered double hydroxides with varying the Mg/Al ratio. Applied Clay Science; 43(1), 79-85.

Wang X., He M., Xi J., Lu X., 2011. Antimony distribution and mobility in rivers around the world's largest antimony mine of Xikuangshan, Hunan Province, China. Microchemical Journal; 97, 4-11.

WHO, Guidelines for drinking-water quality. 4th ed., 2011. Geneva: World Health Organization; ISBN: 978 92 4 154815 1.

Wilson N. and Webster-Brown J., 2009. The fate of antimony in a major lowland river system, the Waikato River, New Zealand. Applied Geochemistry; 24(12), 2283–2292.

Wilson S.C., Lockwood P.V., Ashley P.M., Tighe M., 2010. The chemistry and behaviour of antimony in the soil environment with comparisons to arsenic: a critical review. Environmental Pollution; 158(5), 1169-1181.

Wu X-D., Song J-M., Li X-G., Yuan H-M., Li N., 2011. Behaviors of dissolved antimony in the Yangtze River Estuary and its adjacent waters. Journal of Environmental Monitoring; 13(8), 2292–2303. http:// dx.doi.org/10.1039/c1em10239g

Xu Y.-H., Ohki A., Maeda S., 2001. Adsorption and removal of antimony from aqueous solution by an activated alumina. Toxicological & Environmental Chemistry; 80(3-4), 133-144.

Yang Y., Gao N., Deng Y., Zhou S., 2012. Adsorption of perchlorate from water using calcined iron-based layered double hydroxides. Applied Clay Science; 65-66, 80-86.

Zhang Y. and Li X., 2014. Preparation of Zn-Al CLDH to remove bromate from drinking water. Journal of Environmental Engineering; 140(7). doi: 10.1061/(ASCE)EE.1943-7870.0000835.

Zakaznova-Herzog V.P. and Seward T.M., 2006. Antimonous acid protonation/deprotonation equilibria in hydrothermal solutions to 300°C. Geochimica et Cosmochimica Acta; 70(9), 2298-2310.
.

Appendix I

Physical chemical parameter of water collected at Su Suergiu from 201 to 2014.

Physical chemical parameter of water samples determine at the sampling points.

Sample	Name	Type	Date	Flow	T water	pH	Eh	EC
				L s^{-1}	°C		V	mS cm^{-1}
upstream								
SU8	Villasalto - Armungia	spring	09.05.12	0.03	16	7.6	0.43	0.33
SU15	Monte Genis-fontanelle 1	spring	13.06.12	<0.1	18	6.1	0.43	0.19
MU9	Rio Spigulu	stream	02.05.12	50	17	7.8	0.38	0.36
MU9	Rio Spigulu	stream	28.02.13	250	8	8.2	0.51	0.25
MU9	Rio Spigulu	stream	20.06.13	1	18	7.5	0.44	0.51
MU92	Flumendosa	river	23.05.12	1000	17	8.0	0.45	0.55
MU92	Flumendosa	river	28.02.13	3000	8	7.8	0.51	0.41
MU92	Flumendosa	river	23.07.13	1000	25.9	7.7	0.38	0.55
MU92	Flumendosa	river	09.01.14	4000	10	7.7	0.48	0.49
MU92	Flumendosa	river	20.06.13	1000	24	8.1	0.45	0.52
SU5	Su Suergiu viale dei pini	spring	09.05.12	<0.1	13	7.4	0.46	0.31
SU13	Su Suergiu mine	spring	13.06.12	<0.05	15	7.0	0.49	0.36
SU17	Rio Corr'e Cerbus	stream	28.02.13	8	8	8.2	0.51	0.81
mine area								
SU3	Rio Sessini	stream	09.05.12	0.5	15	7.8	0.43	1.00
SU3	Rio Sessini	stream	11.12.12	20	8	8.2	0.47	0.78
SU3	Rio Sessini	stream	28.02.13	80	8	8.1	0.51	0.41
SU3	Rio Sessini	stream	20.06.13	0.05	19	7.6	0.47	2.30
SU1	Su Suergiu mine	slag drainage	02.05.12	0.05	18	7.9	0.34	1.46
SU1	Su Suergiu mine	slag drainage	09.05.12	0.05	16	7.7	0.35	1.50
SU1	Su Suergiu mine	slag drainage	30.10.12	0.04	10	7.8	0.47	3.03
SU1	Su Suergiu mine	slag drainage	28.02.13	0.3	13	7.6	0.48	2.03
SU1	Su Suergiu mine	slag drainage	01.07.13	0.1	22	8.1	0.44	3.10
SU1	Su Suergiu mine	slag drainage	20.06.13	0.01	22	8.2	0.46	2.70
SU1	Su Suergiu mine	slag drainage	23.07.13	0.07	20	8.0	0.37	2.70
SU1	Su Suergiu mine	slag drainage	26.05.14	0.25	19	7.5	0.40	2.14
SU1	Su Suergiu mine	slag drainage	09.01.14	0.4	14	7.1	0.47	1.78
SU1	Su Suergiu mine	slag drainage	30.06.14	0.03	22	7.8	0.45	2.39
SU2	Su Suergiu mine	slag drainage	02.05.12	0.07	22	8.4	0.36	1.68
SU2	Su Suergiu mine	slag drainage	09.05.12	0.05	22	8.4	0.42	1.79
SU2	Su Suergiu mine	slag drainage	30.10.12	0.1	16	8.5	0.48	3.75
SU2	Su Suergiu mine	slag drainage	28.02.13	0.05	9	8.5	0.49	2.50
SU2	Su Suergiu mine	slag drainage	20.06.13	0.01	25	8.3	0.45	2.60
SU12	Su Suergiu mine	stream	13.06.12	0.01	19	8.1	0.46	2.64
SU20	Rio Sessini	stream	11.12.12	5	11	7.6	0.45	1.25
SU20	Rio Sessini	stream	30.10.12	0.1	16	7.4	0.46	2.44
SU20	Rio Sessini	stream	28.02.13	30	8	8.0	0.50	0.41
SU4	Su Suergiu mine	adit	09.05.12	0.1	14	7.1	0.37	0.79
SU6	Su Suergiu mine	stream	09.05.12	0.05	13	7.8	0.46	0.90
SU7	Su Suergiu mine	adit	09.05.12	0.01	12	7.8	0.47	0.46
SU9	Su Suergiu mine	borehole	23.05.12	0.01	18	7.0	0.44	2.18
downstream								
MU8	Rio Ciurixeda	stream	02.05.12	50	17	8.3	0.40	0.79
MU8	Rio Ciurixeda	stream	23.05.12	40	17	7.9	0.48	0.86
MU8	Rio Ciurixeda	stream	28.02.13	50	8	8.0	0.50	0.71
MU8	Rio Ciurixeda	stream	20.06.13	0.25	19	7.7	0.46	1.10
MU8	Rio Ciurixeda	stream	01.07.13	0.15	20	7.7	0.46	1.20
MU8	Rio Ciurixeda	stream	23.07.13	0.2	22	7.6	0.39	1.15
MU8	Rio Ciurixeda	stream	09.01.14	120	11	7.8	0.49	0.78
MU8	Rio Ciurixeda	stream	13.05.14	1	19	7.9	0.46	1.06
SU11	Flumendosa	river	23.05.12	1000	18	8.0	0.45	0.56
SU11	Flumendosa	river	28.02.13	>1000	8	8.0	0.50	0.41
SU11	Flumendosa	river	20.06.13	200	24	8.1	0.45	0.53
SU11	Flumendosa	river	23.07.13	200	27	7.8	0.37	0.55
SU11	Flumendosa	river	09.01.14	4000	11	7.7	0.49	0.50

Appendix II

Results of chemical analyses of speedy sorption tests.

Concentrations of Sb, Mg, Al and NO_3, and pH values determined in solution during the speed sorption experiments performed with MgAl-NO_3.

	2MgAl-NO_3						3MgAl-NO_3						4MgAl-NO_3					
time	pH	Sb	Mg	Al	NO_3		time	pH	Sb	Mg	Al	NO_3	time	pH	Sb	Mg	Al	NO_3
h		mmoles L^{-1}					h		mmoles L^{-1}				h		mmoles L^{-1}			
0	5.5	10	[a]n.a.	n.a.	n.a.		0	5.4	10	n.a.	n.a.	n.a.	0	5.3	10	n.a.	n.a.	n.a.
1	8.6	5.8	0.13	n.a.	n.a.		1	9.8	7.8	0.19	n.a.	n.a.	1	9.8	8.2	0.16	n.a.	n.a.
2	8.4	5.5	0.13	n.a.	n.a.		2	9.8	7.6	0.20	n.a.	n.a.	2	9.9	8.3	0.17	n.a.	n.a.
3	8.0	5.4	0.14	n.a.	n.a.		3	9.7	7.6	0.18	n.a.	n.a.	3	9.8	7.5	0.20	n.a.	n.a.
5	8.0	5.4	0.16	< 0.06	0.65		5	9.8	7.6	0.20	<0.06	0.39	5	9.7	7.8	0.22	< 0.06	0.39

[a]n.a. = not analyzed

Concentrations of Sb, Mg, Fe and NO_3, and pH values determined in solution during the speed sorption experiments performed with MgFe-NO_3.

	2MgFe-NO_3						3MgFe-NO_3						4MgFe-NO_3					
time	pH	Sb	Mg	Fe	NO_3		time	pH	Sb	Mg	Fe	NO_3	time	pH	Sb	Mg	Fe	NO_3
h		mmoles L^{-1}					h		mmoles L^{-1}				h		mmoles L^{-1}			
0	5.4	10	[a]n.a.	n.a.	n.a.		0	5.4	10	n.a.	n.a.	n.a.	0	5.5	10	n.a.	n.a.	n.a.
1	9.3	9.3	0.38	n.a.	n.a.		1	9.6	9.1	0.29	n.a.	n.a.	1	10.0	9.4	0.23	n.a.	n.a.
2	9.6	9.0	0.43	n.a.	n.a.		2	9.6	8.9	0.31	n.a.	n.a.	2	10.0	9.3	0.25	n.a.	n.a.
3	9.4	8.7	0.44	n.a.	n.a.		3	9.6	8.8	0.35	n.a.	n.a.	3	9.9	9.2	0.26	n.a.	n.a.
5	9.8	8.5	0.49	< 0.02	0.27		5	9.6	8.6	0.36	< 0.02	0.39	5	9.9	9.3	0.28	< 0.02	0.40

[a]n.a. = not analyzed

Appendix III

Results of chemical analyses and mineralogical characterization of preliminary sorption experiments.

Concentrations of Sb, Mg, Fe, Al, Zn and NO_3 and pH values determined in solution during the preliminary sorption experiments.

3MgAl-c					**3Mg(AlFe)-c**						**3MgFe-c**					**3ZnAl-c**					**2ZnAl-c**					**2MgAl-NO_3**				
time	pH	Sb	Mg	Al	time	pH	Sb	Mg	Al	Fe	time	pH	Sb	Mg	Fe	time	pH	Sb	Zn	Al	time	pH	Sb	Zn	Al	time	pH	Sb	Mg	Al
h		mmoles L^{-1}			h		mmoles L^{-1}				h		mmoles L^{-1}			h		mmoles L^{-1}			h		mmoles L^{-1}			h		mmoles L^{-1}		
0	5.4	10.2	[a]n.a.	n.a.	0	5.4	11.1	n.a.	n.a.	n.a.	0	5.4	10.4	n.a.	n.a.	0	5.2	10.3	n.a.	n.a.	0	5.3	10.2	n.a.	n.a.	0	5.2	9.7	n.a.	n.a.
0.5	11.3	8.0	n.a.	n.a.	0.5	10.9	9.2	n.a.	n.a.	n.a.	0.5	10.9	10.1	n.a.	n.a.	0.5	11.7	5.1	n.a.	n.a.	0.5	11.3	4.1	n.a.	n.a.	0.5	7.7	6.2	n.a.	n.a.
1	11.5	7.3	n.a.	n.a.	1	11.3	8.4	n.a.	n.a.	n.a.	1	10.9	10.0	n.a.	n.a.	1	11.8	3.1	n.a.	n.a.	1	11.8	2.6	n.a.	n.a.	1	7.8	5.8	n.a.	n.a.
3	12.0	3.4	n.a.	n.a.	3	12.0	3.3	n.a.	n.a.	n.a.	3	10.9	9.6	n.a.	n.a.	3	11.9	2.3	n.a.	n.a.	3	11.9	1.5	n.a.	n.a.	3	8.0	5.4	n.a.	n.a.
6	12.0	2.2	n.a.	n.a.	6	12.1	1.3	n.a.	n.a.	n.a.	6	11.3	8.1	n.a.	n.a.	6	11.9	1.9	n.a.	n.a.	6	11.9	1.1	n.a.	n.a.	6	7.9	5.2	n.a.	n.a.
24	12.0	1.4	n.a.	n.a.	24	12.1	0.8	n.a.	n.a.	n.a.	24	12.2	1.8	n.a.	n.a.	24	12.0	1.0	n.a.	n.a.	24	12.0	0.6	n.a.	n.a.	24	7.7	5.1	n.a.	n.a.
48	11.9	1.2	<0.01	<0.02	48	12.1	0.7	<0.01	<0.02	<0.01	48	12.2	1.0	<0.01	<0.01	48	12.0	0.8	<0.01	<0.1	48	11.9	0.6	0.04	0.4	48	7.7	5.1	0.26	<0.1

[a]n.a. = not analyzed

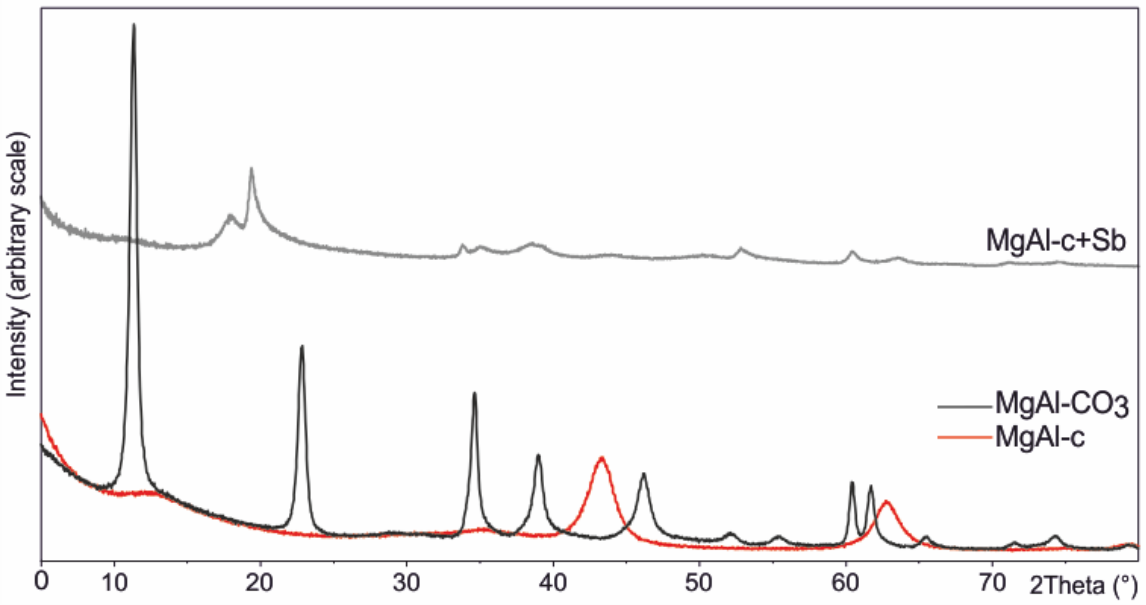

XRD patterns of MgAl-CO_3 and its relative calcined phases before and after the preliminary sorption experiments.

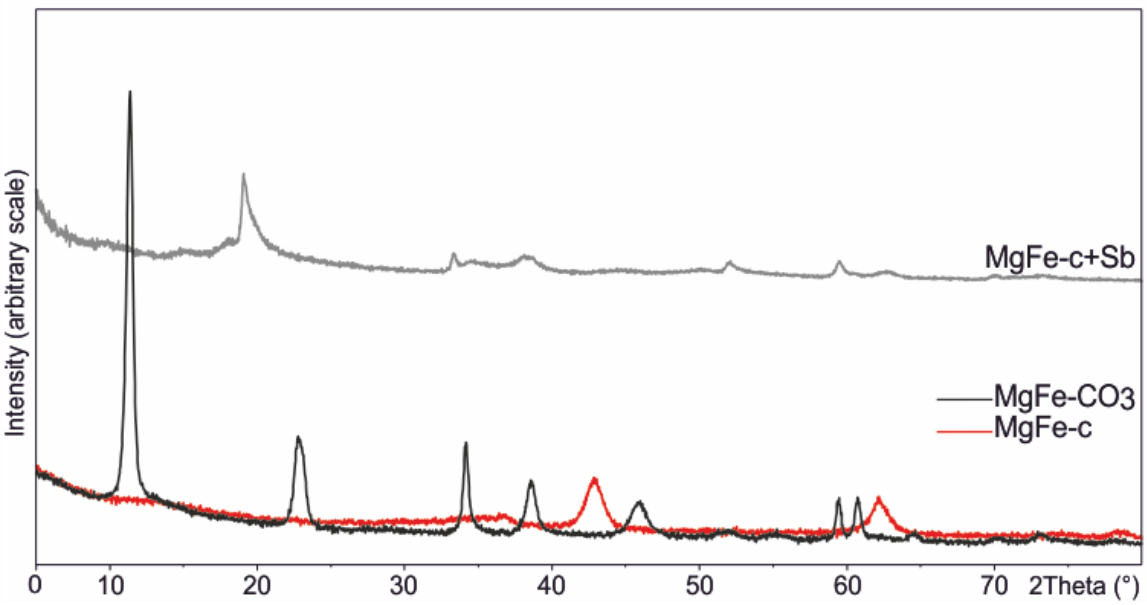

XRD patterns of MgFe-CO_3 and its relative calcined phases before and after the preliminary sorption experiments.

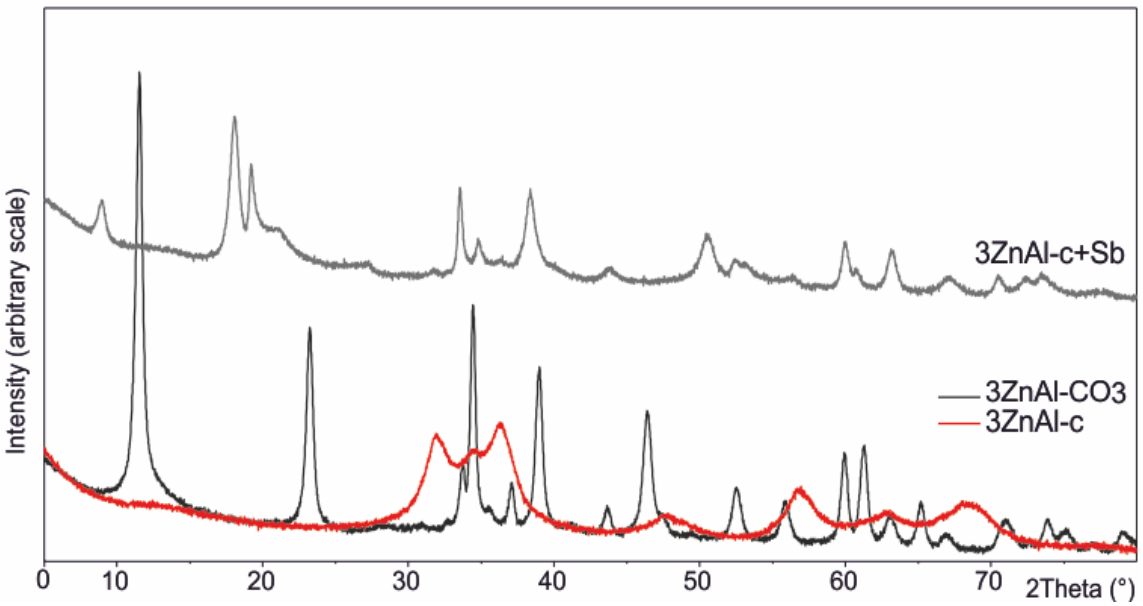

XRD patterns of 3ZnAl-CO_3 and its relative calcined phases before and after the preliminary sorption experiments.

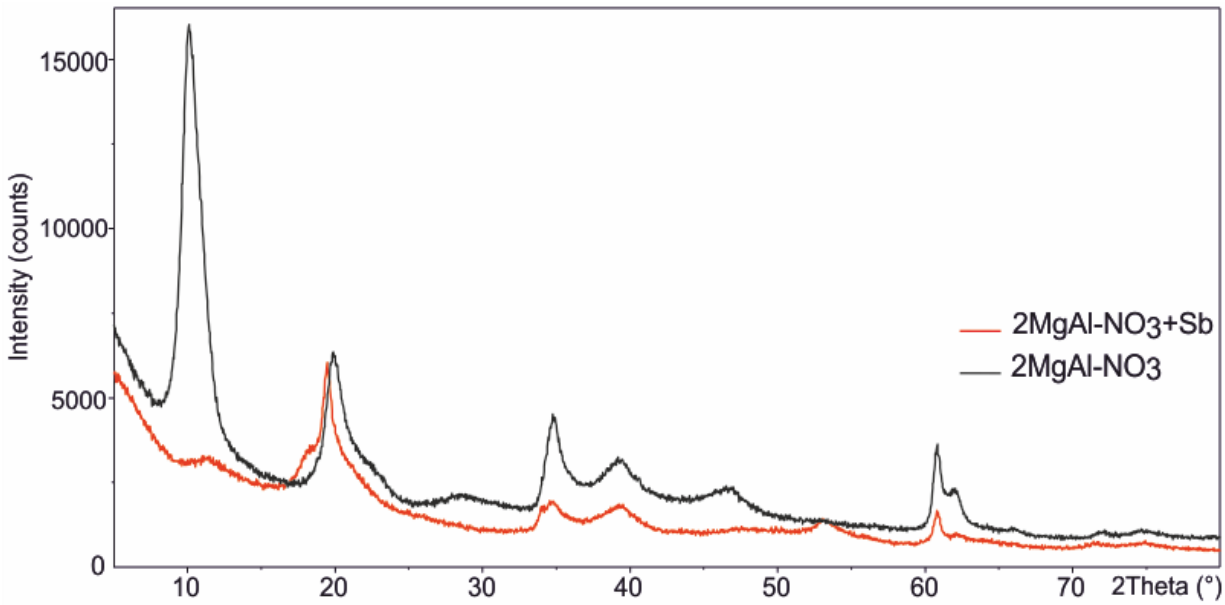

XRD patterns of 2MgAl-NO_3 and its relative calcined phases before and after the preliminary sorption experiments.

Appendix IV

Results of chemical analyses and mineralogical characterization of sorption experiments with circumneutral initial pH.

Concentrations of Sb, Mg, Fe, Al and Zn, and pH values determined in solution during the sorption experiments with circumneutral initial pH.

3Mg(AlFe)-c						2ZnAl-c				
time	pH	Sb	Mg	Al	Fe	time	pH	Sb	Zn	Al
h		mmoles L^{-1}				h		mmoles L^{-1}		
0	7.2	10.10	[a]n.a.	n.a.	n.a.	0	7.2	10.02	n.a.	n.a.
0.5	11.1	9.34	n.a.	n.a.	n.a.	0.5	11.3	5.95	n.a.	n.a.
1	11.3	8.75	n.a.	n.a.	n.a.	1	12.0	3.31	n.a.	n.a.
3	12.0	5.81	n.a.	n.a.	n.a.	3	12.0	1.67	n.a.	n.a.
6	12.1	2.16	n.a.	n.a.	n.a.	6	12.0	0.92	n.a.	n.a.
24	12.1	0.53	n.a.	n.a.	n.a.	24	12.1	0.56	n.a.	n.a.
48	12.2	0.47	<0.01	<0.02	<0.01	48	12.1	0.47	<0.01	0.2

[a]n.a. = not analyzed

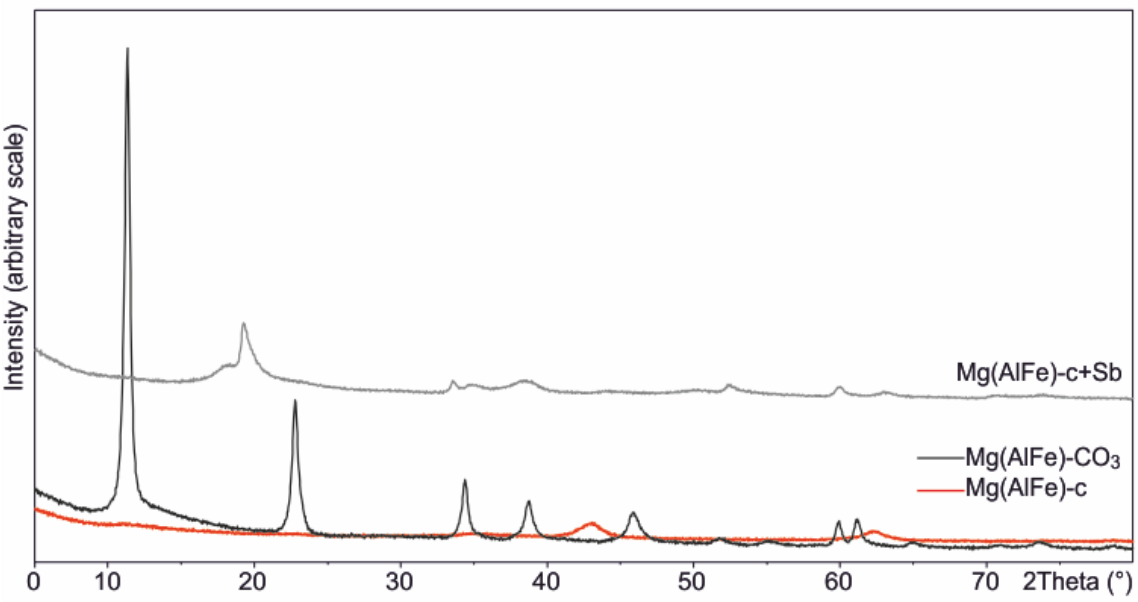

XRD patterns of Mg(AlFe)-CO_3 and its relative calcined phases before and after sorption experiments with circumneutral initial pH.

.

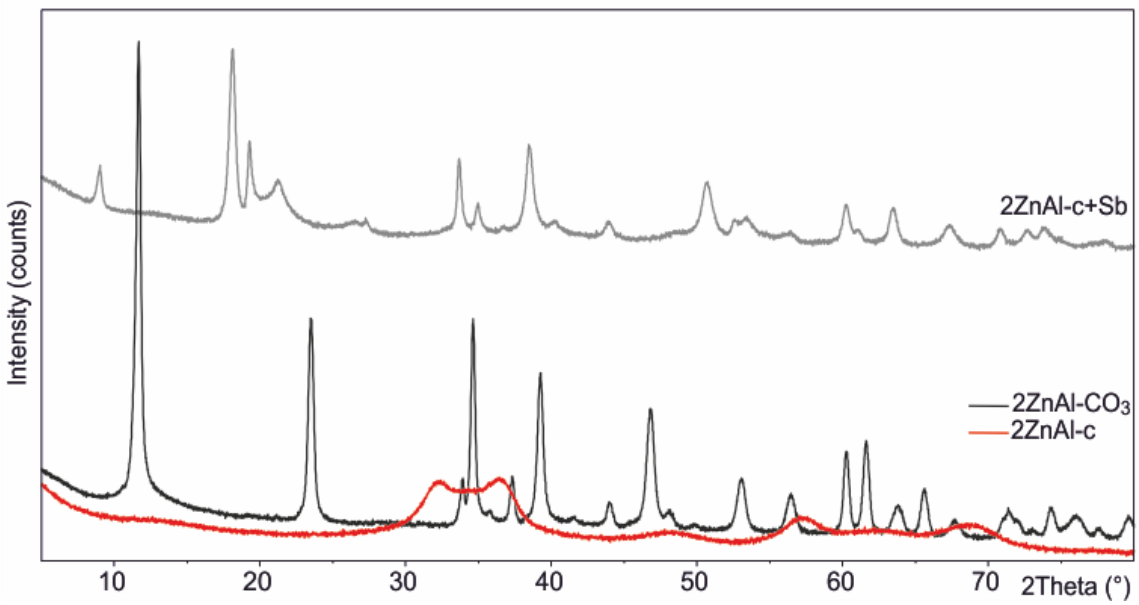

XRD patterns of 2ZnAl-CO_3 and its relative calcined phases before and after sorption experiments with circumneutral initial pH.

Appendix V

Results of chemical analyses of competition sorption experiments.

Concentrations of Mg, Fe and Al determined in solution before the addition of the sorbents and at the end of competition experiments performed with Mg(AlFe)-c.

Mg(AlFe)-c	Sb			$Sb+SO_4^{2-}$				$Sb+HAsO_4^{2-}$				$Sb+HCO_3^-$			
time	Mg	Al	Fe	time	Mg	Al	Fe	time	Mg	Al	Fe	time	Mg	Al	Fe
h	mmoles L^{-1}			h	mmoles L^{-1}			h	mmoles L^{-1}			h	mmoles L^{-1}		
0	< 0.02	< 0.02	< 0.001	0	< 0.02	< 0.02	< 0.001	0	< 0.02	< 0.02	< 0.001	0	< 0.02	< 0.02	< 0.001
48	0.20	< 0.02	< 0.001	48	0.33	< 0.02	< 0.001	48	0.46	< 0.02	< 0.001	48	0.22	< 0.02	< 0.001

Concentrations of Zn and Al determined in solution before the addition of the sorbents and at the end of competition experiments performed with 2ZnAl-c.

2ZnAl-c	Sb		$Sb+SO_4^{2-}$			$Sb+HAsO_4^{2-}$			$Sb+HCO_3^-$		
time	Zn	Al	time	Zn	Al	time	Zn	Al	time	Zn	Al
h	mmoles L^{-1}		h	mmoles L^{-1}		h	mmoles L^{-1}		h	mmoles L^{-1}	
0	< 0.001	< 0.01	0	< 0.001	< 0.01	0	< 0.001	< 0.01	0	< 0.001	< 0.01
48	< 0.001	< 0.01	48	< 0.001	< 0.01	48	0.02	< 0.01	48	< 0.001	< 0.01